

POLITECNICO DI TORINO

Collegio di Ingegneria Chimica e dei Materiali

Master of Science Course
in Materials Engineering

Master of Science Thesis

**DLP-3D printable
cellulose-based hydrogels**



Tutors

prof. Marco Sangermano
dott.ssa Annalisa Chiappone

Candidate

Diana Cafiso

Academic year 2019/2020

Ringraziamenti

Questa tesi simboleggia il termine della mia esperienza da studentessa universitaria; la mia gratitudine va dunque a tutti coloro che mi sono stati accanto in questo percorso e che hanno contribuito al raggiungimento di questo risultato.

Grazie al mio relatore, il professore Marco Sangermano, e ad Annalisa, per avermi guidato nella realizzazione di questa tesi con attenzione e disponibilità.

Grazie ai miei amici Salvo, Damiano, Giulia e Flavia, che mi sono stati vicini anche dopo che i nostri percorsi accademici si sono separati.

Grazie ai miei nonni, ai miei zii e ai miei cugini per il loro affetto incondizionato e sempre tangibile, nonostante la distanza.

Infine, la mia gratitudine più sincera e profonda non può che essere per i miei genitori e mia sorella, che mi sono sempre stati accanto, supportandomi e sopportandomi. Voi rappresentate la mia ancora, il nido che mi legherà alla mia terra, sempre.

INDEX

ITALIAN SUMMARY	1
1. ABSTRACT	1
2. HYDROGELS	2
2.1 Classification	2
2.2 Properties	4
2.3 Applications	5
2.3.1 Regenerative medicine	6
2.3.2 Drug delivery	8
2.3.3 Adsorbents	9
2.3.4 Sensors	10
3. NATURAL HYDROGELS.....	12
3.1 Cellulose and cellulose hydrogels.....	13
4. 3D PRINTING.....	18
4.1 An overview.....	18
4.2 Photopolymerization: stereolithography and digital light processing	20
4.2.1 Photopolymerization	20
4.2.2 Stereolithography and Digital light printing	25
4.2.3 Other photocuring technologies	28
4.3 3D printing of hydrogels via photopolymerization	28
5.METHACRYLATED NATURAL HYDROGELS FOR PHOTOPOLYMERIZATION-3D-PRINTING	33
5.1 Polysaccharides	34
5.1.1 Chitosan.....	34
5.1.2 Hyaluronic acid	36
5.1.3 Alginate.....	36
5.1.4 Alginate and hyaluronic acid	37
5.2 Polypeptides	38
5.2.1 Gelatin	38
5.3 Proteins	39
5.3.1 Silk fibroin.....	39
6. AIM OF THE WORK	42
7. MATERIALS AND METHODS	43
7.1 Materials.....	43
7.2 Cellulose functionalization	44
7.3 Preparation of the hydrogel formulations	45

7.3.1 Neat cellulose hydrogels (M-CMC samples).....	45
7.3.2 Composite hydrogels (CNC/M-CMC samples).....	45
7.4 3D-printing	46
7.5 Characterization	47
7.5.1 H-NMR	47
7.5.2 Photoreology	48
7.5.3 compression tests.....	50
7.5.3.1 Single compression tests	51
7.5.3.2 Cyclic compression tests	51
8.RESULTS.....	53
8.1 H-NMR	53
8.1 Photoreology	54
8.1.1 Neat samples	54
8.1.2 Composite samples	57
8.2 3D printing.....	60
8.3 Compression tests	64
8.3.1 Single compression tests	64
8.3.2 Cyclic compression tests.....	66
9. CONCLUSIONS	70
REFERENCES	71

ITALIAN SUMMARY

SCOPO DEL LAVORO

Lo scopo della tesi è lo studio di idrogeli a base di cellulosa, per la stampa 3D tramite la tecnologia Digital Light Printing (DLP). In particolare modo, sono stati preparati campioni con stampa 3D di idrogeli rinforzati con nanocristalli di cellulosa, in modo da poter analizzare l'effetto di rinforzo dei nano-fillers sul materiale stampato.

INTRODUZIONE: GLI IDROGELI

Gli idrogeli sono materiali polimerici idrofili e reticolati, il cui contenuto di acqua va dal 10 al 99% del peso/volume totale. La proprietà macroscopica maggiormente caratterizzante degli idrogeli è il cosiddetto "swelling", ossia la capacità di gonfiarsi in seguito all'assorbimento di acqua, pur mantenendo integro il network tridimensionale formato dalle macromolecole.

Tra i vari criteri vigenti per la classificazione degli idrogeli, due sono i principali:

- il meccanismo di reticolazione, che, in genere, è fisico o chimico. Per gli idrogeli fisici, la reticolazione si basa su interazioni fisiche tra le catene, che si manifestano in seguito alla variazione di un parametro fisico, quali la temperatura o il pH. Il network degli idrogeli chimici, invece, è tenuto insieme da legami covalenti. Esistono altri meccanismi di reticolazione, come quelli basati sulla chimica sopramolecolare.
- Il polimero costituente, che può essere di origine sintetica o naturale. Gli idrogeli sintetici garantiscono maggiori riproducibilità e controllo sulle proprietà del materiale. Il vantaggio degli idrogeli naturali, invece, risiede sull'elevata biocompatibilità, requisito fondamentale per molte delle applicazioni di questa classe di materiali. I polimeri più diffusi per la produzione di idrogeli naturali e sintetici sono riportati nella tabella sottostante (Tabella 1):

Natural polymers	Anionic polymers: Hyaluronic acid, alginic acid, pectin, dextran sulfate Cationic polymers: chitosan, polylysine Amphipathic polymers: collagen, gelatin, carboxymethyl chitin, fibrin Neutral polymers: dextran, agarose, pullulan
Synthetic polymers	Polyesters: PEG-PLA-PEG, PEG-PLGA-PEG, PLA-PEG-PLA, PHB, P(PF-co-EG)+acrylate end groups, P8PEG/PBO terephthalate) Other polymers: PEG-bis-(-PLA-ACRYLATE), PEG+CDs, PEG-g-P(AAm-co-Vamine), PAAm, PVAC/PVA, P(MMA-co-HEMA), PNVP, P(GEMA-sulfate), P(biscarboxy-phenoxy-phosphazene)
Combination of natural and synthetic polymers	P(PEG-co-peptides), alginate-g-(PEO-PPO-PEO), P(PLGA-co-serine), collagen-acrylate, alginate-acrylate, P(HPMA-g-peptide), HA-g-NIPAAm

TABELLA 1. IDROGELI NATURALI E SINTETICI PIÙ DIFFUSI

Gli idrogeli trovano applicazione in diversi settori.

Il campo di maggiore interesse è quello biomedico. Gli idrogeli possono fungere da *scaffolds* per cellule, impiegati per la rigenerazione dei tessuti o a scopo terapeutico, o per i farmaci, garantendo un rilascio più controllato e graduale di quest'ultimi nell'organismo.

Ulteriori applicazioni riguardano la sensoristica e l'adsorbimento per il trattamento delle acque.

INTRODUZIONE: LA CELLULOSA E IDROGELI A BASE DI CELLULOSA

Questo lavoro di tesi esamina idrogeli a base di carbossimetilcellulosa (CMC), un derivato della cellulosa, un polisaccaride che può essere estratto dalle piante o fermentato da batteri. Le molecole di glucosio, tenute insieme da legami $\beta(1\rightarrow4)$ glicosidici, si raggruppano in fibrille, che a loro volta formano domini ad alta cristallinità (minimo 40-60%) per l'estesa presenza di legami a idrogeno tra e all'interno delle fibrille.

La cellulosa presenta diverse attrattive, tra cui la biocompatibilità, il basso costo, l'elevata reperibilità, una buona rigidezza e la possibilità di essere soggetta a diverse modificazioni chimiche, grazie alla presenza di numerosi gruppi -OH sulla superficie. Quest'ultima caratteristica permette di far fronte a uno dei maggiori limiti della cellulosa, ossia la ridotta solubilità, dovuta alla componente cristallina idrofoba.

Tramite idrolisi acida della cellulosa, che comporta la rottura dei legami glicosidici e la degradazione delle zone amorfe, si ottiene il rilascio di nanocristalli di cellulosa (CNC). I CNC si presentano come nano-tubi con un'ampiezza di 5-20 nm e una lunghezza di 100-2000 nm. In quanto nanomateriali, i CNC possono vantare un'area superficiale e una reattività elevate, nonché proprietà meccaniche migliori rispetto a quelle della cellulosa.

Per quanto riguarda gli idrogeli, la cellulosa può essere usata come polimero costituente o come nano-rinforzo.

Nel primo caso, vengono impiegati gli eteri della cellulosa, che possono produrre idrogeli sia fisici che chimici. Per la formazione di nanocompositi, invece, la nanocellulosa (soprattutto CNC) viene inserita in una matrice di idrogelo per accentuarne le proprietà meccaniche.

INTRODUZIONE: STAMPA 3D PER FOTOPOLIMERIZZAZIONE

La stampa 3D, nota anche come additive manufacturing, comprende una vasta gamma di tecnologie che permettono la realizzazione di componenti tridimensionali tramite la deposizione successiva di strati. Prima della stampa, l'oggetto viene realizzato in forma di CAD, poi convertito in un file STL e suddiviso in micro-strati.

Le caratteristiche vincenti della stampa 3D, che l'hanno resa una valida alternativa alla tradizionale "subtractive manufacturing", sono l'elevata precisione, il design rapido, la riduzione degli scarti, i limiti ridotti in termini di scelta del materiale e la possibilità di fabbricare componenti complessi.

Le tecnologie di stampa 3D sono: material jetting (a getto di materiale), binder jetting, estrusione, laminazione a fogli, stampa a deposizione diretta di energia, stampa per fusione di letto di polveri, stampa per fotopolimerizzazione, biostampa.

La tipologia utilizzata in questo lavoro è la stampa 3D per fotopolimerizzazione.

La fotopolimerizzazione è un processo fotochimico che consiste nella polimerizzazione di un monomero sotto l'influenza di una radiazione luminosa, solitamente ultravioletta. La formulazione iniziale contiene:

- Un foto-iniziatore, ossia un composto in grado di assorbire la radiazione impiegata;
- Un diluente reattivo;
- Il monomero/oligomero da cui si formerà il polimero;
- Eventuali additivi.

In base al fotoiniziatore, la fotopolimerizzazione può essere radicalica o ionica. Quella radicalica è la più diffusa, in virtù della maggiore velocità di reazione.

Nella fotopolimerizzazione radicalica, quando il fotoiniziatore assorbe la radiazione dà vita a dei radicali.

Esistono due tipologie di fotoiniziatori radicalici: di tipo Norrish I e di tipo Norrish II.

I fotoiniziatori Norrish I formano radicali per rottura omolitica del legame, mentre quelli di Norrish II per estrazione di idrogeno da un co-iniziatore.

Il radicale formatosi reagisce con il monomero, formando un macroradicale che si accresce per addizione successiva di monomeri. Questa fase di accrescimento, che non è altro che

la propagazione della polimerizzazione, termina per accoppiamento o disproportionamento.

La velocità di reazione, il basso impatto ambientale e l'elevata versatilità del processo rientrano tra i principali vantaggi della fotopolimerizzazione. Esistono, tuttavia, alcune problematiche, tra cui la scelta del fotoiniziatore, la necessità di post-trattamenti, il ritiro volumetrico del componente, l'inibizione da ossigeno e la ridotta penetrazione della radiazione, che limita l'impiego della fotopolimerizzazione a strutture bidimensionali poco spesse, come film e rivestimenti. Questo problema viene superato, nella stampa 3D, grazie alla suddivisione del componente in strati micrometrici.

In particolare, la stampa 3D per fotopolimerizzazione include due tecnologie principali: la stereolitografia (SLA) e il digital light processing (DLP). Quest'ultima è la tecnologia impiegata in questa tesi.

Nella stampa tramite DLP, la formulazione viene depositata su una base trasparente alla radiazione usata, e irradiata dal basso attraverso un proiettore digitale che permette di polimerizzare un intero strato alla volta. Una volta che uno strato è stato irradiato, la piattaforma di si solleva, cosicché il componente viene costruito dal basso verso l'alto.

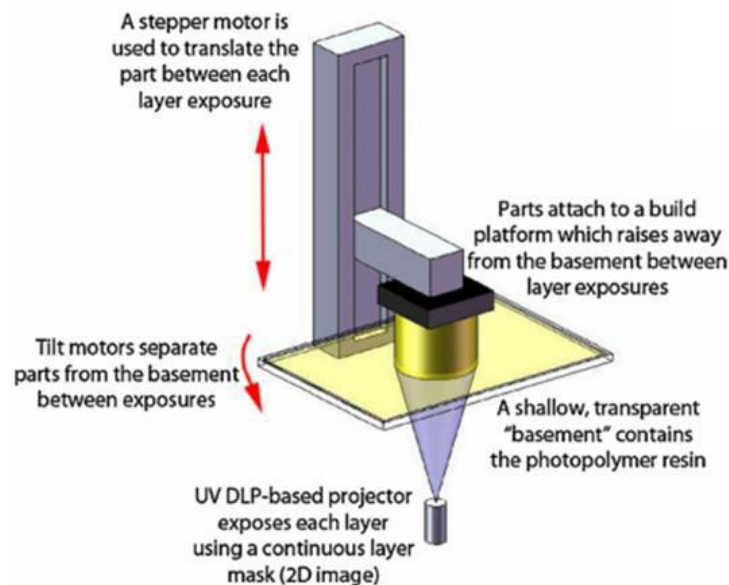


FIGURA 1. TECNOLOGIA DI STAMPA 3D DLP

Al contrario, la SLA realizza gli oggetti tramite un processo top-down e l'impiego di un laser, che irradia la formulazione punto per punto.

Ne consegue che una stampante DLP è più rapida ma caratterizzata da una risoluzione meno fine (35-100 μm contro i 25-85 μm della SLA).

In ogni caso, SLA e DLP possono essere annoverate tra le tecnologie di additive manufacturing che garantiscono la migliore risoluzione.

INTRODUZIONE: STAMPA 3D DI IDROGELI NATURALI METACRILATI

La letteratura scientifica offre diversi studi che esaltano le potenzialità della stampa 3D per fotopolimerizzazione di idrogeli polimerici. Queste tecnologie, difatti, garantiscono l'alta risoluzione necessaria per la realizzazione di strutture complesse e facilmente personalizzabili, proprietà rilevanti non solo per le applicazioni cellulari, ma anche per quelle farmaceutiche e di trattamento delle acque. Sussistono, tuttavia, diversi limiti, tra cui: la limitatezza di monomeri fotopolimerizzabili che siano anche idonei alle applicazioni degli idrogeli; la risoluzione finale, che dipende da diversi fattori (diffusione della luce, profondità di penetrazione della stessa, trasparenza/opacità del materiale); le ridotte proprietà meccaniche di alcuni idrogeli, che ostacolano la realizzazione di componenti che si sviluppano in verticalità.

I monomeri o i pre-polimeri, per essere fotopolimerizzati, devono possedere delle funzionalità fotoattive che, nel caso dei polimeri naturali, vengono inserite aggiungendo o modificando le funzionalità pendenti delle catene.

La metacrilazione è uno dei meccanismi di funzionalizzazione più ricorrente. Molti polimeri a base naturale (gelatina, chitosano, acido ialuronico, fibroine di seta, alginato) sono stati metacrilati per renderli idonei alla stampa 3D per fotopolimerizzazione.

MATERIALI

La carbossimetilcellulosa (CMC) è un etere della cellulosa, che deriva dalla parziale sostituzione di gruppi idrossile con gruppi carbossimetilici idrofili. La CMC e l'anidride metacrilica (MA) sono stati acquistati da Sigma Aldrich.

Come fotoiniziatore è stato usato l'acido bismesitolo fosfonico BAPO-OH, che, all'interno di una foto-formulazione, è in grado di avviare una reazione di fotopolimerizzazione Norrish I quando esposto alla radiazione. Il BAPO-OH è stato gentilmente fornito dal gruppo del Prof. Gruetzmacher (ETH Zurich).

I cristalli di nanocellulosa provengono dai gusci vuoti dei frutti delle palme da olio, e sono stati forniti dalla ricercatrice A.A. Septevani (Indonesian Institute of Sciences).

METODI

La preparazione di un materiale fotoreattivo ha previsto la metacrilazione della carbossimetilcellulosa (CMC), per ottenere la sintesi di carbossimetilcellulosa metacrilata (M-CMC). La funzionalizzazione è stata condotta utilizzando anidride metacrilica (MA) come agente di metacrilazione. In primo luogo, 6,00 g di CMC sono stati sciolti in 300 mL di acqua, mantenendo la soluzione in agitazione magnetica. Il pH è stato portato a 11,0 con idrossido di sodio (NaOH) 0,5M. La soluzione è stata lasciata in agitazione durante la

notte. Dopo aver raffreddato la soluzione a 2 °C, sono stati aggiunti 12 mL di anidride metacrilica. La reazione è stata protratta per 24 ore a 0 °C; il pH è stato periodicamente mantenuto a 8 con la soluzione NaOH. La soluzione è stata poi precipitata e lavata con 1 L di etanolo. Dopo 3 giorni di dialisi in acqua, il prodotto metacrilato (M-CMC) è stato congelato ed essiccato.

Sono state preparate due tipologie di formulazioni:

-formulazioni “neat” a base di acqua, M-CMC e BAPO-OH

-formulazioni “composite” a base di acqua, M-CMC, BAPO-OH e CNC.

La composizione delle formulazioni è riportata nella Tabella 2:

M-CMC [mg]	CNC [mg]	BAPO OH [phr*]
20	--	2
30	--	2
40	--	2
20	10	2
20	20	2

**TABELLA 2. COMPOSIZIONE DELLE DIVERSE FORMULAZIONI TESTATE, RIFERITE A 1 ML DI H₂O.
*PHR RISPETTO ALLA CONCENTRAZIONE DI M-CMC**

La componente polimerica (M-CMC per le formulazioni neat, M-CMC e CNC per le formulazioni composite) è stata dissolta in acqua distillata a 40°C, sotto agitazione magnetica. Una volta completata la solubilizzazione, è stato aggiunto il BAPO-OH.

Le formulazioni sono state studiate tramite un reometro rotazionale piatto-piatto dotato di lampada UV.

Gli studi di flusso hanno permesso di analizzare la viscosità delle formulazioni, in funzione della velocità di deformazione.

Le proprietà viscoelastiche del materiale sono state studiate, invece, con studi in oscillazione, ossia mediante l'applicazione di uno stress/deformazione sinusoidale. In particolar modo, le prove fotoreologiche, condotte ad ampiezza di deformazione e a frequenza costanti (1% e 1Hz), hanno consentito di esaminare la reattività delle formulazioni, in funzione del tempo e in termini di velocità di reazione, nonché di ottenere un'indicazione circa la rigidità del materiale tramite il valore di modulo conservativo finale.

Un materiale viscoelastico è, difatti, caratterizzato da due moduli: il modulo conservativo G' , e il modulo dissipativo G'' , che descrivono, rispettivamente, la componente elastica e viscosa del materiale. Quando la lampada è spenta, la formulazione è allo stato liquido e $G'' > G'$; quando inizia l'irradiamento, si innesca la fotoreticolazione, che comporta la crescita di G' per il procedere della formazione del network polimerico. La reattività della formulazione è data dall'istante di tempo in cui G' comincia a crescere a causa della formazione di legami covalenti tra le catene. Man mano che la reticolazione procede, G' eguaglia e successivamente supera G'' quando il materiale assume una natura solid-like. Il

network è completo quando G' raggiunge il valore di plateau, indice della rigidità del materiale.

Per le prove di stampa è stata impiegata la stampante DLP Asiga Max.
I campioni sono stati stampati dalle formulazioni riportate nella Tabella 3:

M-CMC [mg]	CNC [mg]	BAPO OH [phr*]
20	--	2
20	10	2

TABELLA 3. FORMULAZIONI PER LA STAMPA

I parametri di stampa, che sono stati ottimizzati tramite diverse prove, includono:

- l'intensità della radiazione
- lo spessore degli strati
- il tempo di esposizione di ciascun strato alla radiazione, che influenza l'adesione tra gli strati e la definizione del componente
- burn-in layers ossia il numero di strati che vengono irradiati immediatamente dopo il primo, e i cui parametri di processing possono essere specificatamente impostati
- burn-in exposure time : il tempo di esposizione dei burn-in layers. Di solito è più lungo del tempo di esposizione, per assicurare l'adesione alla piattaforma.

I componenti fabbricati sono stati ulteriormente irradiati tramite una sorgente UV per 90 secondi.

Sono stati fabbricati dei cilindri da sottoporre a test meccanici di compressione, al fine di caratterizzare meccanicamente il materiale (Figura 2).

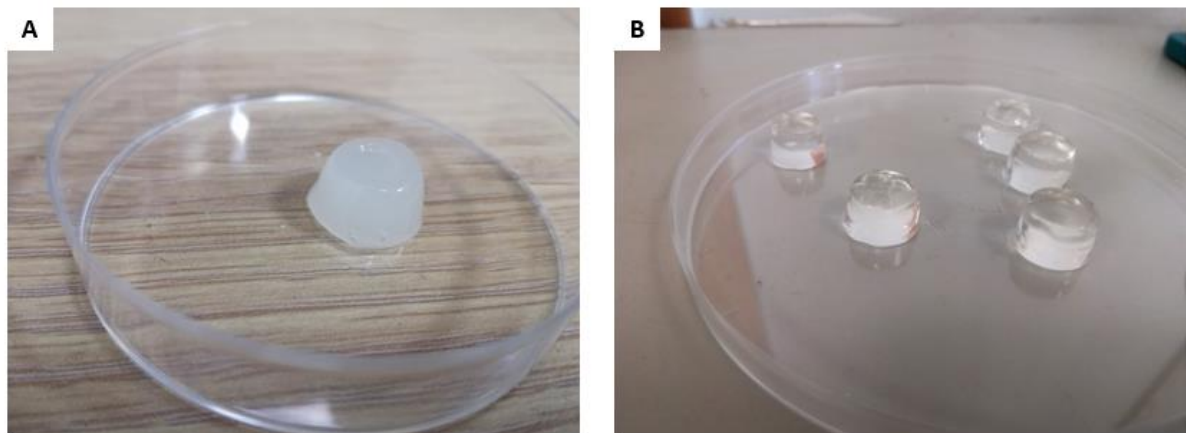


FIGURA 2. CILINDRI STAMPATI PER LE PROVE DI COMPRESSIONE. (A) CAMPIONI CNC/M-CMC (B) CAMPIONI M-CMC

L'apparecchiatura usata è mostrata nella Figura 3.

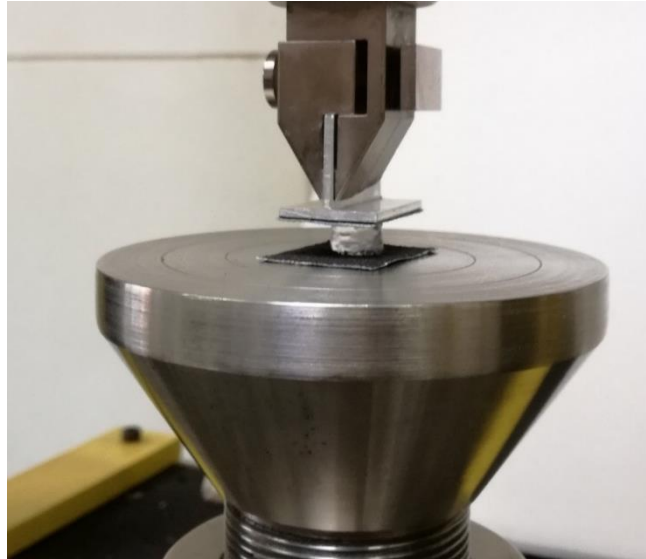


FIGURA 3. TEST DI COMPRESSIONE

Sui campioni stampati, sono state eseguite due tipologie di prove di compressione:

- Test di compressione statica, per determinare lo sforzo e la deformazione a rottura, e il modulo elastico di compressione;
- Test di compressione a fatica, per studiare il comportamento del materiale a fatica.

RISULTATI

La metacrilazione è stata confermata da una spettroscopia di proton risonanza magnetica nucleare (H-NMR), riportata nella Figura 4. Lo spettro della M-CMC presenta dei picchi aggiuntivi corrispondenti ai gruppi vinilici e metilici, che attestano la modificazione del materiale e permettono di calcolare il grado di sostituzione attraverso il rapporto tra l'area integrata dei picchi associati ai gruppi metacrilati della M-CMC e l'area integrata dei picchi correlati alle unità di glucosio anidro dello scheletro della CMC. Il grado di metacrilazione, risultato pari a 0,6, è un fattore importante per diverse caratteristiche di un idrogel. In generale, un suo valore elevato si traduce in una maggiore densità di reticolazione, che comporta migliori proprietà meccaniche e maggiore stabilità del materiale nel tempo. Al contrario, un basso livello di metacrilazione genera una maggiore taglia dei pori, e quindi accentua l'assorbimento di acqua e la capacità di swelling.

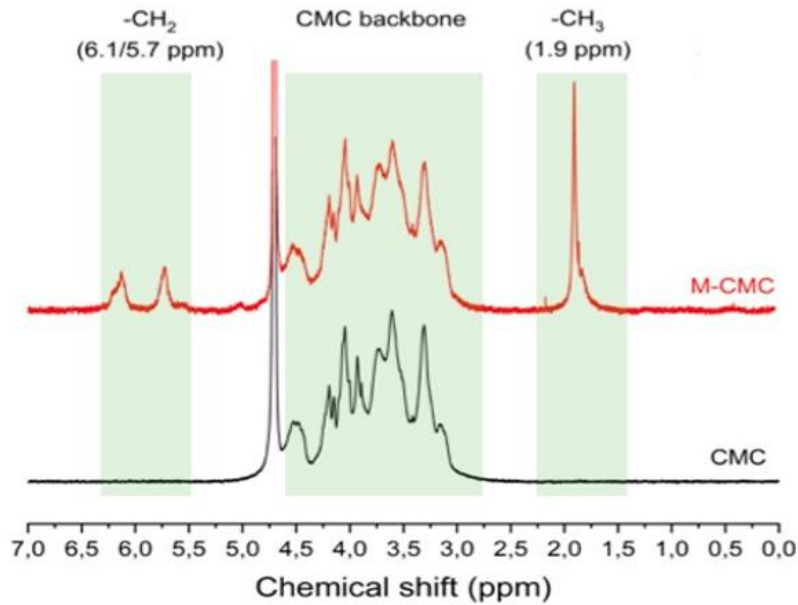


FIGURA 4. SPETTRO 1H NMR DELLA CARBOSSIMETILCELLULOSA (IN ROSSO) E DELLA CARBOSSIMETILCELLULOSA METACRILATA (IN NERO)

Per quanto concerne la reologia, le tre formulazioni di sola M-CMC presentano pressoché la medesima velocità di reazione (data dal tempo in cui il modulo G' inizia a salire, dopo l'esposizione alla radiazione), che è di pochi secondi (Figura 5). La viscosità aumenta al crescere della concentrazione di M-CMC (Figura 6) e così il valore di plateau di G' , che segue l'andamento riportato nella Figura 7.

Neat hydrogels time sweep test

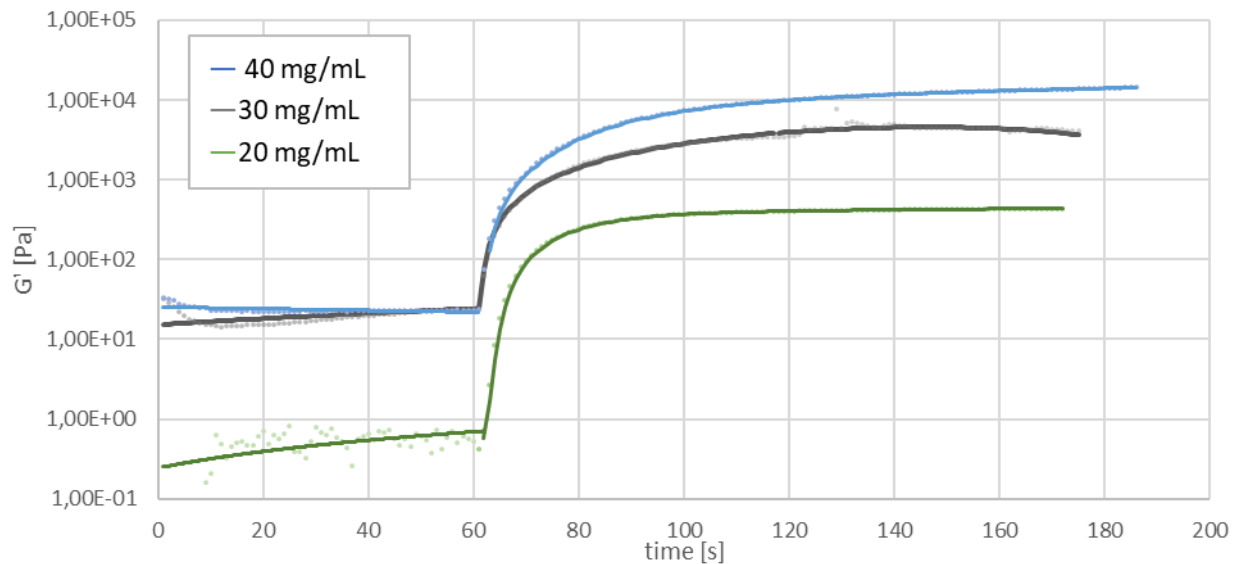


FIGURA 5. TEST DI FOTOREOLOGIA DELLE FORMULAZIONI DI SOLA M-CMC

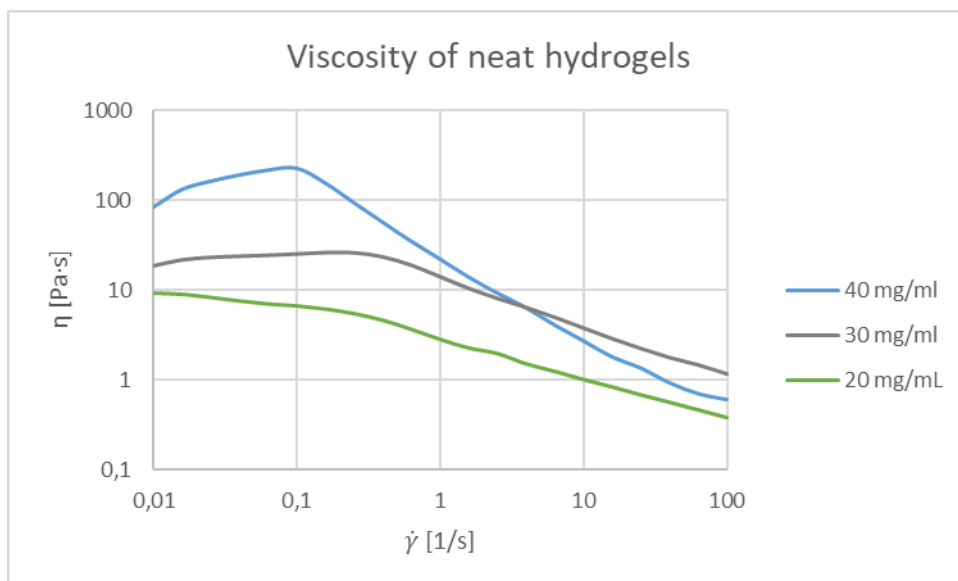


FIGURA 6. VISCOSITÀ DELLE FORMULAZIONI DI SOLA M-CMC

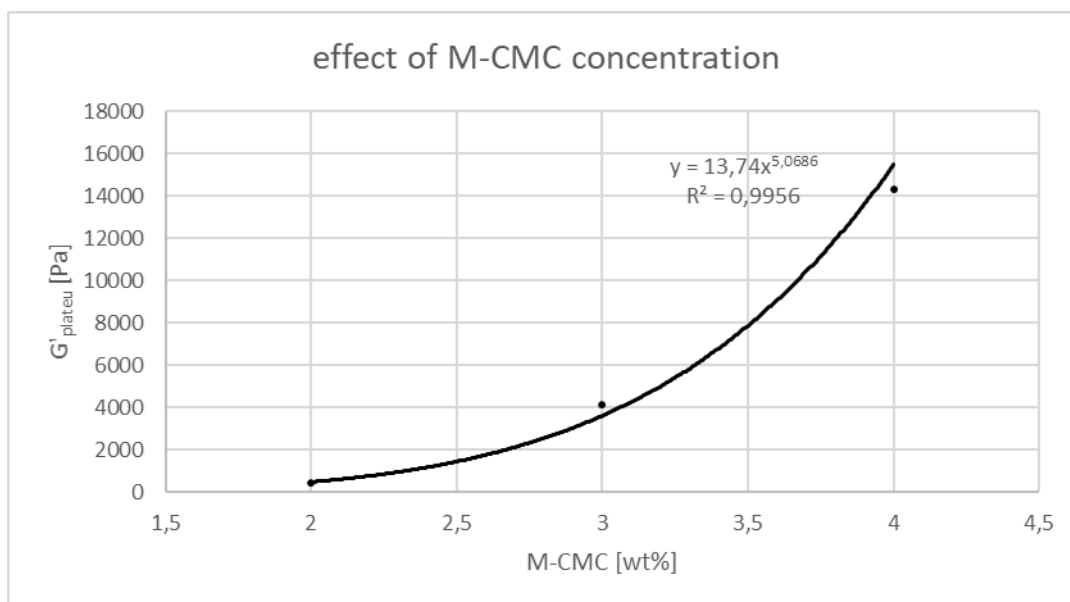


FIGURA 7. ANDAMENTO DEL VALORE FINALE DI G' AL CRESCERE DELLA CONCENTRAZIONE DI M-CMC

Di conseguenza, le necessità di individuare un compromesso tra la bassa viscosità e un valore finale di G' sufficientemente alto, ha determinato la scelta della formulazione di 20 mg/mL per i passaggi successivi.

Dopo l'aggiunta dei nanocristalli, le formulazioni sono state nuovamente testate per esaminare la viscosità (Figura 8) e la reattività (Figura 9).

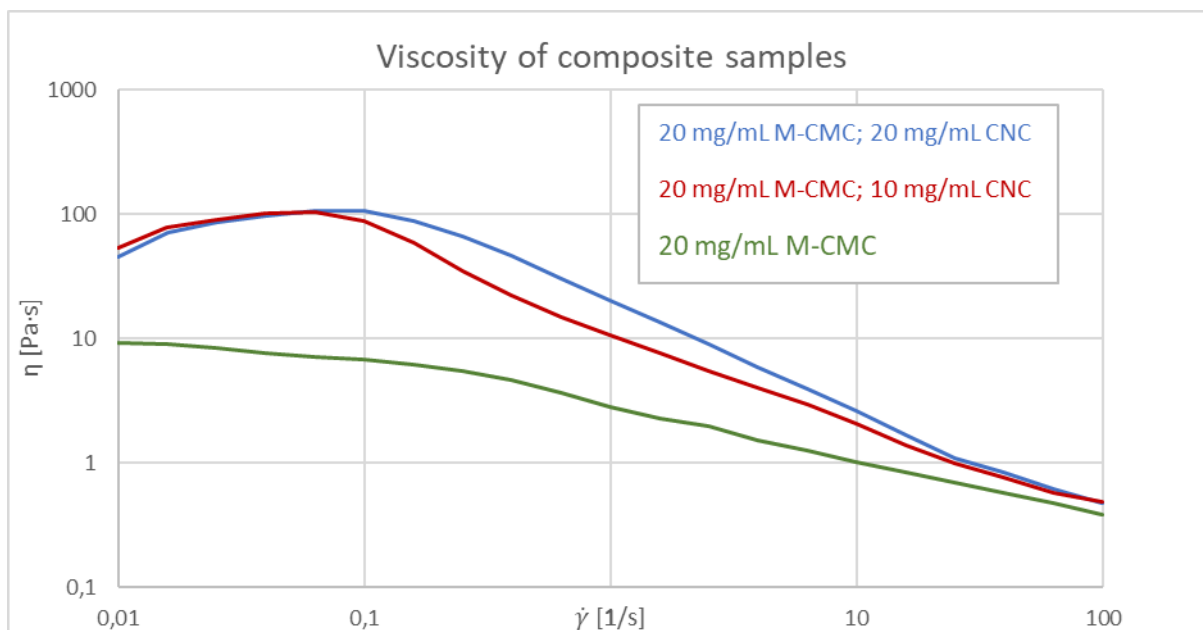


FIGURA 8. VISCOSITÀ DELLE FORMULAZIONI CON CNC E DELLA FORMULAZIONE 20 MG/ML DI M-CMC, 2 PHR BAPO-OH

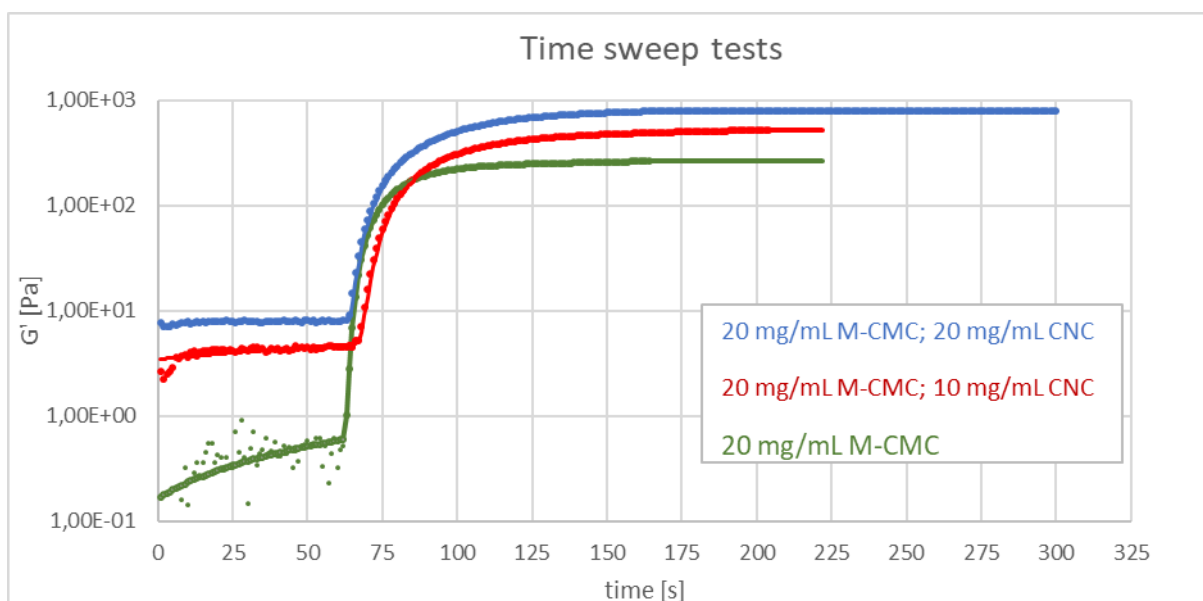


FIGURA 9. TEST DI FOTOREOLOGIA DELLE FORMULAZIONI CON CNC E DELLA FORMULAZIONE 20 MG/ML DI M-CMC, 2 PHR BAPO-OH

In presenza dei nanocristalli, il processo di fotopolimerizzazione è lievemente più lento: ciò può essere imputato all'effetto di schermatura dei CNC verso la radiazione, oppure alla maggiore viscosità della formulazione, che limita la mobilità delle catene. Ciò nonostante, si osserva una crescita del modulo finale G' al crescere della quantità di nanocristalli.

Per la stampa, si è dunque selezionata la formulazione di 20 mg/mL di M-CMC, 10 mg/mL di CNC e 2 phr di BAPO-OH (rispetto alla concentrazione di M-CMC).

Le prove di stampa hanno permesso di selezionare i parametri ottimali:

- l'intensità della radiazione (20-30 mW)
- lo spessore degli strati (50 μm)

- il tempo di esposizione (7-10 s).
- burn-in layers (6).
- burn-in exposure time (10-15 s)

Sono stati stampati diversi componenti, anche complessi (Figura 10); per alcune strutture si è adoperato un colorante, per ridurre la diffusione della radiazione in zone indesiderate e, dunque, per migliorare la risoluzione.

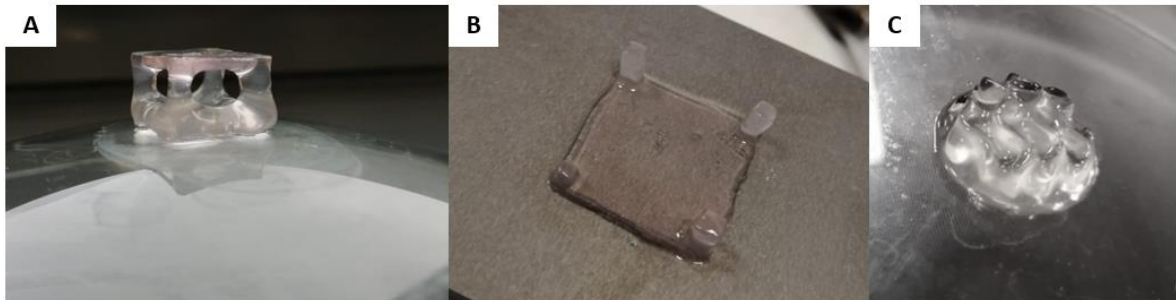


FIGURA 10. STAMPE COMPLESSE, EFFETTUATE CON L'AUSILIO DI UN COLORANTE NEL CASO A E B

I test di compressione statica hanno permesso di ricavare le curve sforzo-deformazione dei campioni (Figura 11):

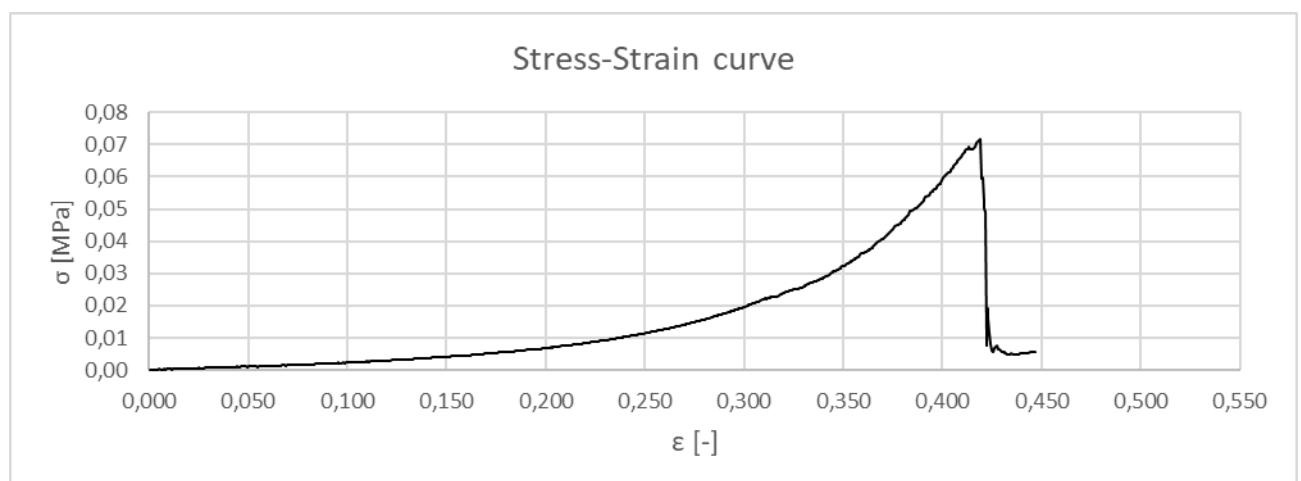


FIGURA 11. CURVA SFORZO-DEFORMAZIONE

Gli idrogeli compositi hanno manifestato una resistenza a rottura più alta, con uno sforzo di rottura σ_{\max} di circa 70 kPa, corrispondente a un incremento del 20% rispetto alla σ_{\max} dei campioni non rinforzati.

Per entrambi i tipi di idrogelo, il modulo elastico aumenta al crescere della deformazione, a causa della risposta non lineare che il materiale manifesta quando soggetto a uno sforzo di compressione. I valori si attestano, comunque, sui 30-65 kPa. Gli idrogeli rinforzati sono più rigidi di quelli privi di CNC; tale differenza si accentua per deformazioni più alte, fino ad un modulo del 20% superiore per gli idrogeli compositi.

Il miglioramento delle proprietà meccaniche può essere correlato a un efficiente trasferimento del carico tra filler e matrice. I nanocristalli di cellulosa assorbono lo stress

esterno a causa della loro maggiore rigidità e lo dissipano attraverso interazioni filler-filler e filler-matrice.

Le prove a fatica hanno rivelato la formazione di un ciclo di isteresi per entrambi i materiali (Figura 12).

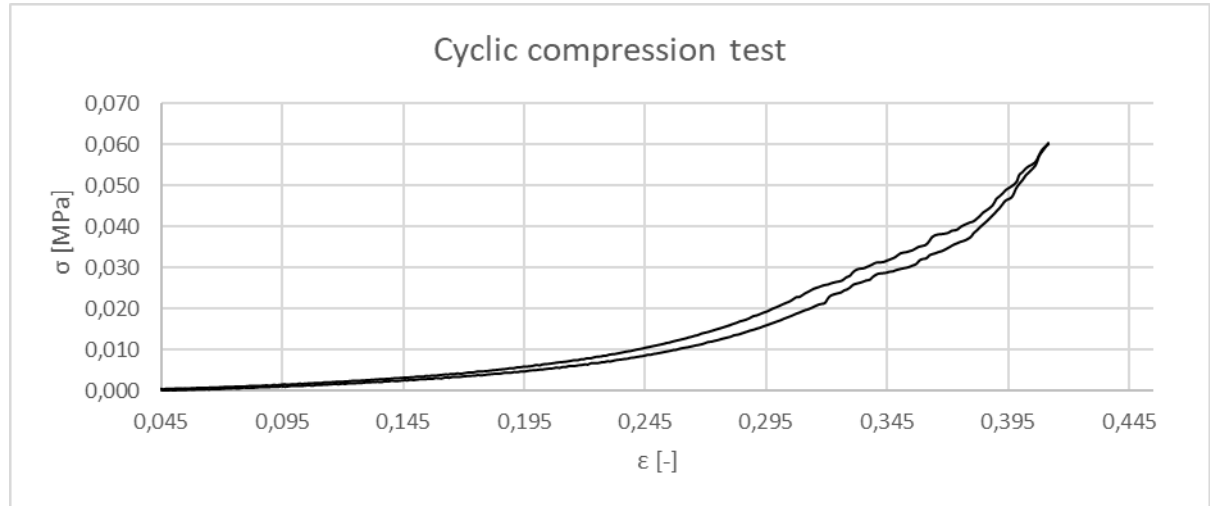


FIGURA 12. UN TIPICO CICLO DI ISTERESI OTTENUTO CON LE PROVE DI COMPRESSIONE CICLICHE

Il numero di test effettuati non è sufficiente per trarre considerazioni conclusive sul comportamento a fatica del materiale; è stato tuttavia possibile effettuare delle osservazioni circa la diversa risposta degli idrogeli con e senza nanocristalli.

L'energia dissipata in un ciclo, quantificabile come l'aria circoscritta dal ciclo di isteresi, aumenta, ciclo dopo ciclo, in modo più accentuato negli idrogeli non rinforzati, nei quali si osserva una significativa riduzione del modulo elastico al progredire dei cicli di carico. In presenza dei CNC, invece, sia l'energia dissipata che il modulo elastico sono soggetti variazioni più graduali. L'andamento delle due grandezze è riportato nella Figura 13.

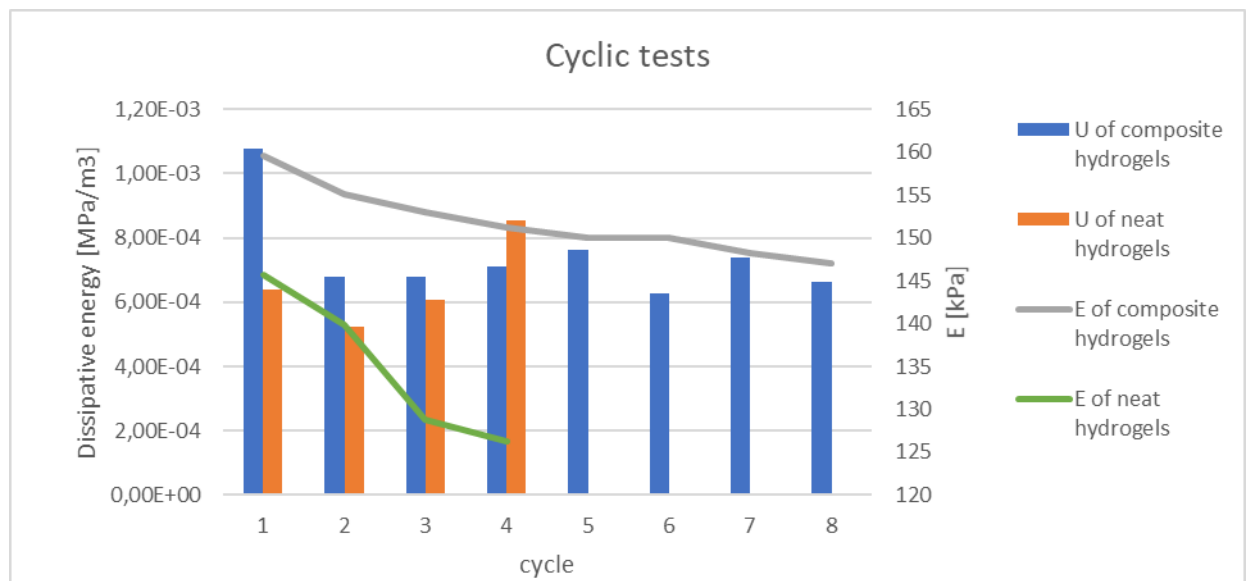


FIGURA 13. VARIAZIONE DELL'ENERGIA DISSIPATA (U) E DEL MODULO ELASTICO (E) CICLO DOPO CICLO, PER I CAMPIONI M-CMC E PER I CAMPIONI CNC/M-CMC

Il lavoro sperimentale di tesi ha, dunque, dimostrato la possibilità di stampare idrogeli a base di carbossimetilcellulosa contenenti nanocristalli di cellulosa, i quali agiscono da rinforzanti meccanici senza però inficiare la reattività e la stampabilità del materiale.

1. ABSTRACT

Hydrogels are polymeric materials that are able to hold large amount of water. They possess attractive and tunable properties -such as swelling properties, biocompatibility, sensitivity to specific stimuli- that make them powerful candidates for a wide variety of applications.

Three-dimensional (3D) printing represents a promising fabrication technique to construct hydrogels into various, even complex, structures. 3D printing has found widespread use in many fields, on account of the freedom of design, rapid prototyping, waste minimisation and the possibility to create complex components. It encompasses several technologies that differ in material selection, fabrication's speed, printing accuracy, price and so on.

This work focused on the 3D-printing of cellulose-based hydrogels through Digital Light Processing (DLP) technology, that relies on photopolymerization. In particular, the aim was printing methacrylated carboxymethylcellulose (M-CMC) hydrogels filled with cellulose nanocrystals (CNCs), so as to investigate the nano-fillers' effect on the mechanical properties of the 3D-printed material.

Firstly, methacrylation of carboxymethylcellulose (CMC) introduced photoactive functionalities in the material and it was confirmed through a H-NMR spectroscopy analysis.

A rheometer equipped with a UV-lamp was used to analyse the viscosity and the reactivity to UV-radiation of two type of aqueous formulations: one containing photoinitiator and M-CMC, one with photoinitiator, M-CMC and CNC.

Both M-CMC and CNC/M-CMC formulations were successfully 3D-printed through DLP. Printed components were subjected to compression tests, that revealed the higher strength and rigidity of the composite samples.

2. HYDROGELS

A hydrogel is a cross-linked hydrophilic polymer that is able to absorb a significant amount of water, while maintaining a three-dimensional network, due to the chemical or physical bonds between polymeric chains. (1) (2)

As a definition, hydrogels are materials whose water's content is at least 10% of the total weight (or volume). (2)

Most of hydrogels are based on biopolymers or polyelectrolites. The most commonly used monomers for the preparation of hydrogels are mono- and multifunctional (meth)acrylates and their derivatives, and natural monomers such as chitosan, alginate, collagen, hyaluronic acid. (3)

In addition, the swelling and the mechanical properties can be modified by adding comonomers. For instance, diethylene glycol dimethacrylate (DEGDMA) is usually utilized with HEMA for preparing poly (HEMA) hydrogel, while triethylene glycol dimethacrylate (TEGDMA) is used with methyl methacrylate (MAA) for making poly(MAA-g- EG) hydrogel. (4) (5)

Hydrophilicity is due to $-NH_2$, $-COOH$, $-OH$, $-CONH_2$, $-CONH$, and $-SO_3H$ groups. Cross-linking is obtainable by different methods, as reported below.

2.1 CLASSIFICATION

Literature provides various hydrogels' classifications.

Firstly, hydrogels can be natural or synthetic, relating to the constituting polymers.

On one hand, natural hydrogels are widely employed in tissue engineering, because the forming polymers either are components of the extra-cellular matrix (ECM) or possess properties that are similar to ECM's ones. Most remarkable natural hydrogels are collagen, gelatine, chitosan, hyaluronic acid, fibrine. For instance, collagen is matter of interest in biomedical field because it is the main component of ECM and the most diffused protein in mammals' tissues. (6)

On the other hand, key aspects of synthetic hydrogels are higher control and reproducibility. In fact, these materials are characterised by a finer control on the architecture and on the chemical composition. For example, products with specific block-structures, molecular weight and with degradable links can be obtained. (6)

Despite of these advantages, synthetic hydrogels suffer of low biological activity, that is necessary for many hydrogels' applications. Therefore, the incorporation of bioactive elements into hydrogel has been developed in order to increase the cellular bioactivity. (6)

Currently, the most thoroughly explored synthetic hydrogels are the polyethylene glycol (PEG)-based ones. In addition, hydrogels made of polyvinyl alcohol (PVA), poly(propylene fumarate (PPF) and polypeptides have been widely studied. (6)

Most common synthetic and natural hydrogels are listed in Table 1.

Natural polymers	Anionic polymers: Hyaluronic acid, alginic acid, pectin, dextran sulfate Cationic polymers: chitosan, polylysine Amphipathic polymers: collagen, gelatin, carboxymethyl chitin, fibrin Neutral polymers: dextran, agarose, pullulan
Synthetic polymers	Polyesters: PEG-PLA-PEG, PEG-PLGA-PEG, PLA-PEG-PLA, PHB, P(PF-co-EG)+acrylate end groups, P8PEG/PBO terephthalate Other polymers: PEG-bis-(-PLA-ACRYLATE), PEG+CDs, PEG-g-P(AAm-co-Vamine), PAAm, PVAC/PVA, P(MMA-co-HEMA), PNVP, P(GEMA-sulfate), P(biscarboxy-phenoxy-phosphazene)
Combination of natural and synthetic polymers	P(PEG-co-peptides), alginate-g-(PEO-PPO-PEO), P(PLGA-co-serine), collagen-acrylate, alginate-acrylate, P(HPMA-g-peptide), HA-g-NIPAAm

TABLE 1. NATURAL AND SYNTHETIC POLYMERS USED FOR SYNTHESIZING HYDROGELS (7)

Secondly, the cross-linking method can define the hydrogel's type. (7)

In physical hydrogels, cross-linking occurs through physical associations between chains and follows the variations of a physical parameter (e.g. temperature, pH, ionic concentration). The network is based on molecular entanglements, and/or secondary forces including ionic, H-bonding or hydrophobic forces. (8)

Physical methods, such as the thermal one, are relatively easy. Nevertheless, linking's mechanisms of most of natural hydrogels (like the collagen) are difficultly controlled by physical-curing methods. On the contrary, chemical hydrogels can boast wider flexibility in the network design, by controlling cross-linking density and structure's properties.

Chemical hydrogels form through covalent bonds between the polymeric chains. As an example, photo-curing represents a process to obtain a chemical hydrogel.

Other methods are Michael-type addition reaction, Click reaction, Schiff base reaction, enzyme mediation. Hydrogels can be obtained by supramolecular interactions, too. (1)

The main limit of chemical hydrogel is the absence of an energy dissipation method, that makes them fragile. Research focuses on the realisation of tough hydrogels, as the nanocomposite (NC) hydrogels and the supramolecular ones.

Relating to NC-hydrogels, Hoffman (9) developed a hydrogel containing cellulose nanocrystals and observed a 7-fold increase in the storage modulus, with a low CNCs loading level of 1.43 wt%, and higher mechanical strength. Feng et al. (9) utilised methacrylated nano-graphene oxide carbon dots to improve the mechanical performance of methacrylated chitosan hydrogel.

Finally, supramolecular curing allows to obtain hydrogels that show simultaneously injectability, self-healing and stimuli-responsive properties. (10) (11)

Both physical and chemical hydrogels are not homogenous. In fact, they contain clusters.

For physical hydrogels, clusters are gatherings of molecular entanglements.

As for chemical hydrogels, the term is referred to regions of low water swelling and high crosslinks' density, dispersed within regions of high swelling and low crosslink density. (8)

Finally, according to many synthesis methods, hydrogels can be categorised as homopolymers, copolymers, semi-interpenetrating network (semi-IPN) hydrogels and interpenetrating network (IPN) ones. (2)

Homopolymeric hydrogels (e.g. PEG, HEMA) are formed by a single monomer, while copolymeric ones are constituted by two monomers, of which at least one is hydrophilic. PEG/ poly(ϵ -caprolactone) (PCL) (12) and PVP-based (13) hydrogels belong to this category.

When a linear polymer inserts between chains of a cross-linked polymer and no covalent bonds between the two species are observed, a semi-IPN hydrogel forms.

An IPN hydrogel is composed of two polymers. One of them is already in solution, whereas the other one is *in-situ* synthesised (or cross-linked). (2) For instance, a genipin-cross-linked chitosan/gelatin IPN hydrogel was successfully obtained by Cui et al. (14)

2.2 PROPERTIES

Swelling is one of the most distinctive properties of hydrogels. When a dry hydrogel is immersed in water, bonds between the material and water molecules are formed. Then, the hydrogel is able to absorb from 10–20% up to thousands of times its dry weight. The absorption of water causes the swelling of the hydrogel's network.

Initially, water molecules enter the network and interact with the most polar and hydrophilic groups, forming the so-called "primary bound water". The following swelling of the hydrogel leads to the exposition of the hydrophobic groups, which create the "secondary bound water". The latter are bonds based on hydrophobic interactions between the water molecules and the hydrophobic groups.

Finally, the hydrogel tends to absorb more water (free water) but swelling is counterbalanced by the cross-links. Therefore, the equilibrium swelling level is reached. (8)

Swelling depends on several factors.

One of them is the chemical structure: the presence of hydrophilic groups enhances the swelling degree.

Furthermore, cross-links, that can be obtained by the abovementioned methods, affect the swelling. The crucial parameter is the degree of cross-linking (CrD), defined as:

$$CrD = \frac{n_{cross-linkers}}{n_m}$$

Where $n_{cross-linkers}$ are the moles of the cross-linker agents and n_m are the moles of the repeating monomers. (5)

A high-CrD hydrogel shows a lower swelling, due to the tighter structure. On the contrary, hydrogels that are characterised by a lower CrD have more mobile polymeric chains. Then, their swelling ratio is higher.

Moreover, the chemical (or physical) cross-links prevent hydrogels from dissolving in aqueous media, by keeping intact the material's network.

“Sensitivity” is a further, attractive feature of hydrogels. In fact, the so-called sensitive-hydrogels can respond to changes in surrounding environment. Variations in temperature, in pH or in ionic concentration, or the presence of an electric or magnetic field can modify the swelling ratio, as well as the network structure, the permeability and the mechanical strength of these materials. (5)

Finally, mechanical strength of hydrogels is a function of the synthesis method, the cross-linking degree and the base polymers.

2.3 APPLICATIONS

Applications of hydrogels extend to various fields.

Their primary use is biomedical area (regenerative medicine and drug delivery). Obviously, hydrogels used in this field need to be biocompatible. A material is biocompatible if it can perform its function while stimulating appropriate and undamaging answer of the living host-system. An excellently biocompatible hydrogel causes minimal inflammatory responses, thrombosis, and tissue damage. (15)

However, hydrogels demonstrated successful applications in other fields, because of their multiple properties, such as porosity, sensitivity, swelling ability. Some examples will be discussed below.

2.3.1 REGENERATIVE MEDICINE

Regenerative medicine relies on the cellular cultures, that can be utilised in both cellular therapy and tissue-regeneration.

The first one consists in releasing therapeutic cells across “target tissue”, to treat specific pathologies. Cells’ source can be the patient itself -then, the therapy is regarded as autologous- or a donor, in the case of allogenic approach. Typical examples of cell-based therapies include hemoglobin injection and platelet and bone marrow implantation. The number of cells injected usually ranges from several million to hundreds of millions of cells. The release of cells through an appropriate carrier can extend the duration of the therapeutic effects. This advantage is particularly beneficial in the case of chronic diseases (e.g. diabetes). (1)

On the contrary, tissue-regeneration, that is also called tissue engineering, uses cells, signal molecules and scaffold to repair and regenerate damaged human body’s tissues. This science implies a deep understanding of biomaterials, cells’ and tissues’ biology, physio-chemical processes and bioengineering design. (1) Up to now, regeneration of skin and cartilage is clinically available (1). Furthermore, significant developments have been achieved in regeneration of bladder (16) (17), liver (18) (19) (20), cardiac tissue (21) (22) (23) and bones (20) (24) (22).

In regenerative medicine, cells need to be encapsulated in biomimetic scaffolds, which emulate the 3D nano-environment of ECM in the body. As an artificial ECM, a scaffold must have adequate mechanical properties and a porous structure. The latest allows the diffusion of nutrients and waste products. Moreover, the scaffold’s degradability must be compatible with the rate cells’ growth, so that it can provide spatial and temporal control on encapsulated cells. Finally, it must be produced by easy methods that minimise cell’s damage and cytotoxic products.

The main challenges of using hydrogels in the field of regenerative engineering are the creation of a biocompatible and biodegradable ECM having a connected porosity for active nutrient transport, and the control of the cells with adequate growth factors. (1)

In the past decade, many synthetic and natural materials have been used to make hydrogels used in this field. Natural polymers have been widely employed for their excellent biocompatibility. Similarly, there is a wide variety of synthetic polymers whose chemical and physical properties suit regenerative engineering. However, synthetic polymers may lack the structure to stimulate a positive biological response from cells. As a result, the use of synthetic polymers requires modification of them. (6)

A hydrogel can be utilised as a cell carrier when it possesses proper degradation rate and mechanical properties. In general, these properties can be refined through variations in the chemical structure and lattice density. For a certain hydrogel, the activity of inseminated cells can be regulated by functionalizing the polymer matrix with specific bioactive groups (macromolecules and proteins). (6)

The properties of a hydrogel affect their ability to promote adhesion and cell extension. For instance, the extent of neural ganglia, the growth of fibroblasts and the differentiation in stem cells depend on the rigidity of the hydrogel. Moreover, hydrogels with a positive charge interact with cells that have negative net surface charge, allowing for a sharper adhesion. In addition, the elastic module of the hydrogel must be similar to that of the original tissue. (25)

Since injection is the most common technique to implant hydrogels in the body, another key aspect is the injectability. This property reduces the need of invasive treatments and allows the homogenous distribution of the cells. Cells' growth and proliferation have been proved to be promoted by highly hydrated hydrogels, that mimic more accurately the ECM.

In tissue engineering, for example, hydrogel's precursors are loaded with growth factors and/or cells. Then, they are injected in the wound's site. Once in the body, the precursors undergo to the sol-gel transition, triggered by chemical or physical stimulus. So, the hydrogel assumes the shape that adapts to the surrounding tissues, while entrapping the cells. When cells start secreting new ECM to repair the damaged tissue, the hydrogel is ready to degrade. (6) This procedure is explained in Figure 1.

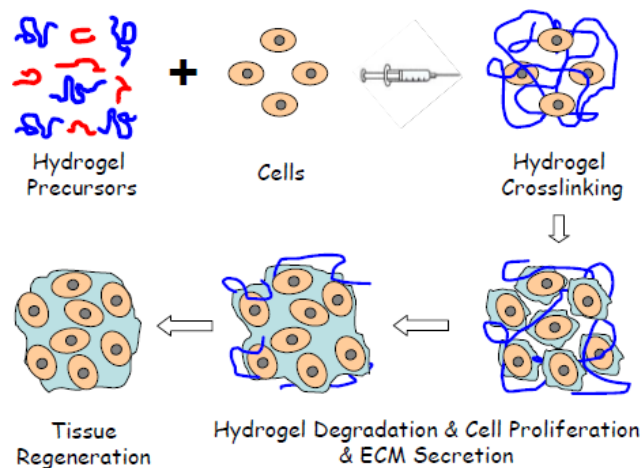


FIGURE 1: PROCEDURE TO INJECT THE CELLS-LOADED HYDROGEL PRECURSOR. THE HYDROGEL FORMS IN-SITU, THUS THE TISSUE REGENERATION OCCURS IN A NO-INVASIVE MANNER (6)

The advantage of using injectable hydrogels is not only to keep the plant inside the defect, but also to provide the immediate support of the weight, thanks to the instant achievement of the final stiffness and resistance.

Nevertheless, nowadays there are few hydrogels that are suitable for long-term cells encapsulation. Most of hydrogels, in fact, can't be cross-linked through completely biocompatible agents. Another problematic is the low stability of hydrogels in the body. In addition, hydrogels favour proliferation of cells when they are loaded with growth factors, that must be inserted in a controlled manner. This requisite, fundamental for a correct working of the hydrogel, is not easy to be achieved. (1)

Hydrogels intended for regenerative medicine can be prepared using non-toxic chemical cross-linkers or enzymes, to obtain biological crosslinking, or exploiting physical interactions, such as hydrophobic and ionic ones. Supramolecular chemistry can also be used. (26) (27) (28)

Each type of hydrogel has advantages and disadvantages, when employed in regenerative medicine. Hydrogels prepared by chemical reticulation have shown to have good mechanical properties, but in vivo applications are limited, due to the possible cytotoxicity of linking agents. In contrast, physical hydrogels can be formed without reactive chemicals, but they are characterized by low stability and reduced mechanical properties, once inserted into the body.

2.3.2 DRUG DELIVERY

Hydrogels have gained large applications in drug delivery. When a pharmaceutical therapy is needed, having an effective and controlled drug delivery system gives economic and therapeutic benefits. (6)

figure 2 shows the comparison between classical therapy, in which the drug is given to the patient via doses (conventional dosing), and the one in which the drug is released through appropriate carriers (controlled release).

In both cases, there is a therapeutic window, the lower limit of which represents the minimum level for the drug to be effective, while the upper limit indicates the concentration above which the medicine is harmful.

In conventional dosing, it is possible observing some peaks that exceed the therapeutic window. The following collapse of the concentration highlights the need of an additional dose.

On the contrary, in controlled release, the concentration of the drug maintains at the desired level for longer periods.

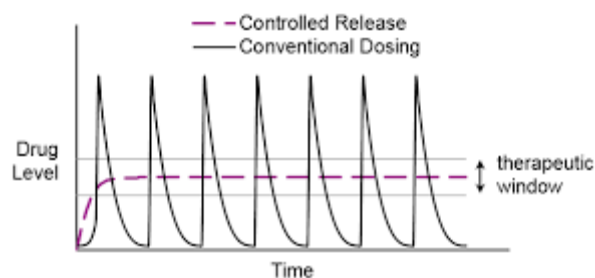


FIGURE 2. TREND OF DRUG'S CONCENTRATION. IN CONVENTIONAL DOSING THE DRUG IS GIVEN BY DOSES; CONTROLLED RELEASE CONSISTS IN A GRADUAL RELEASE FROM CARRIERS.

Hydrogels have become preferred materials for the design of such drug delivery systems, especially those that are sensitive to changes in pH or temperature. The goal is to release the drug into certain time intervals (time-modulation) (6).

Properties that make hydrogels suitable for drug delivery are the water content, the biocompatibility, the controllable pore size distribution and the chemical adaptability. An ideal drug delivery system must provide the drug in the target sites and at the desired time. Hydrogels can achieve this aim. When the drugs are loaded into the hydrogel, this behaves as a depot in which the drugs' elution occurs slowly. This keeps drugs at a high concentration for an extended time.

The release of drugs is regulated by controlling swelling, crosslinks' density, and degradation. (15)

In this context, the main challenge is the hydrophilicity of hydrogels, which can inhibit the quantity and distribution's homogeneity of hydrophobic drugs (e.g. cancer drugs, antioxidants, anti-inflammatory drugs). The solution to this problem may be the use of liposomes and micelles, hence the use of block-based hydrogels. (29)

In literature, there are studies also about the use of injectable hydrogels combined with biodegradable microspheres for drug delivery applications. (30) (31)

2.3.3 ADSORBENTS

Hydrogels have been studied as adsorbents for removal of heavy metal ions and toxic compounds from various effluents. (32) (33) (34)

The hydrogel-based adsorbents are of great interest because their unique properties.

Firstly, their structure is a three-dimensional network in which chains create voids. Voids can form during the synthesis, due to the phase separation, or they may exist as smaller pores within the network. (8)

Pores' size and distribution determine the so-named "tortuosity" of the hydrogel. (8)

Secondly, the hydrophilicity provides compatibility to water and the swelling ability.

The high porosity and the presence of hydrophilic groups allows the adsorption of large amount of water and pollutants. (35) (36)

The sorption capacity depends on the functional groups.

Furthermore, most of hydrogels are biocompatible and biodegradable, thus they are eco-friendly and suitable for water treatments. In fact, biopolymers-based hydrogels have been studied for treating water pollution, i.e. the removal of heavy metal ions from aqueous media. (35)

Nanocomposite hydrogels have aroused much interest, due to their improved mechanical strength and their higher surface area. Many clay-hydrogel nanocomposites such as poly(acrylic acid)/bentonite and chitosan/montmorillonite have been utilised for adsorption of Pb^{2+} from aqueous solution. (37)

Moreover, polyelectrolyte hydrogels are particularly used for their ability to form complexes with opposite charge ions. (2)

Similarly, magnetic hydrogels are important for this field. For instance, a chitosan-based magnetic hydrogel was prepared for the removal of textile dyes from industrial effluent. (35)

2.3.4 SENSORS

Sensitive hydrogels are materials that can respond to specific stimuli. Consequently, they are successfully applied as sensors. Some examples are described below.

pH-sensitive hydrogels change their volume when pH varies. Then, they can deform or strain the transducer, that translates the mechanical work in a signal. As an alternative, transducers can directly observe the modification of the material. pH-sensitive hydrogels can be utilized in medical applications, because pH changes at many specific or pathological body sites. (2)

A smart application is reported by A. Pathak and V.K. Singh (38). They used a polyacrylamide hydrogel to coat a fiber sensor. The pH-variations in surrounding liquids led to the swelling of the hydrogel, causing changes in refractive index (RI) of the liquids. RI modification resulted in a specific output transmission wavelength dip.

Moreover, hydrogels can be used as biosensors.

A biosensor is a device that can receive a biochemical data and transform it in a useful signal, through the transducer. The biosensor has a specific bio-element, which receives the information and must be protected from undesired reactions with surrounding

molecules. Therefore, hydrogels are employed as matrix to immobilize and defend the bioelement of biosensors. (2)

Finally, hydrogels have attracted a lot of interest for the preparation of flexible, temperature-sensors. Temperature-sensors have applications in bioelectronics and in biomedical diagnosis. Temperature-sensitive hydrogels can respond to heat and produce an electric signal. The properties of these materials can be enhanced by the addition of proper fillers. Such as an example, Ran An et al. (39) added multi-wall carbon nanotubes to a polyacrylamide/Fe³⁺-polyacrylic acid hydrogel to increase the material's thermal conductivity and enhancing the response to temperature.

3. NATURAL HYDROGELS

Natural hydrogels are natural polymers-based materials that offer a wide set of advantages.

First of all, they resemble ECM structure and do not cause inflammatory or immunological reactions; they are mostly biocompatible and biodegradable. (40) (41)

Moreover, they promote cell adhesion and proliferation.

Consequently, natural hydrogels have attracted interest in biomedical applications, as cells' scaffolds and drug carriers. (40) (41) (42)

Nonetheless, these materials were reported to be applied in other fields. For instance, Tadeau et al. (35) studied hydrogels based on chitosan, maltodextrin and gum arabic (with and without magnetite nanoparticles) as adsorbents for removing Cd^{2+} from aqueous solutions. Owing to the hydrogels' structure, the no-toxicity and the ease and speed of the application, polysaccharide's hydrogels proved to be ideal adsorbent of heavy metals from water.

However, the lack of adequate mechanical properties limits natural hydrogels' application prospects.

This problem has led to various researches about enhancing mechanical performances.

Bao et al. (42) summarized methods used to address this challenge: the creation of double-network hydrogels, the incorporation of nanophases (nanofibers, nanoparticles, nanorods), the realisation of Click chemistry-based hydrogels and the use of supramolecular chemistry.

Nevertheless, some challenges remain, like the toxicity of residual chemical reagents and the industrial production.

Generally, natural hydrogels are formed of proteins or polysaccharides.

Proteins-based hydrogels are mainly composed of collagen, gelatine, fibrin, silk-fibroin.

While for polysaccharides, chitosan, hyaluronic acid, agarose and alginate are the main employed materials, especially for cartilage tissue engineering.

Polysaccharides are a family of degradable, natural polymers that largely exist in microbials, plants and animals. Polysaccharides consist of repeating saccharide (carbohydrate) units that are covalently linked with O-glycosidic bonds.

Each polysaccharide is characterised by the groups that substitute the saccharide units, the linkage site and types, and the molecular weight. All these factors define the physical

properties (strength, solubility, gelling behaviour etc) and superficial and interfacial characteristics. (41)

Cellulose, which is the subject of the current thesis, belongs to this materials' family.

3.1 CELLULOSE AND CELLULOSE HYDROGELS

As the primary component of plant and natural fibers, cellulose is the most largely available natural polymer of glucose.

It is composed of glucose units held together by 1,4- β -glucosidic linkages (Figure 3,a), which aggregate to form cellulose fibrils.

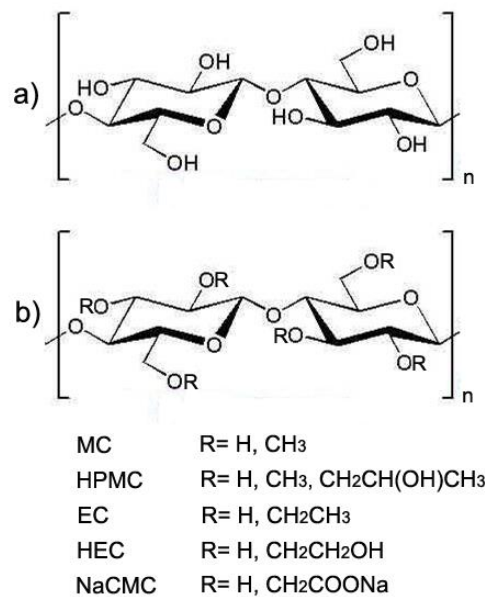


FIGURE 3: (A) REPEATING UNIT OF CELLULOSE, THE 'CELLUBIOSE'. (B) REPEATING UNIT OF CELLULOSE DERIVATIVES. "R" REPRESENTS THE SUBSTITUENT GROUPS FOR EACH DERIVATIVE, SUCH AS METHYLCELLULOSE (MC), HYDROXYLPROPYL METHYCELLULOSE (HPMC), ETHYL CELLULOSE (EC), HYDROXYETHYL CELLULOSE (HEC) AND SODIUM CARBOXYMETHYLCCELLULOSE (NACMC). (43)

The high density of hydroxyl groups (that create intra and inter-molecular bonds) and the stiffness of glycosidic bonds lead to the formation of crystalline domains. (44) As shown in figure 4, there are amorphous portions among the high-ordered ones.

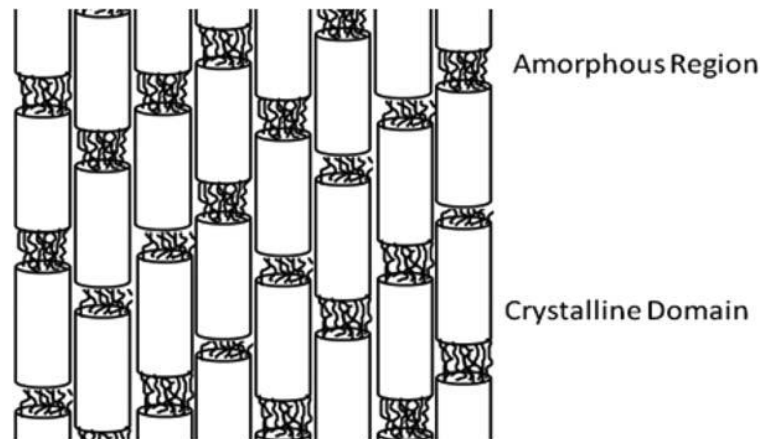


FIGURE 4. AMORPHOUS AND CRYSTALLINE REGIONS IN CELLULOSE FIBRILS (44)

Cellulose exists in both form of bacterial cellulose (BC) and plant cellulose (PC).

PC is extracted from plants; BC is produced by some bacteria from various sugars, through a fermentation process (45).

Both BC and PC are highly crystalline (respectively, 40-60% and more than 60%) and insoluble in water. In fact, the extended hydrogen-bonds structure of the cellulose complicates the choice of an appropriate solvent. (46) Recently, ionic liquids have emerged as green solvents to dissolve cellulose materials. (47) (48)

BC and PC differ from one another in structure and purity.

BC's network is finer, constituted by nanosized fibers; this structure grants large water holding capacity and higher tensile strength than PC's ones. In addition, BC can be regarded as totally pure, whereas PC, that contains other polymers in the form of lignin and hemicellulose, requires further modifications. (45)

Cellulose and its derivatives are biocompatible, biodegradable and bio-durable. This last term refers to the lack of resorption of cellulose in animal and human tissues.

The biodegradation rate can be further improved by lowering the crystallinity and by increasing the water solubility. Cellulose is transformed into water-soluble products by the separation of the molecules in a cellulose fiber and the derivatization of some of their hydroxyl groups. This prevent molecules to rearrange through intermolecular hydrogen bonds over enough of their length to determine insolubility. (49)

In this regard, etherification of cellulose produces more soluble derivatives (figure 3,b). The degree of substitution, namely the average number of substitute hydroxyl groups in a glucose unit, affects the behaviour in water solutions of the so-modified cellulose derivatives. (43)

Moreover, cellulose possesses high mechanical stiffness, low density, hydrophilicity, amenability to various chemical modifications, especially due to the abundant hydroxyl groups on the surface. (46)

The low cost of cellulose, which is the most diffuse polysaccharide, is another advantage.

Nanocellulose (i.e. cellulosic material with nanometric size at least in one dimension (50)) has attracted much attention because of its properties.

As a nanostructured material, nanocellulose boasts high aspect ratio, specific surface area, reactivity and improved strength and stiffness. (51) (52)

Moreover, it retains the advantages and properties of cellulose, that have been formerly addressed. (50)

CNCs are obtained by an acid hydrolysis of cellulose, that produces the cleavage of the glycosidic bonds. This results in the degradation of the amorphous domains and in the release of cellulose, crystalline nanoparticles.

Following steps involve centrifugation, dialysis and ultrasonication.

As regards the hydrolysis, sulfuric acid is the most common acid, because it allows a stable dispersion of the nanocrystals in solvents. (53) (54) (55) (56)

In fact, during the hydrolysis, sulfuric acid and surficial -OH groups react, leading to the grafting of anionic sulfate ester groups to the CNCs' surface. Consequently, CNCs result negatively charged and, once dispersed, they repulse each other, preventing their flocculation. (44)

CNCs appear as highly crystalline nanorods with a width of 5-20 nm and length ranging from 100 nm to 2000 nm. (10)

Further forms of nanocellulose are nanofibrillar cellulose and bacterial nanocellulose. (50)

Cellulose hydrogels can be formed from aqueous solutions of cellulose ether (such as methylcellulose, hydroxypropyl methylcellulose, ethyl cellulose, hydroxyethyl cellulose) by either chemical or physical methods.

The formers include chemical cross-linkers or photocuring. Photo-crosslinking requires specific functionalization of cellulose. In recent years, radiation crosslinking has been examined as a tool to obtain an environmentally sustainable production process.

Instead, physical hydrogels form through a sol-gel process which involve hydrophobic associations. The starting solution usually contains methylcellulose and/or hydroxypropyl methylcellulose (concentration is 1-10% by weight). (43)

Epichlorhydrin, multifunctional carboxylic acids, aldehydes and aldehyde-based reagents, urea derivatives and carbodiimides are among the most widely employed crosslinkers agents for cellulose hydrogels. (43)

Cellulose hydrogels have been recently regarded as a valid material for superabsorbent for personal care, such as diapers, napkins, hospital bed sheets, sanitary towels. Currently,

these products are usually made in acrylate-based superabsorbent hydrogels, whose major limit is the non-biodegradability. In contrast, cellulose hydrogels are completely biodegradable. Sodium carboxymethylcellulose (NaCMC) and hydroxyethyl cellulose (HEC) hydrogels, for example, have a microporous structure, achieved by a phase inversion desiccation technique in acetone. The so-done network increased the water adsorption and the swelling capabilities. (43)

Studies have been carried out to employ cellulose hydrogel superabsorbent in agriculture, as water reservoirs. This application relies on the water storage ability of hydrogels. Again, being an eco-friendly material is a plus-point of cellulose. (57) (58) (59) (60)

Likely to other natural hydrogels, cellulose-based ones are used in biomedical field. For instance, pH-sensitive cellulose hydrogel can be administered orally; the hydrogel swells in the intestine, due to the changes in pH. Then, it can be used to absorb water and treat some pathological conditions, such as renal failure and diuretic-resistant oedemas. For such a purpose, polyelectrolyte NaCMC/HEC hydrogels have been studied. (61)

Hydrogels containing NaCMC have been also investigate as drugs' carriers. (29).

Finally, cellulose hydrogels functionalised with hyaluronic acid has were proposed as a scaffold for regenerative medicine (43), whereas a carboxymethylcellulose (CMC)/methylcellulose(MC) hydrogel was formulated to replace nucleus pulposus. (62)

More frequently, cellulose is used as nano-reinforcer in hydrogels. Combining nanofillers and hydrogel matrix produces significantly flexible and tough materials, with improved strength and stiffness.

Specifically, cellulose nanocrystals (CNCs) are the most common form of nanocellulose.

The most common way to introduce the nanofillers in the matrix is the simple stirring with the reaction solution before the gelation step. (46)

The presence of numerous reactive hydroxyl groups on the CNCs' surface enables a facile surface functionalization which can influence the interaction with the hydrogel matrix and thus the properties of the final composite.

For instance, Du et al. (10) prepared CNCs hydrogel by the solution-mixing of poly(glycerolmonomethacrylate) (PGMA), grafted with CNCs (CNC-g-PGMA), and phenylboronic acid-containing binary copolymers. The resulting material was an injectable self-healing nanocomposite (NC) hydrogel dominated by reversible boronic ester bonds.

Other forms of cellulose nanofillers exist, like nanofibrils and microgranules. It was demonstrated that little amounts of micro-granulated cellulose can increase the Young's modulus of a PAAm hydrogel up to 1.5 times. (46)

An alternative solution to achieve a substantial improvement of mechanical performances is producing IPN hydrogels (e.g. cellulose-PAAm and cellulose polyacrilic acid compounds).
(46)

4. 3D PRINTING

4.1 AN OVERVIEW

3D printing or additive manufacturing is a process that builds up a three-dimensional object by adding material layer-by-layer.

In the International Organization for Standardization (ISO)/American Society for Testing and Materials (ASTM) 52900:2015, 3D printing is defined as the “process of joining materials to make parts from 3D model data, usually layer upon layer, as opposed to subtractive manufacturing and formative manufacturing methodologies”.

The part is produced from a CAD file, which is converted into the STL-format (standard triangulation language) and then divided into thin (order of microns) layers.

3D printing technologies are emerging as alternatives to subtractive or formative manufacturing technologies. The success of AM processes is ascribed to their remarkable properties (63), such as:

- high precision;
- wide variety in terms of material;
- shortening of design cycle;
- potentially no limits in parts' complexity;
- low waste of material;
- reduction of mistakes' costs.

These characteristics make 3D printing attractive for fields that require the low production of high value and highly complex objects (e.g. aerospace and biomedical industries).

The ASTM 52900:2015 standard has identified seven main classes of 3D printing technologies, that are:

- Material jetting: the part is created by depositing droplets of a photosensitive material, that solidifies under UV irradiation.
- Binder jetting: the three-dimensional part is built up from powders that are joined together by a bonding agent. This is dropped by the printing head. a layer of powder is spread on the platform, the printing head drops
- Material extrusion: powders are pushed out through a nozzle on a substrate, where they solidify.

- Sheet lamination: the layers of the object are constituted by sheets of material, that are bonded by the use of ultrasound or a laser.
- Direct energy deposition: a continuous flow of powders is hit by a thermal source, such as a laser. The energy heats the substrate on which the material is deposited and melts the powders. Direct energy deposition is usually used in powder metallurgy.
- Powder bed fusion: likely to direct energy deposition, powder bed technologies rely on a thermal source which heats and melts the powders. The fundamental difference is that, in powder bed fusion, the laser hits a pre-deposited layer of powders. This kind of technologies are remarkable for their flexibility.
- Photopolymerization (or Vat photopolymerization): the solidification of a photo-curable resin in a solid, three-dimensional object is achieved by a chemical reaction called photopolymerization. Photopolymerization involves specific compound, photo-initiators and the use of a light source. (see chapter 4.2 Photopolymerization: stereolithography and digital light processing , page 20).
- Bioprinting: an AM process that prints cells, bioactive molecules, biomaterials. These bioprintable materials are known as bioinks. Cells can be incorporated in a matrix (e.g. a hydrogel) in the so-called scaffold-based bioinks; free-scaffold bioinks exploit the biological self-assembly or mini-tissues as building blocks, in order to print the cells and molecules without the support of the scaffold. (64)

Some of these typologies are furtherly categorized in subclasses (figure 5).

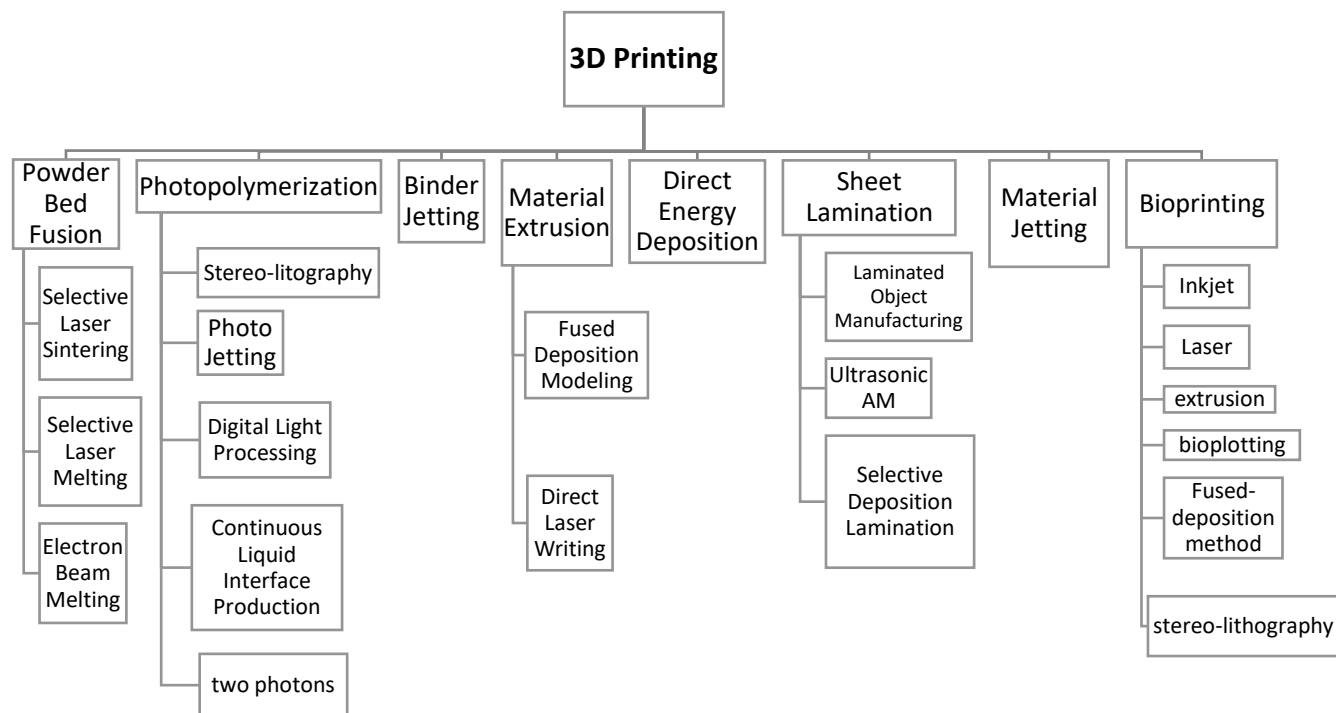


FIGURE 5. CLASSIFICATION OF 3D PRINTING TECHNOLOGIES (64) (65)

AM processes	System	Specific energy density (J cm ⁻³)	Fabrication speed (cm h ⁻¹)	Resolution (elements mm ⁻³)
Binder jetting	CJP	0.026	1.27-1.9	1900
Direct energy deposition	LENS	50.000	4.4	17
Material extrusion	FDM	N.A	0.05	46
Material jetting	Polyjet	0.06	0.4	15.200
Powder bed fusion	SLS	300	2.5	211
Sheet lamination	LDM	336	0.45	1907
Vat photopolymerization	DLP/SLA	0.94	1.5	3152

TABLE 2. VALUE OF SPECIFIC ENERGY DENSITY, FABRICATION SPEED AND RESOLUTION OF MOST COMMERCIALY COMMON AM PROCESSES (66)

The main positive and negative aspects of each of the 3D printing classes concern the range of potential materials, the resolution and the accuracy, the utilization rate of the raw materials, the final properties of the parts and the need of post-processing operations. (66)

For instance, material extrusion processes are low-cost, versatile and easy to customize. Furthermore, many materials can be processed. The main issues are the low precision and the long build time. On the contrary, photopolymerization grants high resolution, accuracy and high fabrication speed. Nevertheless, post-processes are required, such as a post curing step to improve the strength of the part. (66)

The use of 3D printing extends from the automotive to the medical field, from the aerospace industry to the jewellery and civil sectors. Even the food (67) (68), the textile (69) (70) and the clothing (71) markets started to rely on AM processes.

Among the main challenges about improving 3D printing technologies, two are targeted as priority:

- 1) Obtaining higher speed and resolution and lower energy consumption (concerning parameters of current AM technologies are reported in Table 2).
- 2) Studying and developing new 3D printable materials.

4.2 PHOTOPOLYMERIZATION: STEREOLITHOGRAPHY AND DIGITAL LIGHT PROCESSING

4.2.1 PHOTOPOLYMERIZATION

Photopolymerization is a photochemical process that consists in the curing of a liquid monomer, thanks to the use of light.

The photopolymerization of monofunctional monomers produces thermoplastic polymer; if the number of functional groups is higher, the result is a thermoset.

Broadly speaking, a photochemical process occurs when a molecule absorbs a radiation. This happens if the wavelength of the radiation equals the energy gap between the unexcited and the excited states of the molecule.

Photopolymerization usually uses UV radiation, which corresponds to higher energy than those of IR and visible radiations. However, monomers and oligomers rarely absorb UV radiations. Then, the starting formulation must include molecules that are UV-reactive (i.e. the photoinitiators).

Therefore, a photocurable formulation usually contains:

- A photoinitiator, i.e. an organic/inorganic compound which is thermally stable. It must have proper absorption at the wavelength of the applied radiation (visible or UV);
- A reactive diluent, which controls viscosity and is involved in the photopolymerization;
- The oligomer from which the polymer forms;
- Additives.

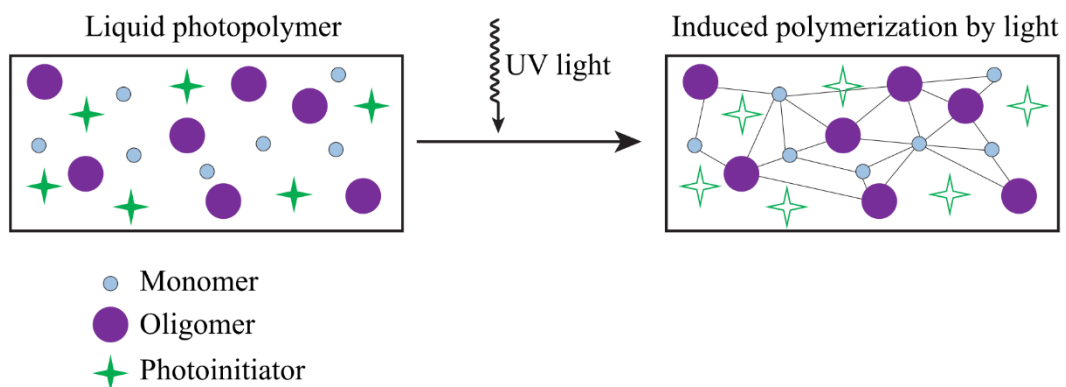


FIGURE 6. SCHEME OF PHOTOPOLYMERIZATION (72)

The instant the photoinitiator absorbs the radiation, it forms a reactive specie. This step is referred as activation, and it is a photochemical reaction.

The reactive specie sets off the polymerization, which is a thermal chain reaction (the heat of the reaction, for an acrylate monomer, is around 85 kJ/mol (73)). The result is a polymer.

So, in summary, the basic steps in photopolymerization are:

- Absorption of light;
- Generation of reactive species;
- Polymerization (polyaddition process).

Depending on the photoinitiator, the polyaddition reaction can be radical or ionic.

In the radical photopolymerization, the photoinitiator absorbs the radiation and forms free radicals that are capable of adding to vinylic or acrylic double bonds to initiate the polymerization. The most efficient photoinitiators include benzoin ether derivatives, benzyl ketals, hydroxyalkylphenones, amino ketones, and acylphosphine oxides (73).

The most common radical photopolymers are acrylates. When the photoinitiator reacts, acrylates form long polymeric chains by adding monomer segments. Once the polymer chains are long enough to become close to one another, cross-linking occurs. (73) Further radical photocurable monomers include polyester resins, methacrylates, thiol-ene systems.

In the ionic photopolymerization, the reactive species are anions or, more commonly, cations. Cationic photoinitiators are neutral salts. Their cationic part absorbs the radiation and degrades, releasing H^+ acids and starting an ionic polyaddition reaction. This reaction proceeds by heterolytic cleavage of π -bond. Epoxies and vinyethers are common cationic photopolymers.

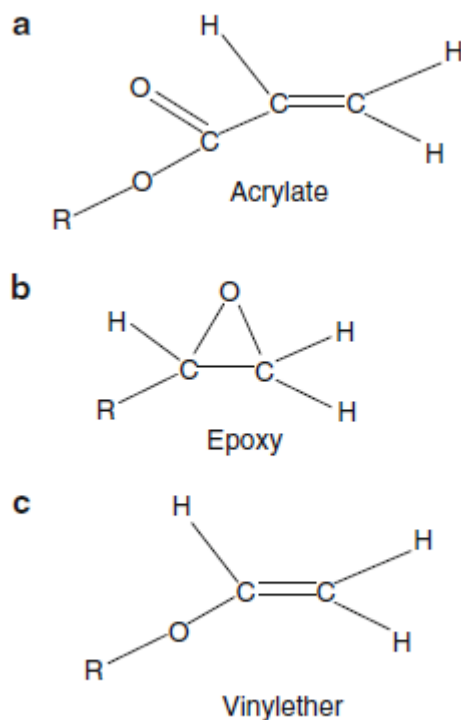


FIGURE 7. MOLECULAR STRUCTURE OF PHOTO-MONOMERS (73)

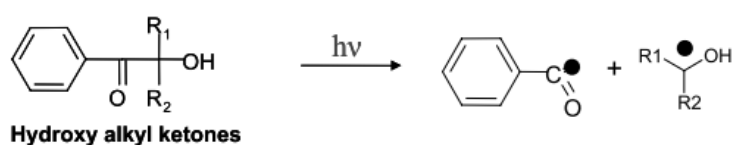
The present work uses radical photopolymerization, which is the most commercially widespread, because of the higher reaction rates.

Radical photoinitiators (Norrish type-I and type II) produce a radical polyaddition, which consists of three phases: initiation, propagation and termination. They are chromophores that absorb the radiation and create radicals, through two different processes.

Type-I photoinitiators cause a homolytic cleavage, that produces two radicals that may both initiate the polymerization. The cleavage usually occurs at the α -position of a carbonyl group. (74)

Instead, type II photoinitiators undergo hydrogen abstraction. They need a co-initiator, such as a tertiary amine, ether, ester, thiol, etc., that acts as the hydrogen donator. (74)

α - cleavage type photoinitiators (type I)



H-abstraction type photoinitiators (type II)

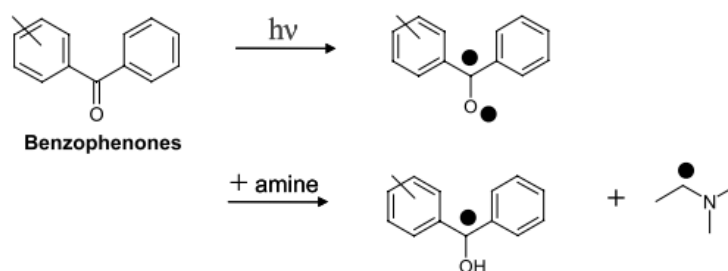


FIGURE 8. PHOTOINITIATORS (TYPE I AND TYPE II). (75)

The different steps of a radical photopolymerization reaction are reported in figure 9.

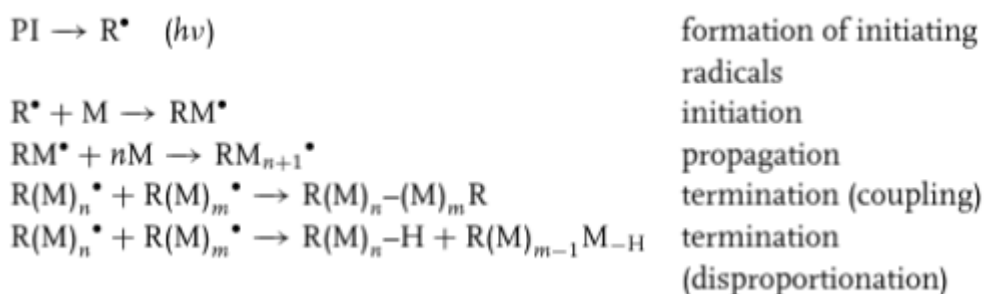


FIGURE 9. RADICAL PHOTOPOLYMERIZATION REACTION'S STEPS. PI IS THE PHOTOINITIATOR, THAT ABSORBS THE RADIATION AND CREATE A RADICAL SPECIE. THE REACTION PROCEEDS WITH THE FORMATION OF A MACRORADICAL (INITIATION) AND ITS GROWTH BY THE ADDITION OF OTHER MONOMERS (PROPAGATION). THE REACTION ENDS WITH THE TERMINATION STEP. (76)

Radicals R^\bullet interact with the monomer M and create the first macroradical RM^\bullet (initiation). On average, for every two photons of the laser, one radical will be produced (73). Then, the macroradical grows by the subsequent addition of monomers. This phase represents the propagation of the reaction, in which one radical can cause the polymerization of over 1000 monomers. (73)

The last step of the reaction is the termination. It occurs by coupling (joining of two radicals) or disproportion (cancelation of one radical by another, without joining).

Photopolymerization gained wide applications because of its economic and ecological advantages.

In fact, the production speed is high, and the reaction can be performed rapidly and at room temperature, hence minimizing the energy costs. The energy saving and the reduction of waste material guarantee a low ecological impact. Moreover, photopolymerization grants high quality products and it is versatile in terms of both applications and materials. (75)

As for the drawbacks, one criticism concerns the choice of the photoinitiator, that must be based on the absorbance coefficient and the final purpose of the material (e.g. the formation of cytotoxic free radicals is harmful in biomedical applications). The photoinitiator influences the polymerization rate, and its chemical selectivity is crucial for the resolution of fine features: the polymerization must involve the desired portion of material without causing a cascade of free-radical crosslinking. (77)

Another disadvantage is the low penetration depth of the radiation, that limits the applications to thin, bidimensional structures (e.g. films, coatings). 3D printing overcomes this problematic, thanks to the slicing of the part, that allows a layer-by-layer photopolymerization (see 4.2.2 Stereolithography and Digital light printing).

Moreover, the final part is subjected to a volumetric shrinkage (up to 20% for acrylates) that prevents the fabrication of massive objects. Moreover, the shrinkage is challenging for coatings, because it affects the adherence to the substrate. (78)

Finally, for radical photopolymerization, the oxygen inhibition must be considered. (74) (78)

In fact, oxygen can either quench the photoexcited photoinitiator (quenching) or create peroxides by combining with the free radical from the photocleaved photoinitiator (scavenging). (79)

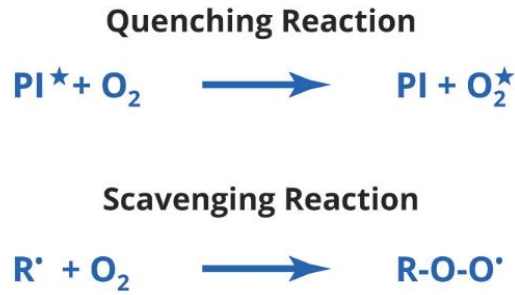


FIGURE 10. QUENCHING AND SCAVENGING REACTIONS (80)

So, the process can be performed in void or in inert atmosphere. Another solution is adding some molecules that are more likely to bond to oxygen, avoiding the interaction between the radical species and the oxygen. (78) (81) (82)

4.2.2 STEREOLITHOGRAPHY AND DIGITAL LIGHT PRINTING

The most common 3D processes based on the photopolymerization are stereolithography (SLA) and digital light printing (DLP).

Commonly, radical photopolymerization is involved in both processes.

In SLA, a laser is used to print the object from the resin, which fills a tank. A support-platform lowers into the tank. The laser is directed to the appropriate coordinates by a computer-controlled mirror. The solidification occurs only in points hit by the radiation. In fact, SLA can be seen as a point by point process. Once a layer is made, the support platform rises according to the layer thickness (typically about 0.1 mm), and the laser delineates the following layer.

The component is built top-down from a series of layers, which correspond to the cross section of the CAD model.

When the whole part is completed, the platform rises out of the tank and the excess resin is drained. Then, the model is removed from the platform, washed of excess resin, and finally placed in a UV oven for final curing, in order to increase strength and stability.

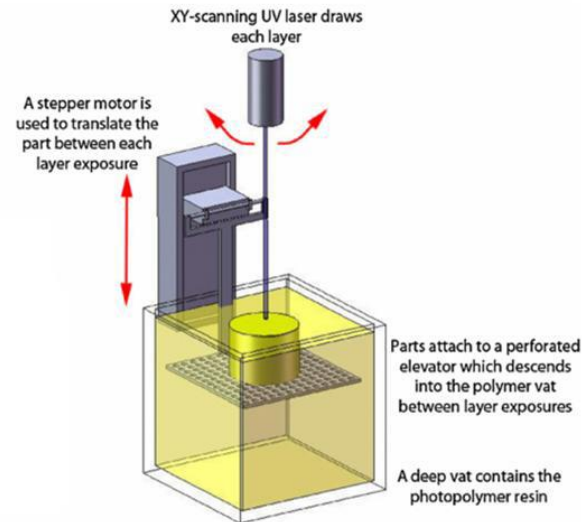


FIGURE 11. STEREO LITOGRAPHY (SLA) (83)

On the contrary, DLP produces the object from the bottom, and one layer is irradiated by a single-shot. This is achieved by a digital processor screen (i.e. a dynamic mask consisting of microscopic-size mirrors in a matrix on a semiconductor chip) instead of a laser. Therefore, DLP is faster than SLA, but resolution is lower, because it corresponds to pixel size.

The DLP process is described in figure 12.

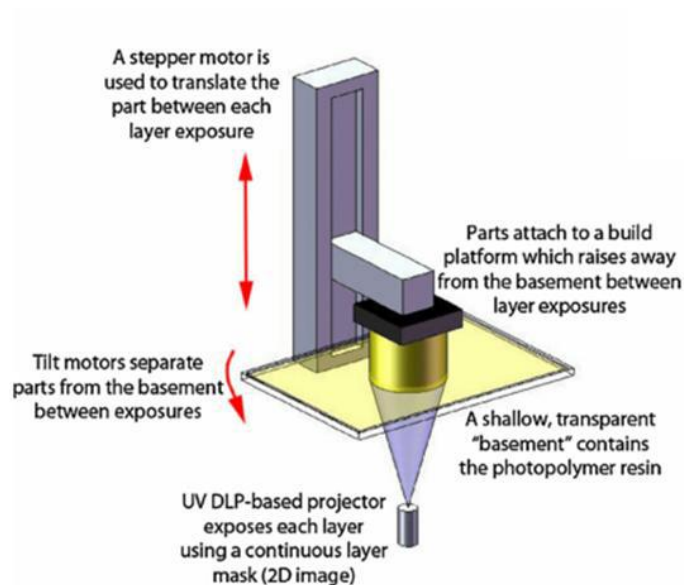


FIGURE 12. DIGITAL LIGHT PROCESSING (DLP) (83)

DLP printers ensure a faster and more efficient production than SLA printers. In addition, DLP allows to use a wider range of wavelength.

Finally, DLP technology offers higher flexibility in terms of volumes of photoreactive polymers for printing: unlike for SLA printers, even small amount of resin can be used. SLA and DLP both offer some of the finest Z resolutions of all 3D printing processes.

As for X-Y resolution, in DLP is affected by the square pixels' size (thus from the screen's resolution) and is usually between 35 to 100 microns. (84)

On the contrary, the X-Y resolution of SLA depends on the laser's spot size and it varies in a range of 85-25 microns. (84)

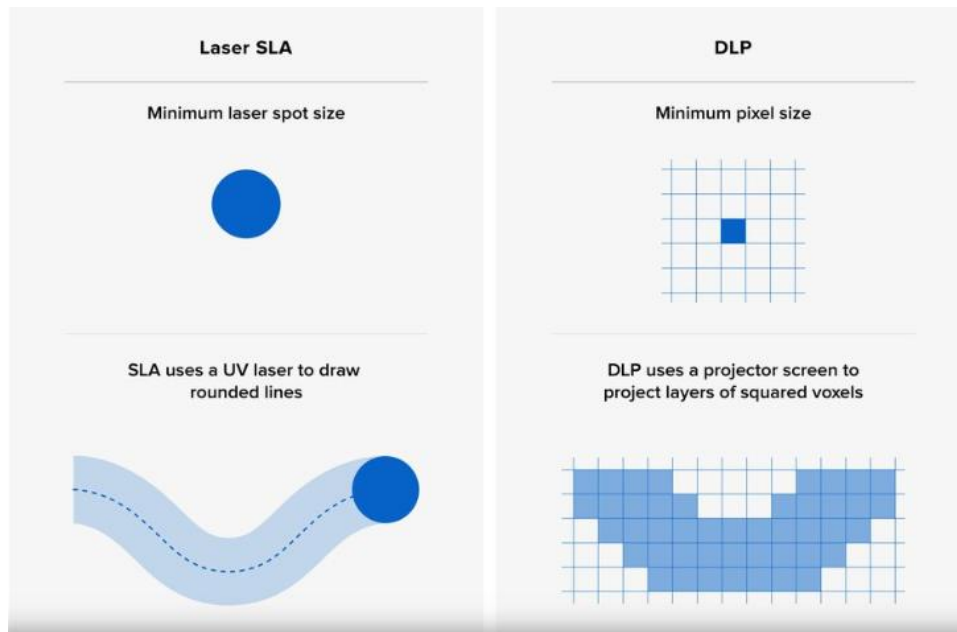


FIGURE 13. COMPARISON BETWEEN SLA AND DLP. (84)

The high resolution is one of the main benefits of photopolymerization 3D-printing.

This feature significantly depends upon the light exposure, that must be properly defined. If the light exposure dose is too low, photopolymerization can't occur adequately; if it is too high, it causes photopolymerization even in undesired regions.

However, the correct light exposure window is very narrow, and selecting the proper dose, such as the other printing parameters, is a trial and error process.

Resolution is affected by the curing time and the depth cure (i.e. the thickness of each layer), too. They define the kinetics of the curing reaction, that can be fine-tuned by changing the scanning speed, the light intensity, the ratio of monomer to photo-initiator etc (85)

Finally, it is possible to define the specific energy W^* as:

$$W^* = \frac{W'_c}{l_c} \exp(l_c/l_p)$$

where W'_c is the curing exposure for solid-liquid transition, l_c is the curing depth and l_p is the depth of penetration. The specific energy is the amount of radiant energy to solidify a unit of the photo-resin and describes the photosensitivity of the polymer. (66)

4.2.3 OTHER PHOTOCURING TECHNOLOGIES

Continuous liquid interface production (CLIP) is an upgrade of DLP that obtains faster printing. It takes advantage of the oxygen inhibition. The innovation consists in an oxygen-permeable window below the resin bath, that allows the formation of the so-called dead zone, a thin uncured liquid layer between the window and the cured part surface. (79)

Differently to DLP printers, where the movement of the platform and the UV exposure represent discrete steps of the procedure, CLIP ensures a continuous and 25 to 100 times faster process. (86)

Nevertheless, this process is strongly affected by the viscosity of the resin. (86)

Recently, there has been an increasing trend toward nanoscale fabrication processes. They require a finer resolution, that can be achieved by 2 photons polymerization (2PP) processes.

The other photopolymerization technologies (SLA, DLP and CLIP) are based on the absorption of a single photon by the atom.

When an atom absorbs a photon, the process is characterised by a virtual state of transition, whose life is of the order of femtoseconds. Multi-photons absorption is possible if the second photon is absorbed before the decay of the virtual state (83).

Then, 2PP technology uses a pulse N-IR laser, so that the interaction between the radiation and the material is in the range of femtoseconds. As a consequence, the absorption of two photons occurs. The nature of nonlinear excitation triggers the reaction only in the focal point of the laser beam. The result is the fabrication of a 3D construct with a resolution close to 100 nm. (87)

4.3 3D PRINTING OF HYDROGELS VIA PHOTOPOLYMERIZATION

Applications of hydrogels have been already discussed in previous chapters.

Since the most common field is the biomedical's one, hydrogel need to be processed by technologies that achieve very fine resolution. In this context, photopolymerization-based 3D printing techniques can produce complex 3D architecture with micron-scale features. In fact, literature contains examples of hydrogel cells' scaffolds obtained by vat-photopolymerization. (88) (89) (90) (91) (92).

In order to use these scaffolds to deeply investigate cell's behaviour, micrometric and sub-micrometric resolution, that can be achieved only by vat photopolymerization printing, is needed. Moreover, several papers demonstrated that highly organized 3D structures promote cells' mechanisms and their proliferation. (89) (90) (93) (94) (95) (96)

For instance, SLA and DLP enable the production of hydrogel scaffolds showing graded properties (e.g. porosity) which mimics the ECM of native tissues (see figure 14). (90) (92)

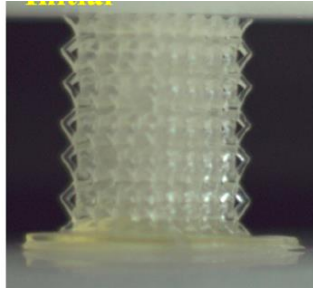


FIGURE 14. A PEGDA HYDROGEL CELL-SCAFFOLD PRODUCED BY DLP. THE MODIFICATION OF EXPOSURE TIME ALLOWED THE PRODUCTION OF A STRUCTURE WITH REGIONALLY VARIED STIFFNESS. (92)

Relating to the drug delivery, the main advantage of vat photopolymerization is that drugs can be incorporated in the resin before the printing. In addition, there are further pros in using SLA or DLP for printing hydrogels drugs carriers. As instance, Kadry et al. (97) utilised DLP to print a tablet for drug content, avoiding the use of temperature and overcoming the limit of printing material containing thermolable substances (figure 15). Furthermore, these technologies yield the production of small batches of tablet, that possess size and release features that refer to specific patient.

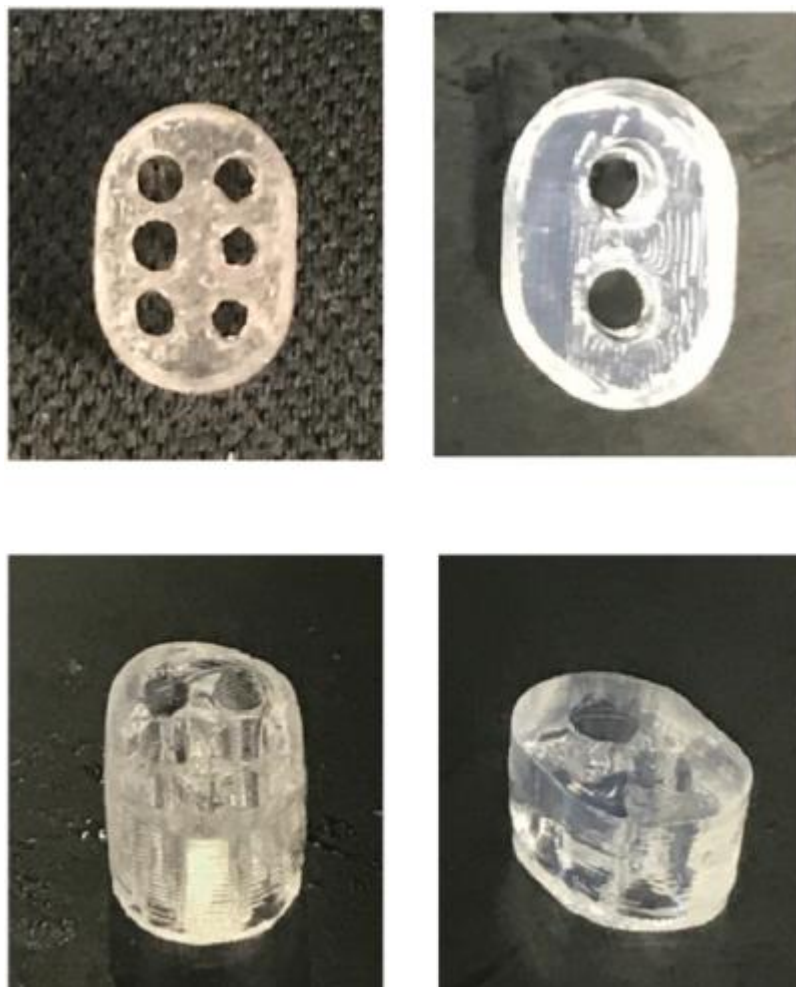


FIGURE 15. DLP PRINTER TO FABRICATE TABLETS FOR DRUG CONTENT, USING PEGDA AND PEGDMA AS PHOTOREACTIVE (97)

As for membrane separation and water treatment applications, 3D printing represents a fast-speed and unexpensive route to produce shapes with potentially no limits in complexity. In fact, optimizing the spacers' design reduces the pressure drop along the channels and enhances the filtration efficiency. (98) (99) (100) In particular, Kerdi et. al (101) and Ali et. al. (102) fabricated and tested spacers printed by DLP and attested the improving of hydrodynamic performances (figure 16).

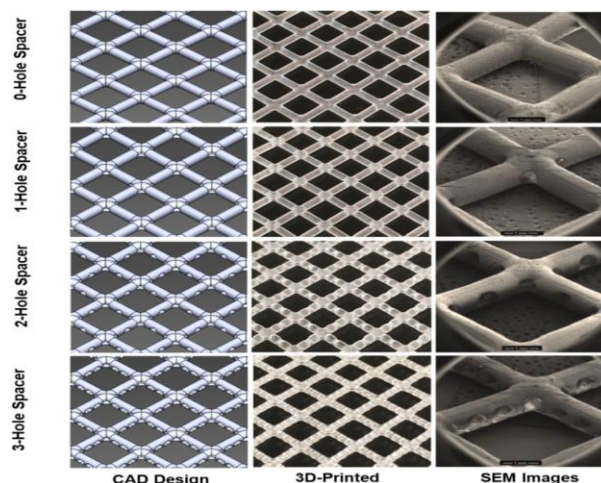


FIGURE 16. MEMBRANES' SPACERS PRODUCED BY DLP TECHNOLOGIES. (101)

Therefore, 3D-printing represents a promising fabrication technique of hydrogels constructs for the removal of pollutants from aqueous environments. (103) (104). For instance, Appuhamillage et al. (105) proved the metal absorption of extrusion-3D-printed chitosan/iacrylated Pluronic F-127 (cDAP) hydrogels (figure 17).

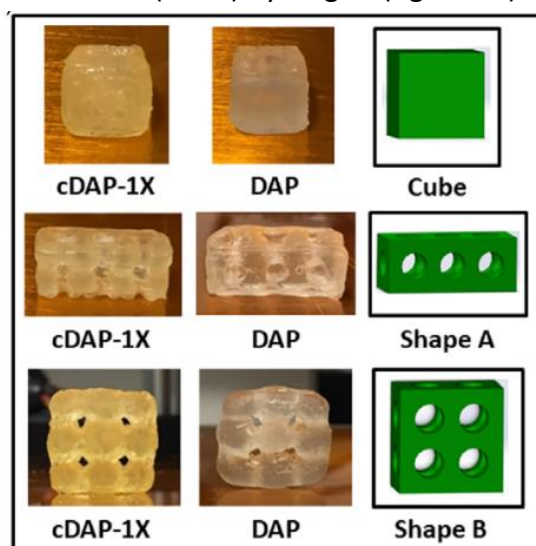


FIGURE 17. cDAP HYDROGELS WITH DIFFERENT CONCENTRATION OF CHITOSAN AND DYACRYLATED PLURONIC F-127 WERE PRINTED INTO VARIOUS SHAPES (105).

Despite the potential applications, few examples of hydrogels printed by DLP can be found in literature.

The low availability of water-soluble initiators and photocurable monomers is among the main reasons for this. Furthermore, the high amount of water during printing can result problematic. The most investigated systems are poly(ethylene glycol) diacrylate (PEGDA) (106) (107), poly(2-hydroxyethyl methacrylate) (pHEMA) (108), poly(ethylene glycol) dimethacrylate (PEGDMA) (109) (110), poly(propylene fumarate)/ diethyl fumarate (PPF/DEF) (111) (112).

Methacrylated gelatin (88) (113) (114) (115), chitosan (116) (117), alginate (118) (119) and hyaluronic acid (120) (121) are among the most explored, natural materials for

photopolymerization. As regard DLP, systems based on gelatin-methacrylate/silk fibroin (122), silk fibroin- glycidyl methacrylate (123), a mixture of gelatin-methacrylate and glycidyl methacrylate-hyaluronic acid (124), chitosan (116) and a mixture of polyethylene glycol diacrylate and gelatin-methacrylate hydrogel (125) have been studied.

As concerns the 3D printing of cellulose hydrogels, very few studies have been described, and almost none of these involve vat photopolymerization.

Cellulose nanofibrils (CNF) hydrogels are the most extensively investigated systems for 3D printing, but only as inks for extrusion 3D printing. (126) (127)

Methyl cellulose hydrogels have been used as blenders to help the 3D printing of hyaluronic acid (by a bioprinter) or alginate (by extrusion) (128) (129)

Negrini et al. (130) optimized the bioprinting of MC hydrogels by extrusion.

The main challenges in DLP- 3D printing of hydrogels are:

- The final resolution, which depends on the exposure time. Regarding hydrogels, there are three factors that can lead to the resolution deterioration. Firstly, the light scattering, due to the optically-clear media. Secondly, the cure depth, that depends on the material. When the cure depth is greater than the optical depth of field, the result is an unwanted polymerization. Even the free-radicals diffusion in un-illuminated regions (that is the third factor) can cause unwanted polymerization. These issues can be addressed by adding light absorbers (dyes) in the initial formulation. The light scattering remains significantly challenging, still. In fact, it increases during photopolymerization because many hydrogels, that are transparent liquids at the beginning, becomes translucent once they are cured, thus causing scattering. In these circumstances, light exposure should be avoided, but it can't be achieved because current printers use a continuous light source (e.g. mercury lamp, light emitting diode). The outcome is the photopolymerization of unwanted regions, that provokes a low print fidelity. (131)
The scattering can be enhanced by phase-separation, too.
- The lack of self-supporting of the layers during the printing, that can lead to the collapse of the structure. This problem is especially critical for objects that are relatively "tall" in Z direction. This problematic requires the optimization of the formulation (e.g. concentration of the solution, addition of other polymers) and printing parameters.

5. METHACRYLATED NATURAL HYDROGELS FOR PHOTOPOLYMERIZATION-3D-PRINTING

As for photo-3D-printing, all polymers require photoactive functionality. Most common photopolymerizable functionalities include acrylates, methacrylates and epoxides.

The functionalization of natural polymers is usually achieved by adding/altering pendant functionality on the polymer backbone. Nevertheless, some challenges exist: the limited solubility in common solvents and the presence of multiple reactive sites or pendant functionality on each backbone repeating unit, that leads to uncertainty in molecular weight between crosslinks, make these polymers difficult to be functionalized. (132)

Natural oligomeric polymers are commonly modified by introducing methacrylate groups in the backbone, in order to obtain hydrogels by photopolymerization. Methacrylates possess highly reactive double bonds, that are involved and consumed in the photo-cross-linking process. The photo cross-linking mechanism is rendered mainly by chain-growth radical polymerization of methacrylate.

Common natural polymers include polysaccharides and polypeptides. As described in previous chapters, they possess enzymatically biodegradable, biofunctional groups that afford the attachment, proliferation and growth of cells and that can be modified by introducing methacrylate groups for photo-curing 3D printing.

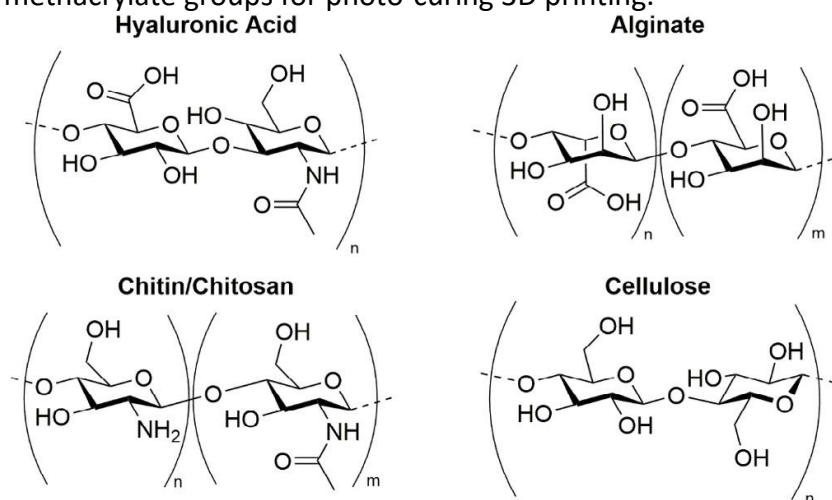


FIGURE 18. REPEATING UNITS OF COMMON POLYSACCHARIDES (132)

Several methods have been developed for synthesizing methacrylate-modified natural polymers; the most frequent protocols involve the use of methacrylic anhydride (133) (89) (116) (113) (134) (115) or glycidyl methacrylate (135) (136).

Photoinitiators of Irgacure family (89) (134) (137) (41) (136) (138) and lithium acylphosphinate salt (LAP) (123) (133) (139) (113) (134) (137) (140) are the most commonly used.

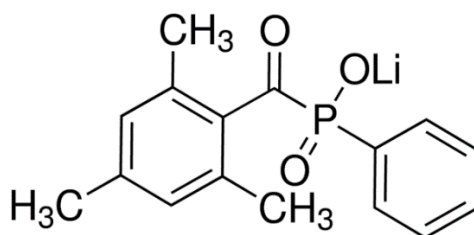


FIGURE 19. CHEMICAL STRUCTURE OF LITHIUM ACYLPHOSPHINATE SALT (LAP) (141)

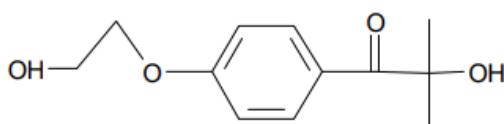


FIGURE 20. CHEMICAL STRUCTURE OF 1-[4-(2-HYDROXYETHOXY)-PHENYL]-2-HYDROXY-2-METHYL-1-PROPANE-1-ONE (IRGACURE 2959) (142)

Beside ensuring the photopolymerization, the degree of methacrylation impacts the gelation time and the properties of the cured material.

The cross-linking density, the mechanical properties and the swelling ratio can be fine-tuned by varying the degree of modification, as explained in some of the following case studies (chapters 5.1-5.6).

In general, a high degree of substitution provides high cross-linking density, that turns into enhanced mechanical properties and stability in time (these features are generally favourable to cells response) (136).

A low level of methacrylation creates defects in the hydrogel network, thus larger pore sizes. The consequence is a higher water absorption and swelling ability (136).

Since natural polymers are usually used for biomedical applications, addressing the biocompatibility/cytotoxicity issue of methacrylated natural polymers is fundamental. For instance, the presence of unreacted methacrylic groups can be cytotoxic; the formation of methacrylic acid, due to the eventual hydrolytic degradation of methacrylate-based complex, can endanger the physiological properties. (143)

In addition, water-solubility is required so to not interfere with cell survival during the photo-crosslinking scaffold fabrication process (144). In water, methacrylates tend to degrade slower and to a lesser extent than acrylates (132). In fact, the methacrylation adds extra hydrophobic methyl groups on the backbone; this results in less hydrophilicity (compared to acrylates) and in steric constraints that hinder the hydrolyzation of the ester bonds.

Nevertheless, the examples below are only a few of the many studies that proved that photo-polymerized methacrylated natural hydrogels are ideal materials for the realization of 3D constructs for bioengineering and biomedical applications.

5.1 POLYSACCHARIDES

5.1.1 CHITOSAN

Chitosan is a linear, cationic polysaccharide deriving from chitin, which is found in crustacean shell. Chitosan is obtained from the deacetylation of chitin, that results in the substitution of acetyl groups with reactive amino group (-NH₂). (145)

Chitosan is a very attractive material for biomedical applications because of its biocompatibility and biodegradability. Especially, ultraviolet (UV) sensitive methacrylated chitosan (CHI-MA) has been extensively used for tissue engineering applications, and subjected to various techniques, such as micropatterning, injectable transdermal curing, extrusion-based 3D printing (146) (147).

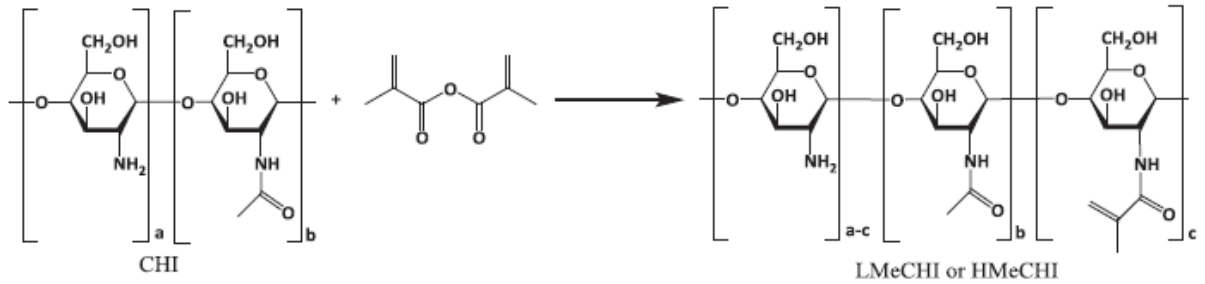


FIGURE 21. REACTION SCHEME FOR THE SYNTHESIS OF METHACRYLATED CHITOSAN (MECHI). LMECHI AND HMECHI ARE CHITOSAN WITH RESPECTIVELY LOW AND HIGH DEGREE OF MODIFICATION. (117)

For instance, CHI-MA was used to yield complex 3D hydrogel structures through DLP. (116) CHI-MA was synthesized by conjugating methacryloyl groups to amino groups of CHI. The incorporated methacryloyl groups endowed the material with hydrosoluble ability and UV crosslinkable ability.

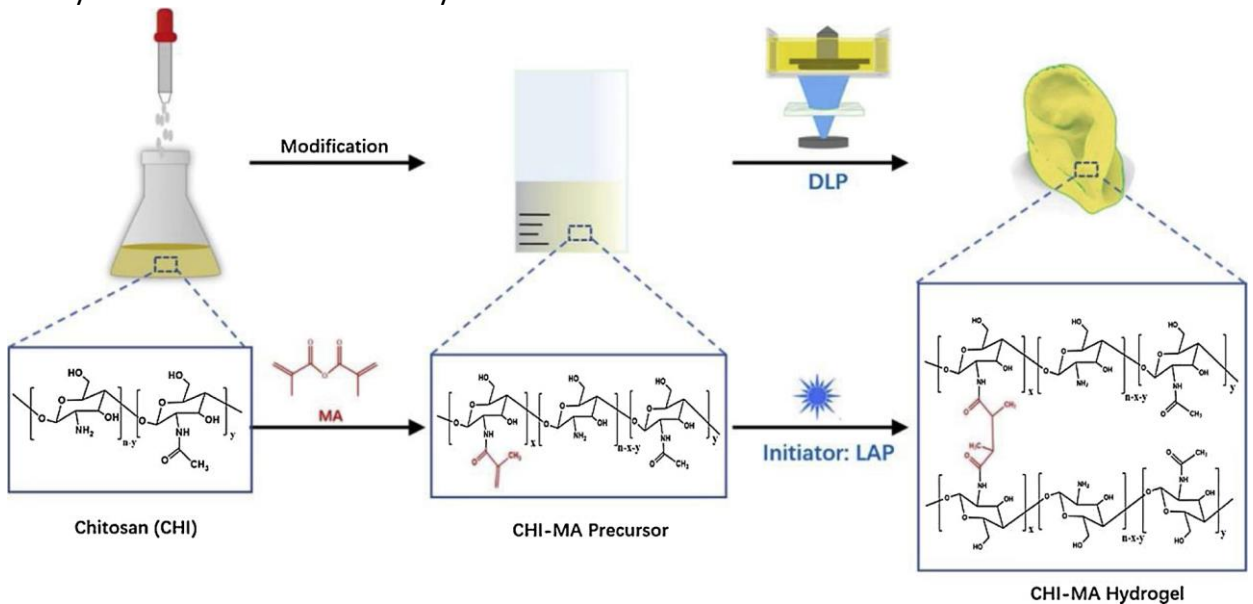


FIGURE 22. MODIFICATION AND DLP-3D PRINTING OF CHITOSAN (109)

The researchers used blue light instead of UV light and LAP photoinitiator. The study revealed that a higher degree of substitution of CHI-MA enhanced the photo-curing efficiency, leading to faster curing time. The so-fabricated hydrogels showed good biocompatibility and high resolution.

Matsuda et al. (148) functionalized a system of chitosan, heparin and hyaluronan with methacryloyl groups. This material was used with methacrylated gelatin to produce tubular structures for tissue engineering applications, through the use of visible light.

Kufelt et al. (135) adapted chitosan, by the addition of glycidyl methacrylate moieties, to two-photon polymerization (2PP) processing. The biocompatibility of the 2PP-fabricated scaffold materials was proved with human pulmonary microvascular endothelial cells (HPMEC).

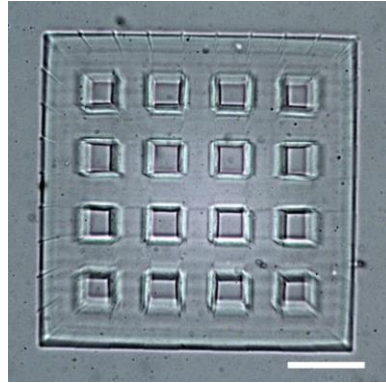


FIGURE 23. MAGNIFICATION OF A CHI-MA SCAFFOLD PRODUCED BY 2PP (135)

5.1.2 HYALURONIC ACID

Hyaluronic acid (HA), also known as hyaluronan, is a glycosaminoglycan linked by $\beta(1,4)$ and $\beta(1,3)$ glucosidic bonds.

Sun et al. (149) used visible light-SLA to produce scaffolds of methacrylated PDLLA-PEG and HA, for cartilage regeneration (figure 24). The material demonstrated good cell viability and relatively high mechanical strength (compressive modulus of 780 kPa).

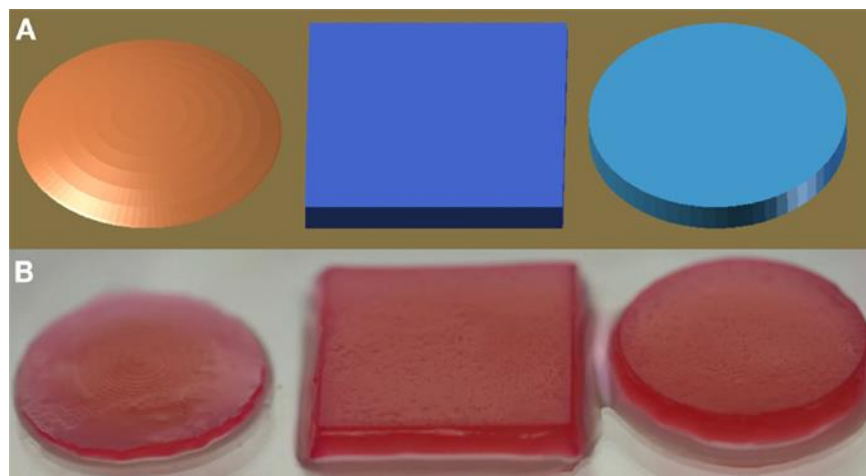


FIGURE 24. CONSTRUCTS OF VARIOUS SHAPES (B) MIMICK PERFECTLY THE CAD MODELS (A) IN PAPER (149)

Another study (150) reported the 3D printing of photopolymerizable MeHA with encapsulated valvular interstitial cells. Physical properties of MeHA were tuned by varying the degree of methacrylation and/or by copolymerizing with PEGDA.

5.1.3 ALGINATE

Alginate is a polysaccharide that has two repeating monomer units, β -D-mannuronate and α -L-guluronate, that are joined by a $\beta(1-4)$ linkage.

Zorlutuna et al. applied SLA on a hydrogel system of oxidized methacrylic alginate (OMA) (linked with RGD), poly(ethylene glycol) methyl ether methacrylate (PEGMEM) and

various cells. The stiffness of the hydrogel (≈ 12 kPa) was demonstrated ideal for culturing skeletal muscle tissue. (151)

Another study analysed a photo-cross-linkable OMA, modified with RGD peptides, and the proliferation of angiogenic cells. The cells activity increased with the increasing of ECM stiffness, that was ascribed to a higher degree of methacrylation. (152)

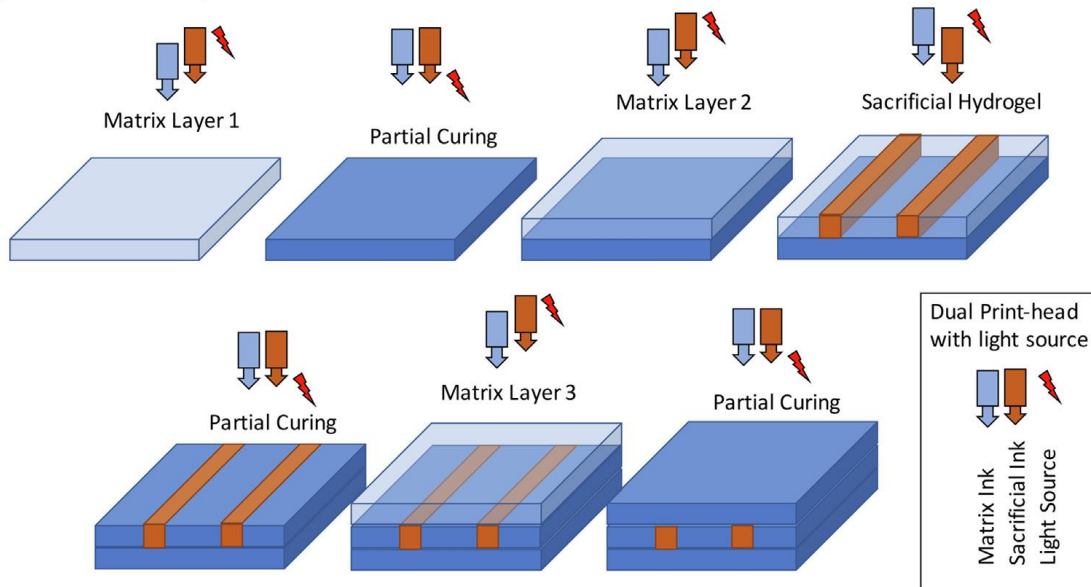
Rouillard et al. (153) examined the roles of the photoinitiators in affecting the cells' viability. They photopolymerized 3D scaffolds of methacrylate-modified alginate and studied cell (chondrocyte) viability. The photoinitiator VA-086 proved to be noncytotoxic at w/v concentrations up to 1.5%; at this concentration, 2-hydroxy-1-[4-(2-hydroxyethoxy) phenyl]-2-methyl-1-propanone (Irgacure 2959) lowered the cell viability. The modulus of 3D constructs was in the 10-20 kPa range.

5.1.4 ALGINATE AND HYALURONIC ACID

A system of methacrylated alginate (MeAlg) and methacrylated hyaluronic acid (MeHA) were used in a novel approach that exploits a sacrificial ink (Pluronic) to produce a robust platform with channels for fabricating vascularized tissues. (133)

MeAlg and MeHA, in the presence of a photoinitiator LAP, formed a hydrogel when exposed to UV light. After complete crosslinking of the hydrogel layer, the sacrificial hydrogel was washed away to create channels.

PRINTING APPROACH



POST-PRINTING PROCESS

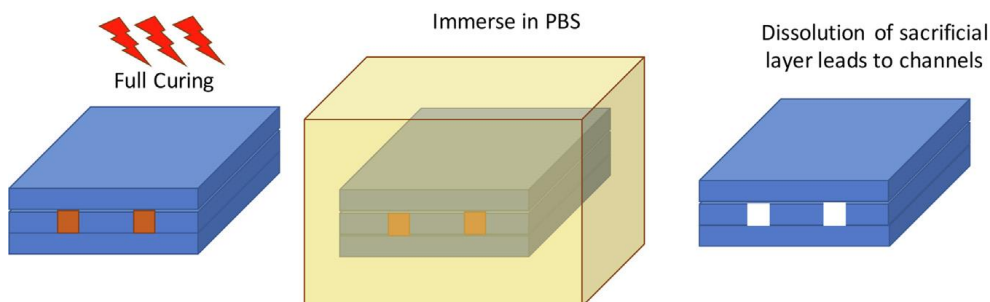


FIGURE 25. PRINTING APPROACH THAT USES A SACRIFICIAL INK (131)

Endothelial cells were incorporated into the photocurable inks formulations and remained highly viable within the hydrogel. The researchers analysed how methacrylation allows the photopolymerization and influences the degree of crosslinking. In addition, they highlighted the fact that methacrylates undergo a Michael-type addition reaction with thiols, thus allowing the incorporation of bioactive molecules containing cysteine groups into hydrogel matrix. This could be useful to enhance the stem cell adhesion (e.g. by tethering RGD-peptide).

5.2 POLYPEPTIDES

5.2.1 GELATIN

Gelatin is obtained by denaturing the triple helix structure of collagen, the major component of musculoskeletal tissue. (132)

The functionalisation of gelatin introduces methacryloyl substitution groups on the reactive amine and hydroxyl groups and produces GelMA (gelatin methacryloyl or methacrylated gelatin)

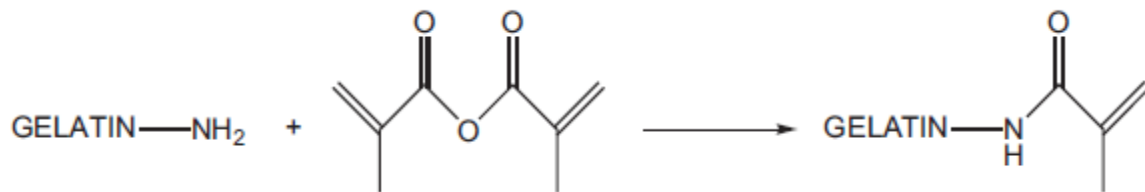


FIGURE 26 SYNTHESIS OF GELMA (154)

Among all the natural hydrogels, gelatin is probably the most extensively studied so far, as concerns 3D printing and photopolymerization. Many studies have demonstrated the successful applications of GelMA in bioprinting, especially using photopolymerization (115) (155) (156). The methacryloyl groups allow the photopolymerization, whereas the gelatin backbone grants the biocompatibility.

As for photoinitiators, Irgacure 2959 (138) and (LAP) (140) are the most frequent choices. Billiet et. al. (115) used a bioplotter to print a macroporous GelMA construct, using VA-086 as photoinitiator. They controlled the printing parameters (temperature, needle's pressure, curing irradiation dose and so on) to obtain mechanically stable scaffolds, that display high viability and an interconnected pore network in the range of 10-20 w/v%.

Wadnap et al. fabricated tubular structures of GelMA hydrogels, through DLP process. The cells' viability was confirmed, but the study revealed that the tensile properties slightly decreased when living cells are encapsulated. (134)

DLP was similarly used by Krishnamoorthy et al. (157) to create GelMA 3D four-branch vascular-like scaffolds (figure 27).

The study attested the GelMA degree of functionalization as the main factor influencing the photopolymer solution's optical properties. In fact, the researchers observed an increase in the GelMA degree of functionalization corresponded to a reduction of the UV penetration depth.

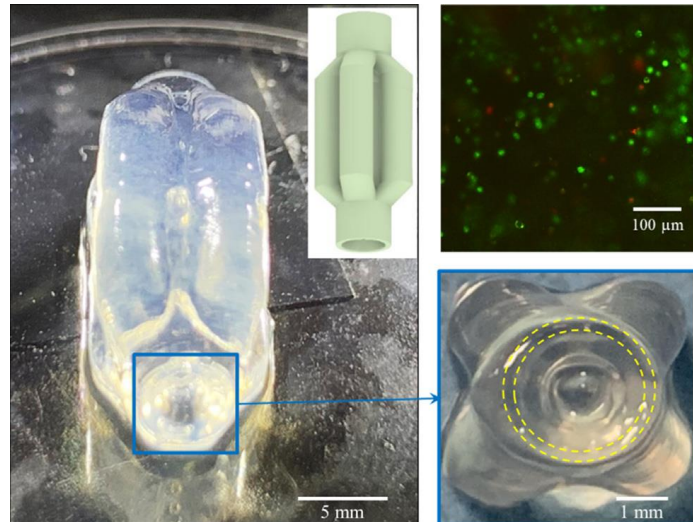


FIGURE 27. FABRICATED 3D VASCULAR-LIKE CONSTRUCT AND THE CELL VIABILITY TEST. THE PART POSSESSES A HOLLOW CROSS SECTION (157)

Finally, DLP was used to develop a GelMA-hydrogel multichannel construct, that mimics the intricate structure of the nerve. (158) The scaffold provided support and proliferation of cells for neural regeneration. The mechanical strength of the hydrogels proved to be inferior than native nerve; so the researchers suggested the addition of some component to enhance the mechanical properties of GelMa. In general, developing hybrid hydrogels based on GelMA has been used as a tool to increase the mechanical strengths of GelMA hydrogels. Generally, GelMA is commonly blended with methacrylated hyaluronic acid (159), alginate (160), or alginate blends.

5.3 PROTEINS

5.3.1 SILK FIBROIN

Silk is a natural fibrous polymer composed of two proteins, fibroin and sericin. Silk fibroin (SF) has aroused much interest for biomedical applications due to biocompatibility, biodegradability, high tensile strength, and excellent biological characteristics such as proliferation of various cells.

Hong et al. (139) modified Silk fibroin with glycidyl-methacrylate to obtain glycidyl-methacrylate silk-fibroin (Silk-GMA) for DLP 3D printing.

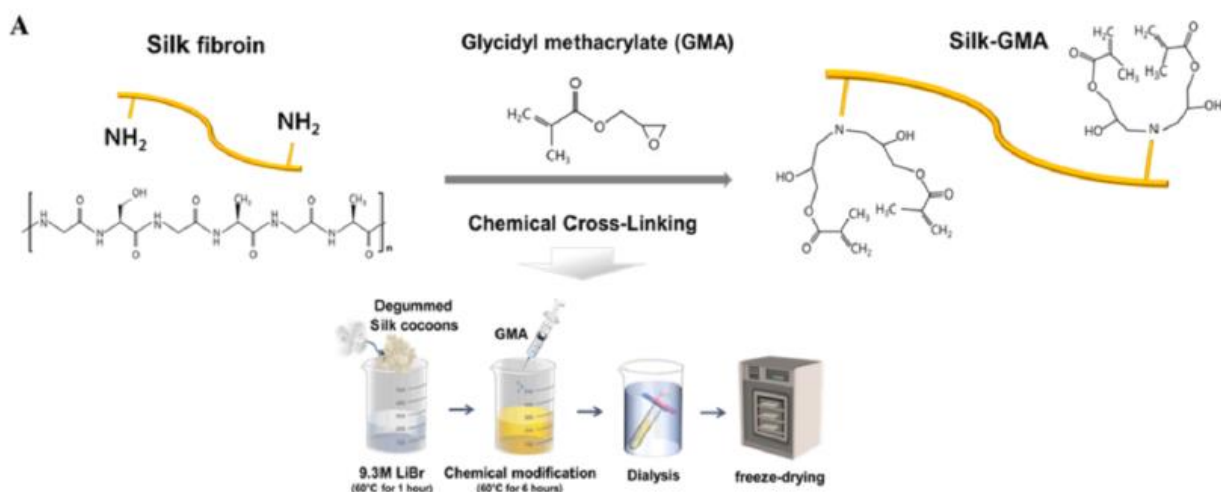


FIGURE 28. SYNTHESIS OF SILK-GMA (137)

SF modification consists in the addition of methacrylate groups to amine residue groups of hydrogels.

The study focused on the clinical application for trachea injury patients. Artificial trachea was printed by DLP printer with chondrocyte from rabbit ear (figure 29).



FIGURE 29. CELL-LOADED ARTIFICIAL TRACHEA FABRICATED BY DLP PRINTER (137)

Kim et al. (161) chemically modified SF with glycidyl methacrylate (GMA) to obtain Silk-GMA. The material was DLP 3D printed with chondrocytes.

In another study (162), SF-methacrylate (SFMA) was synthesized with the addition of 2-isocyanatoethyl methacrylate (IEM) to hydrolysed SF (that was previously dissolved in dimethyl sulfoxide (LiCl/DMSO)). The hydroxyl groups of SF played a key role in IEM functionalization, as shown in figure 30.

The degree of methacrylation, that increased with an increase of input IEM in synthesis, was the main factor that shorten gelation time. A higher degree of substitution increased the effect of polymer concentration on the hydrogel properties. Finally, the photo-cured SFMA hydrogel was compared to physically crosslinked SF one: the photo-crosslinked material demonstrated higher elasticity.

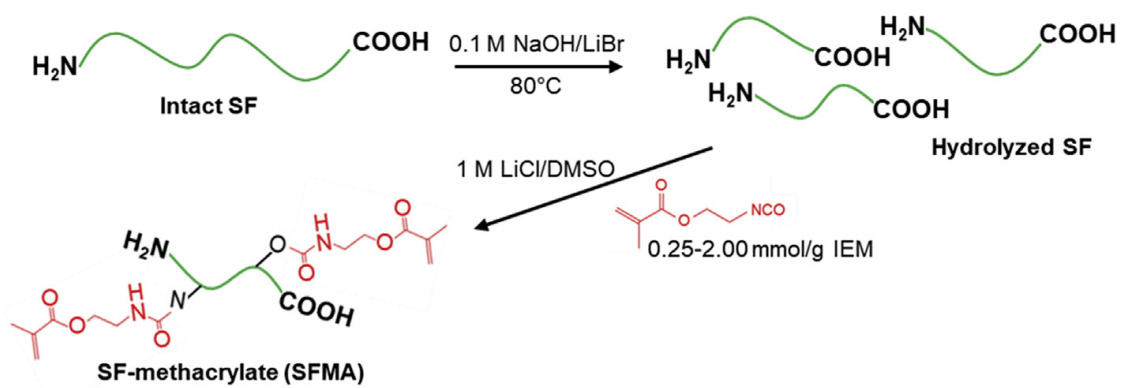


FIGURE 30. SYNTHESIS OF SFMA (139) WITH IEM

6. AIM OF THE WORK

This thesis focused on combining the benefits of DLP-3D-printing as a fabrication technique and the peculiarities of hydrogels. These last were based on carboxymethylcellulose, that was methacrylated in order to produce a photoreactive (and then, DLP-printable) material.

In particular, this work was aimed at the printing of methacrylated carboxymethylcellulose (M-CMC) hydrogels filled with cellulose nanocrystals (CNCs), so as to investigate the nano-reinforcers' effect on the mechanical properties of the 3D-printed material.

Unfortunately, the experimental activity was interrupted due to the lockdown imposed by the Covid-19 emergency. This affected the number of mechanical tests and the statistical validity of the results. Therefore, the thesis reports considerations that can be drawn from these preliminary results.

7. MATERIALS AND METHODS

7.1 MATERIALS

Carboxymethyl cellulose is a cellulose ether. This water-soluble polyelectrolyte derives from the partial substitution of the 2, 3, and 6 hydroxyl groups of cellulose by hydrophilic carboxymethyl groups. (163) (59)

The CMC sodium salt appears as a white, granular, tasteless and odourless powder, soluble in water or in alkaline solutions.

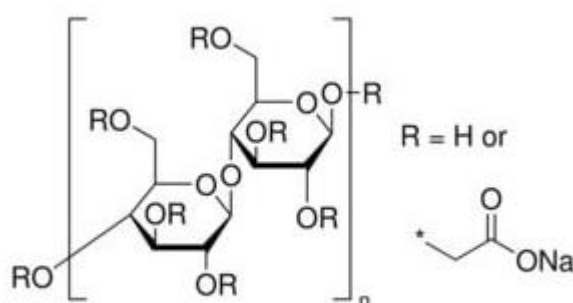


FIGURE 31. CARBOXYMETHYL CELLULOSE SODIUM SALT CHEMICAL STRUCTURE (164)

Main properties of CMC are hydrophilicity, due to the carboxylate groups, bioadhesion, related to polyanionic nature, non-toxicity and gel-forming ability. (165)

Carboxymethyl cellulose sodium salt (CMC) medium viscosity and methacrylic anhydride (MA) were purchased from Sigma Aldrich.

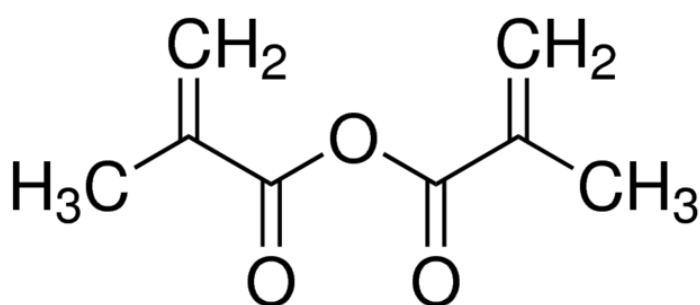


FIGURE 32. METHACRYLIC ANHYDRIDE (166)

The photoinitiator is the bismesitylphosphinic acid BAPO-OH, that derives from the functionalization of phenylbis-(2,4,6-trimethylbenzoyl)-phosphine oxide (BAPO, figure 33) with a OH group. BAPO's derivatives are used in UV-curable formulations, where they start a Norrish type I reaction upon light exposure. (167) The BAPO-OH photoinitiator was kindly provided by Prof. Gruetzmacher's group (ETH Zurich).

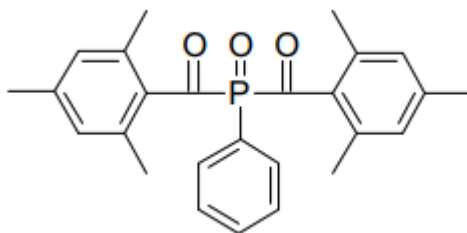


FIGURE 33. BAPO CHEMICAL STRUCTURE. (168)

Nanocellulose can be produced from various cellulosic sources: plants, wood, cotton, animals, bacteria and oil palm biomass (OPB). (169) (170)

Chang (171) reported that the production of 1 tons of palm oil from a fresh fruit bunch generates 2.3 tons of biomass (palm fibers, palm shells, empty fruit bunches...), that represents an unexpensive, renewable source. In particular, nanocellulose crystals can be isolated from the empty fruit bunches to replace synthetic or petrochemical-based materials as reinforcers in nanocomposites.

Oil palm empty fruit bunch based cellulose nanocrystals (OPEFB-CNC) used in this work were provided by researcher A.A. Septevani, from the Indonesian Institute of Sciences.

7.2 CELLULOSE FUNCTIONALIZATION

First, 6.00 g of CMC were dissolved in 300 mL of water, under magnetic stirring. The pH was adjusted to 11.0 with 0.5 M sodium hydroxide (NaOH). The solution was left under stirring overnight. After cooling the solution at 2 °C, 12 mL of MA were added dropwise. The reaction proceeded for 24 hours at 0°C; the pH was periodically adjusted to 8.0 with the NaOH solution. The following steps involved precipitation and washing of the solution with 1 L of ethanol, to remove the unreacted methacrylic acid and methacrylic anhydride. After 3 days of dialysis against water, the methacrylated product (M-CMC) was freeze dried.

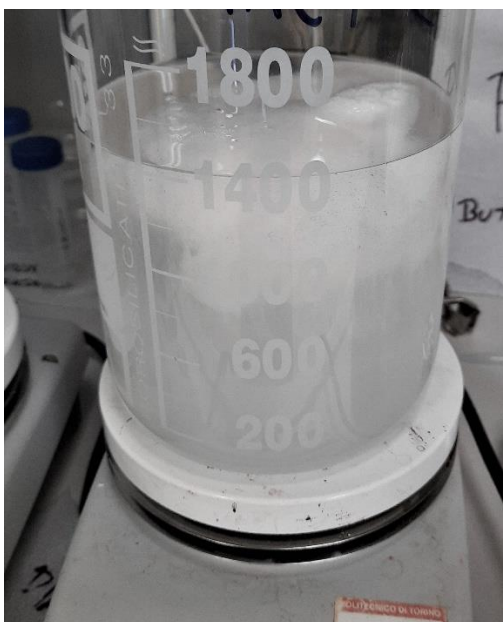


FIGURE 34. CMC AND MA SOLUTION AFTER WASHING WITH ETHANOL

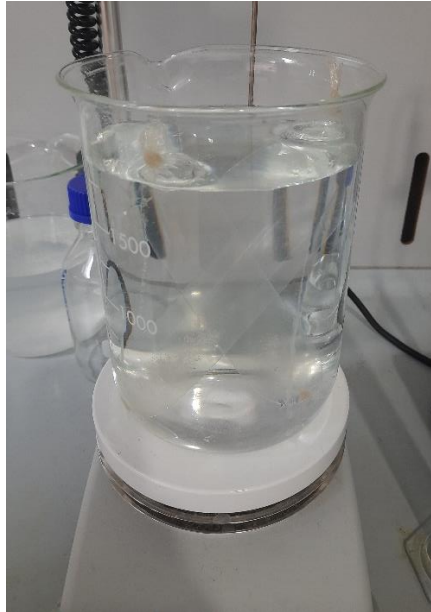


FIGURE 35. DIALYSIS

7.3 PREPARATION OF THE HYDROGEL FORMULATIONS

This study focused on two types of hydrogels:

- “Neat hydrogels”, composed of water, methacrylated carboxymethyl cellulose M-CMC and bismesitoylphosphinic acid BAPO-OH.
- “Composite hydrogels”, that are neat hydrogels reinforced with oil palm empty fruit bunch based cellulose nanocrystals OPEFB-CNC (they will hereafter be referred as CNCs).

7.3.1 NEAT CELLULOSE HYDROGELS (M-CMC SAMPLES)

Different concentrations of M-CMC (methacrylated carboxymethylcellulose) were dissolved in water.

The mixture was left under magnetic stirring at 40 °C until a homogenous solution was achieved.

Then, 2 phr (per hundred resin) of BAPO-OH were added with respect to M-CMC.

The prepared samples are summarized in Table 3.

7.3.2 COMPOSITE HYDROGELS (CNC/M-CMC SAMPLES)

The cellulose nanocrystals were added in a 20 mg/mL water solution of M-CMC, prepared under magnetic stirring at 40 °C. Afterwards, 2 phr (respect to M-CMC) of BAPO-OH were added.

The formulations' compositions are reported in Table 3.

M-CMC [mg]	CNC [mg]	BAPO OH [phr*]
20	--	2
30	--	2
40	--	2
20	10	2
20	20	2

TABLE 3. COMPOSITION OF THE TESTED SAMPLES FOR 1 ML OF WATER (*PHR WITH RESPECT TO M-CMC)

7.4 3D-PRINTING

3D printing via Digital Light Processing was done in ASIGA MAX™, connected to a UV source (figure 36).

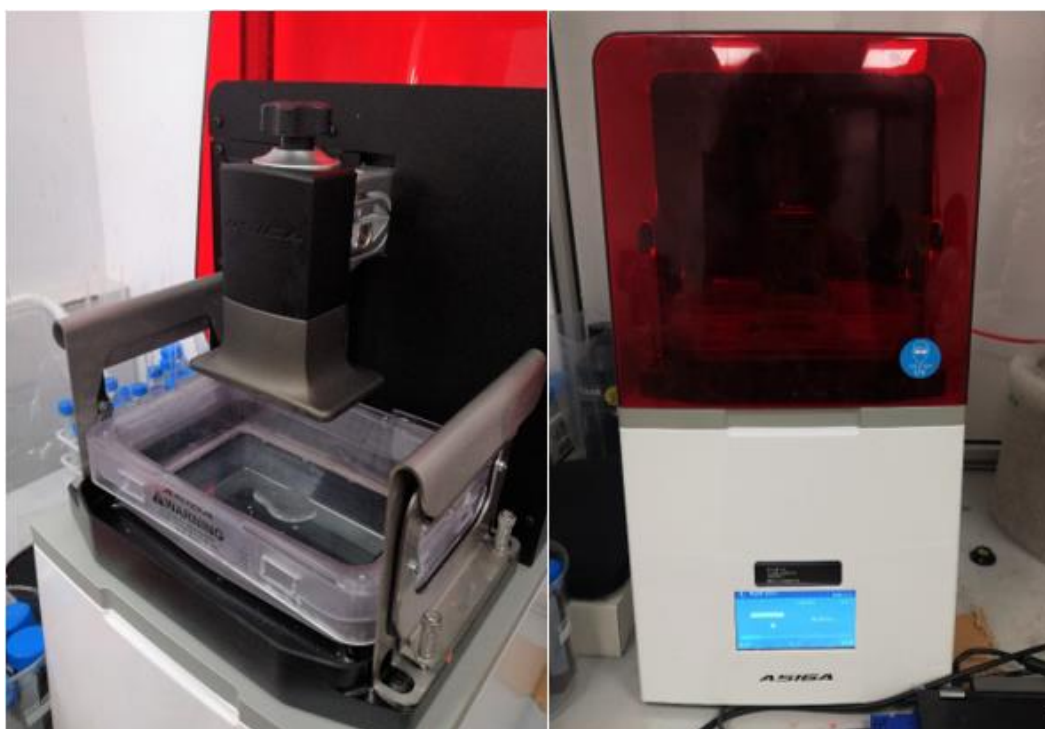


FIGURE 36. DLP PRINTER

20 mg/mL concentration of M-CMC was used for both M-CMC and NC/M-CMC samples. M-CMC/DMEM formulations were printed, too. Parts of shapes various were printed, each corresponding to a STL file.

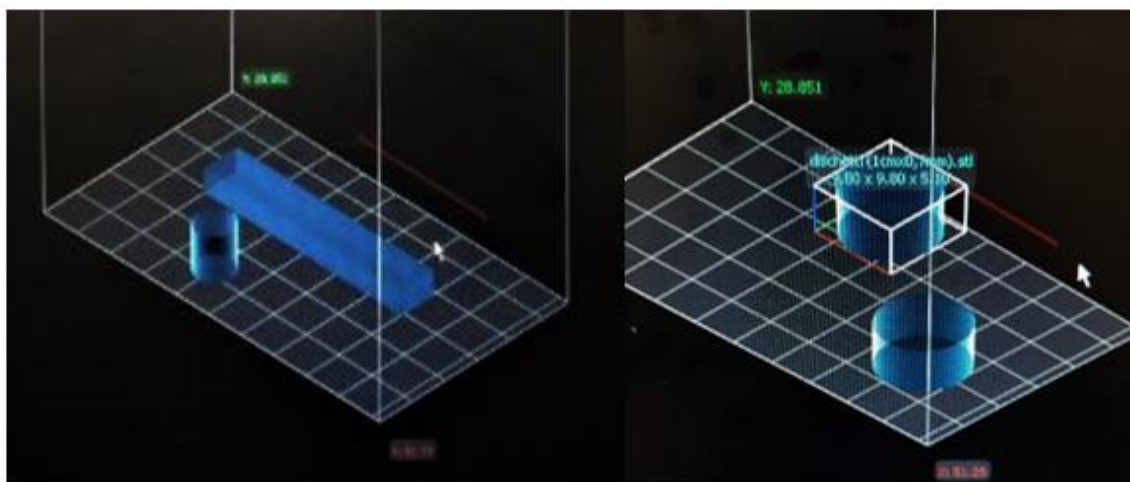


FIGURE 37. STL FILES FOR THE 3D PRINTING OF VARIOUS PARTS

Before printing, the build parameters must be settled up.

In particular, the optimization of the process goes through the selection of five parameters:

-the **light intensity**

-the **slice thickness**: i.e. the layer thickness, that usually is between 16 μm and 150 μm (172)

-the **exposure time** of each layer under the light source. If it is too low, it affects the adhesion between layers; if it is too high, the definition of the build decreases. (172)

-the **burn-in layers** is the number (usually less than 10) of layers that are cured right after the first one and whose parameters can be specifically settled.

-the **burn-in exposure time** is the exposure time of the burn-in layers. It is usually longer than the exposure time to ensure the adhesion to the building platform.

The choice of the optimal parameters is commented in the Results section (chapter 8.2 3D printing).

The printed parts were then post-cured under UV light for 90 seconds.

7.5 CHARACTERIZATION

7.5.1 H-NMR

Proton nuclear magnetic resonance (H- NMR) spectra were collected to confirm the functionalization and to determine the methacrylation conversion of modified CMC.

H-NMR is a spectroscopic technique that gives access to details of the molecules' structure by observing the atomic nuclei's response to a magnetic field.

^1H NMR spectra were recorded by a Bruker advance DPX-400 nuclear magnetic resonance spectrometer at 25°C in D_2O .

The ^1H NMR spectrum of neat CMC was collected for reference and compared to that of the modified material.

The degree of substitution was calculated as the ratio between the total integral of the peaks in M-CMC related to methacrylate side groups and the total integral of the anhydrous glucose unit of CMC backbone.

7.5.2 PHOTOREOLOGY

Photoreology tests aim to describe the rheological behavior and the photoreactivity of the formulations. Rheometers can operate with either continuous rotation or rotational oscillation.

The former mode's output is the flow curve, that provides the evaluation of viscosity as a function of shear strain (or shear stress), time or temperature.

Instead, the viscoelastic properties (i.e the combination of elastic and viscous behaviour when the material is sheared) are assessed with oscillatory tests, based on the application of a sinusoidal strain or stress. Then, the response of the material can be observed in function of temperature, time, amplitude or frequency. In particular, for viscoelastic material there are two parameters of interest: the storage shear modulus G' and the loss shear modulus G'' , namely the elastic and viscous components of material's behaviour. In fact, G' is related to the stored deformation energy, while G'' represents the deformation energy that is dissipated through internal friction when flowing.

The analysis of these parameters under proper conditions provides useful information about the kinetics of curing.

The tests were performed with an Anton Paar rheometer (Physica MCR 302) in parallel plate mode, equipped with a UV-light source (Hamamatsu LC8 lamp, light intensity 25 mWcm^{-2}). The light passes the bottom, quartz plate, on which the formulation is placed. While moving, the upper plate applies the shear stress on the material.

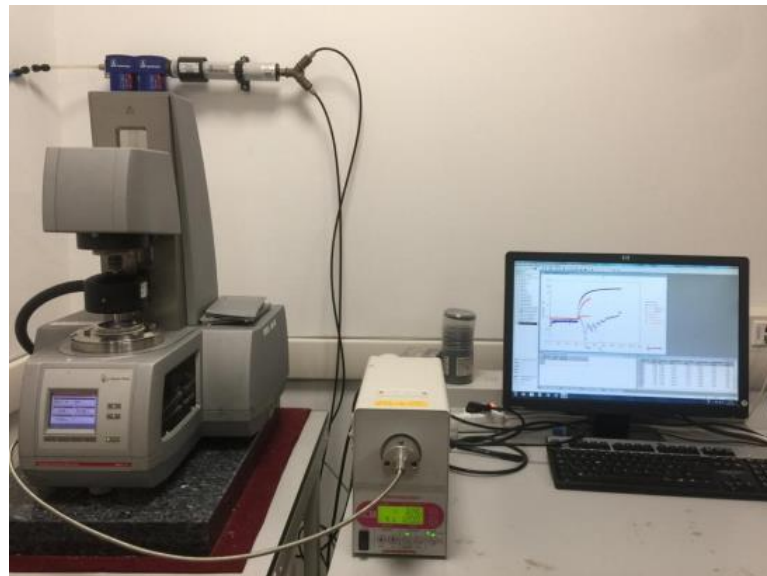


FIGURE 38. PHOTO-RHEOMETER EQUIPMENT

The tests were performed at room temperature.

The analysis that were carried out are as follows:

-Amplitude sweep test. For this test, the shear frequency was kept at a constant value (1 Hz) and the shear amplitude was step-wise increased from 0.01% to 100%. The test was performed twice, prior to and following the photopolymerization. The result is a graph

with strain (or shear stress) plotted on the x-axis and G' and G'' plotted on the y-axis. The range of strain rate in which G' and G'' are constant is the linear viscoelastic region (LVR), where the material shows a linear response. The LVR also represents the range of strain rate in which the test can be performed without destroying the structure of the sample. As for the cured samples, the value of G' in LVR indicates the stiffness of the hydrogel. The evaluation of G' curve gives information on the stability of the material, too. In fact, its downturn represents the limit of LVR, after which the solid structure of the hydrogel starts breaking.

-**shear rate test** on the uncured material, to measure viscosity with the increasing of the shear.

The rheometer operates with continuous rotation and records values of shear rate and shear stress.

The software measures the shear rate from the angular velocity Ω [rad/s] of the motor, the plates' radius r of the plates and the distance h between plates (see equation 1).

$$\dot{\gamma} = \Omega \times \frac{r}{h}$$

EQUATION 1. SHEAR RATE EQUATION

Shear stress is measured using equation 2:

$$\tau = \frac{2}{\pi r^3} \times M$$

EQUATION 2. SHEAR STRESS EQUATION

where M [N m] is the torque of the rheometer.

Then, the software calculates the viscosity applying the law of viscosity for each measuring point:

$$\eta = \frac{\tau}{\dot{\gamma}} = \frac{M}{\Omega} \times K$$

EQUATION 3. VISCOSITY EQUATION

In equation 3, K is a constant related to the geometric configuration of the rheometer.

The output is the curve η vs $\dot{\gamma}$, that describes the flow behavior under a shear rate ramp.

- **Photorheology: time sweep test** to study the photo-reactivity of the material. In time-sweep tests, the shear-strain amplitude and (angular) frequency are kept constant (1% and 1 Hz). As a result, G' and G'' time-dependent functions can be analysed. Light was switched on after 60 s to allow the system to stabilize before the onset of polymerization. What is expected is that G'' remains larger than G' before the photocuring and that, after the lighting of the lamp, G' increases and becomes larger than G'' , proving the hydrogel formation.

Two time-points can be evaluated. The first is t_{cr} , that represents the time G' starts raising, displaying the beginning of the curing process; the second one is t_{gel} , that is the gel transition point, where $G'=G''$. In addition, the final values of G' and G'' can be evaluated.

7.5.3 COMPRESSION TESTS

A MTS Qtest/10 instrument equipped with 10N cell load was used.

The samples were cylinders obtained by DLP.

The dimensions set in STL files were: diameter $\phi=8.80$ mm, height $h=6.10$ mm. The accuracy of the printing was about ± 0.5 ; then each sample was measured before testing.

The formulations chosen for the compression tests are summarized in table:

M-CMC [mg]	CNC [mg]	BAPO-OH [phr*]
20	-	2
20	10	2

TABLE 4. COMPOSITION OF THE PRINTED SAMPLES FOR 1 ML OF WATER (*PHR WITH RESPECT TO M-CMC)

A piece of sandpaper was placed below the samples to prevent the hydrogel to slip away during the test (figure 39).

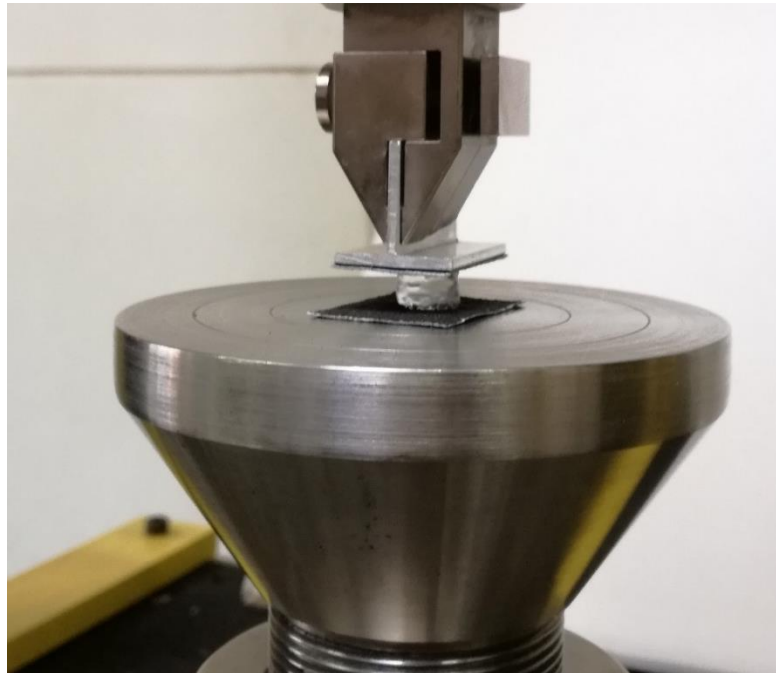


FIGURE 39. HYDROGEL SAMPLE SUBJECTED TO COMPRESSION TEST

The test was stopped at the failure of the sample.

Load (N) and displacement of the crosshead (mm) were collected during the experiments; stress and strain were derived as the ratio of load to area and the ratio of displacement to height. The values of area and height were referred to the uncompressed samples.

Samples were tested in single compression mode and in cyclic compression mode.

7.5.3.1 SINGLE COMPRESSION TESTS

The single compression tests were carried out as a displacement-controlled test. The specimen was clamped between the upper and bottom plates. The upper plate moved down at constant rate, compressing the sample. The load cell measured the load supported by the sample at any particular displacement. Independently of the load trend, the displacement increased.

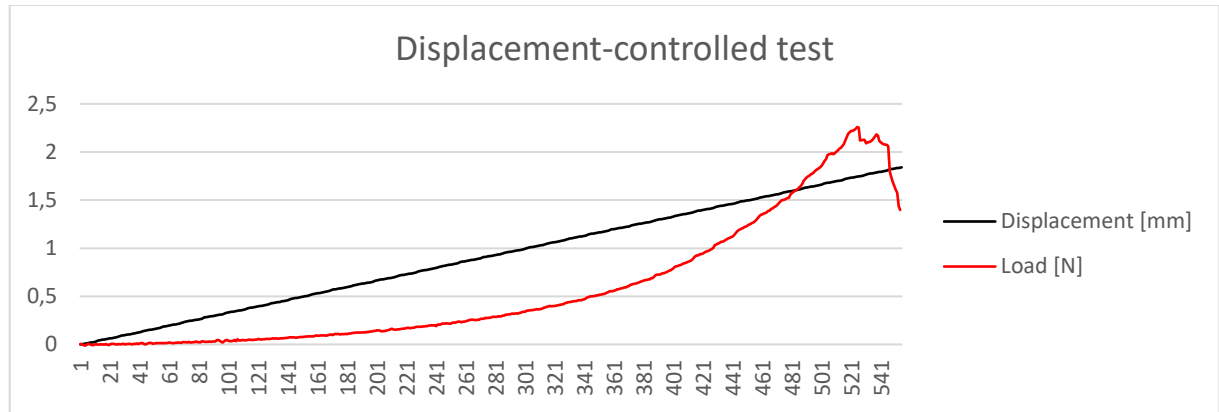


FIGURE 40. DISPLACEMENT-CONTROLLED TEST. THE DISPLACEMENT INCREASES REGULARLY AND THE MACHINE MEASURES THE INSTANTANEOUS LOAD SUSTAINED BY THE SAMPLE

The parameters of single compression tests were:

- minimum load: 0.01 N
- maximum load: -5 N
- test speed: 1 mm/min

The compressive modulus was calculated as:

$$E = \frac{\Delta\sigma}{\Delta\varepsilon}$$

$\Delta\sigma$ is the stress increment, $\Delta\varepsilon$ is the strain increment in an appropriate range of deformation.

7.5.3.2 CYCLIC COMPRESSION TESTS

The cyclic tests were performed by imposing the maximum stress. At each cycle, the displacement increased until the load reached the value corresponding to the settled maximum stress.

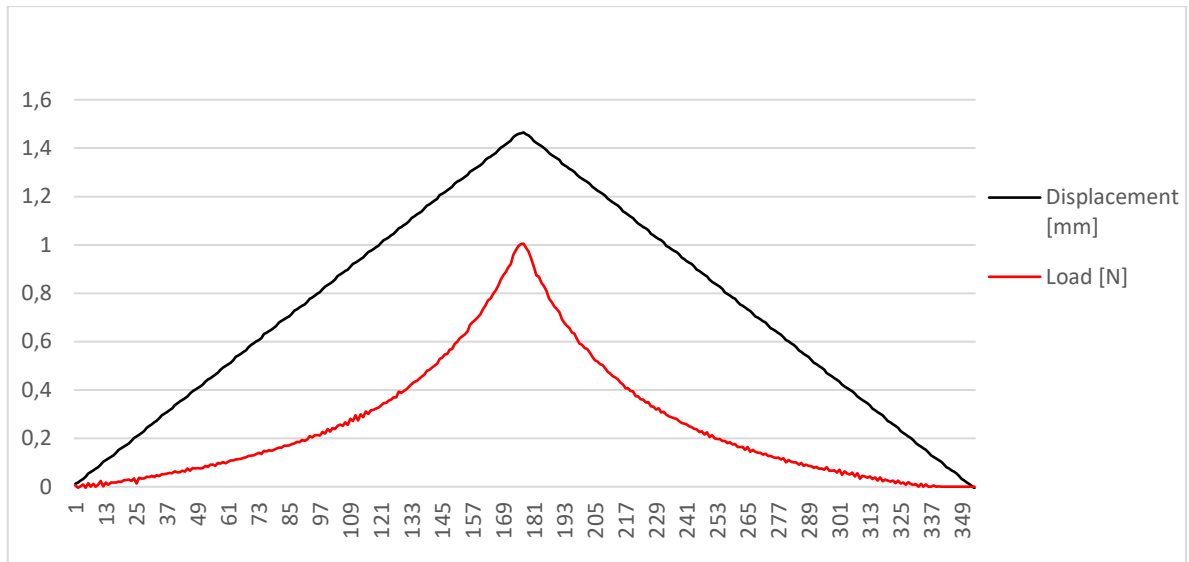


FIGURE 41. TREND OF LOAD AND DISPLACEMENT IN A CYCLE

The parameters for cyclic tests were:

-minimum load: 0.025 N

-test speed: 5 mm/min

- maximum load was set to obtain a maximum stress of 60 MPa.

For each cycle, the value of E corresponding to the maximum stress σ_{max} was evaluated as

$$E_{max} = \frac{\sigma_{max}}{\epsilon_{max}}$$

Where ϵ_{max} is the strain measured when $\sigma = \sigma_{max}$.

The dissipative energy, for each cycle, was measured as:

$$U = \int_{loading} \sigma d\epsilon - \int_{unloading} \sigma d\epsilon$$

8.RESULTS

8.1 H-NMR

The methacrylation CMC process was performed using methacrylic anhydride (MA) as methacrylation agent. In these conditions, the reaction of fully deprotonated alcohol groups of CMC and MA led to graft methacrylate functional groups distributed along the CMC backbone (M-CMC) (fig.42).

The effective functionalization of the polymer was evaluated by H-NMR (figure 43). In the spectrum of neat CMC, the resonance of CMC skeleton was located between $\delta = 2.7$ and 5 ppm. For M-CMC, additional peaks were observed at $\delta = 6.1/5.7$ ppm and at $\delta = 1.9$ ppm, which are respectively related to vinyl and methyl groups. Their presence attested the successful methacrylation of the material. The peaks related to methacrylic groups are associated with 5 hydrogen, the anhydrous glucose unit are related to 8.4 hydrogen. Taking this into account, the degree of substitution was measured 0.6, according to the method reported previously.

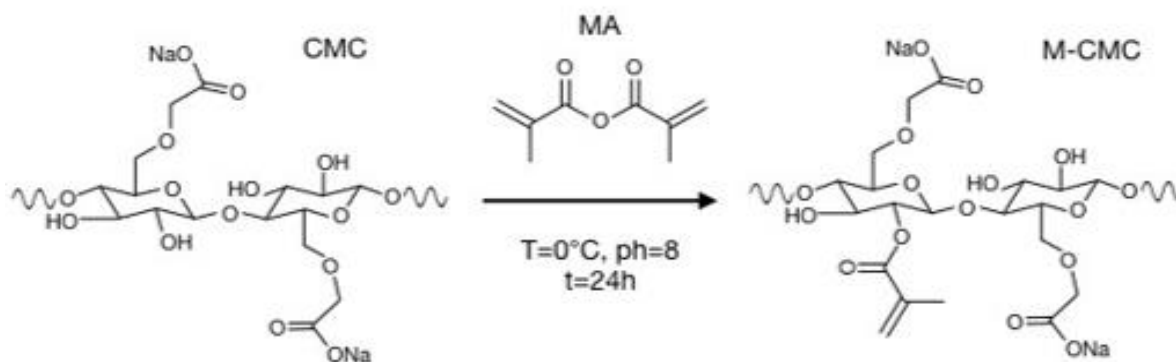


FIGURE 42. POSSIBLE SCHEME FOR METHACRYLATION OF CMC

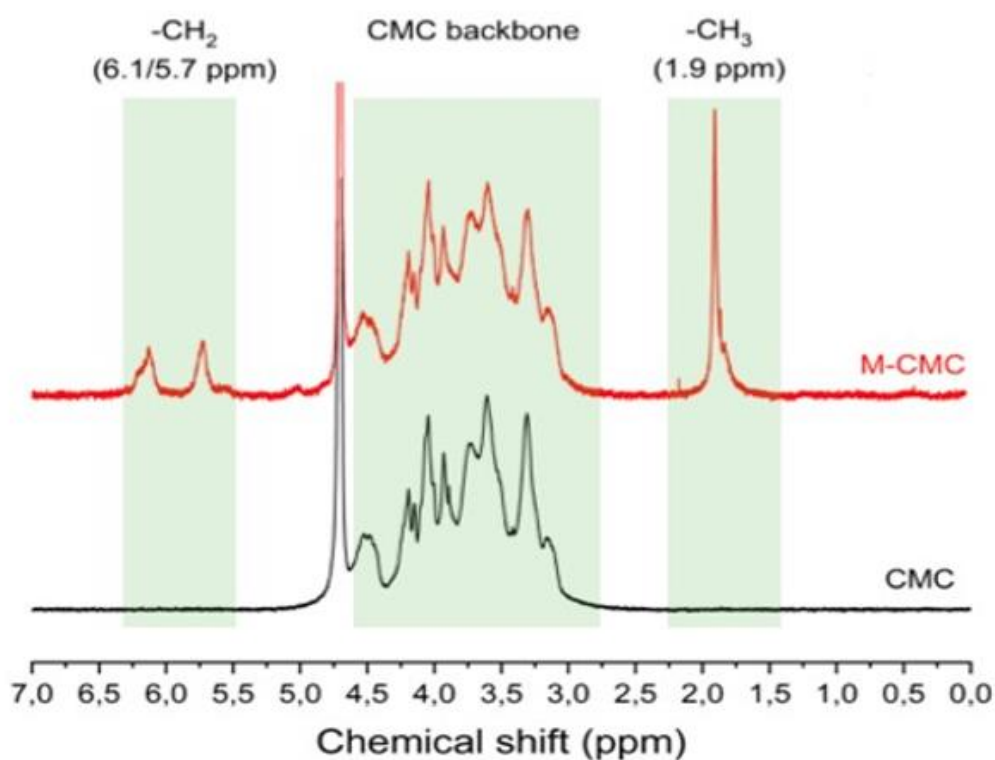


FIGURE 43. ¹H-NMR SPECTRA FOR M-CMC (RED) AND NEAT CMC (BLACK).

8.1 PHOTOREOLOGY

According to the results of the amplitude sweep tests on the uncured material, for each formulation the oscillatory experiments were performed in the LVR (strain amplitude of 1%).

8.1.1 NEAT SAMPLES

Viscosity is a fundamental aspect in evaluating the printability of a material. As a rule of thumb, viscosity should be low, to obtain good fluidity and shorter fabrication time. In fact, low viscosity facilitates the interaction between the reactive functionalities, thus

increasing the cure rates. In addition, low viscosity is beneficial for many hydrogels' applications, such as drug delivery (173) and cells' cultures (174).

The solutions of neat M-CMC showed a shear-thinning (or pseudoplastic) behavior, characterized by decreasing viscosity with increasing shear rate (figure 44)

In addition, viscosity increased with M-CMC concentration, as expected.

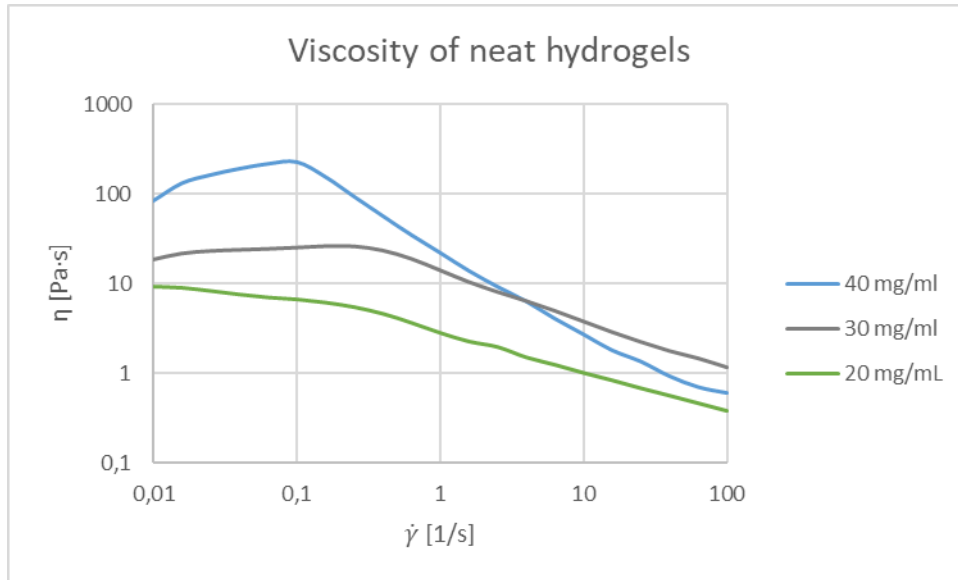


FIGURE 44. VISCOSITY VS SHEAR RATE CURVES OF NEAT M-CMC SAMPLES

Photoreology is a useful tool to investigate the reactivity of the formulations. It provides, as indication, the time required to reach the gel point, that is a helpful information for the selection of the exposure time during the 3D-printing. figure 45 displays the output of the time sweep tests of the neat samples.

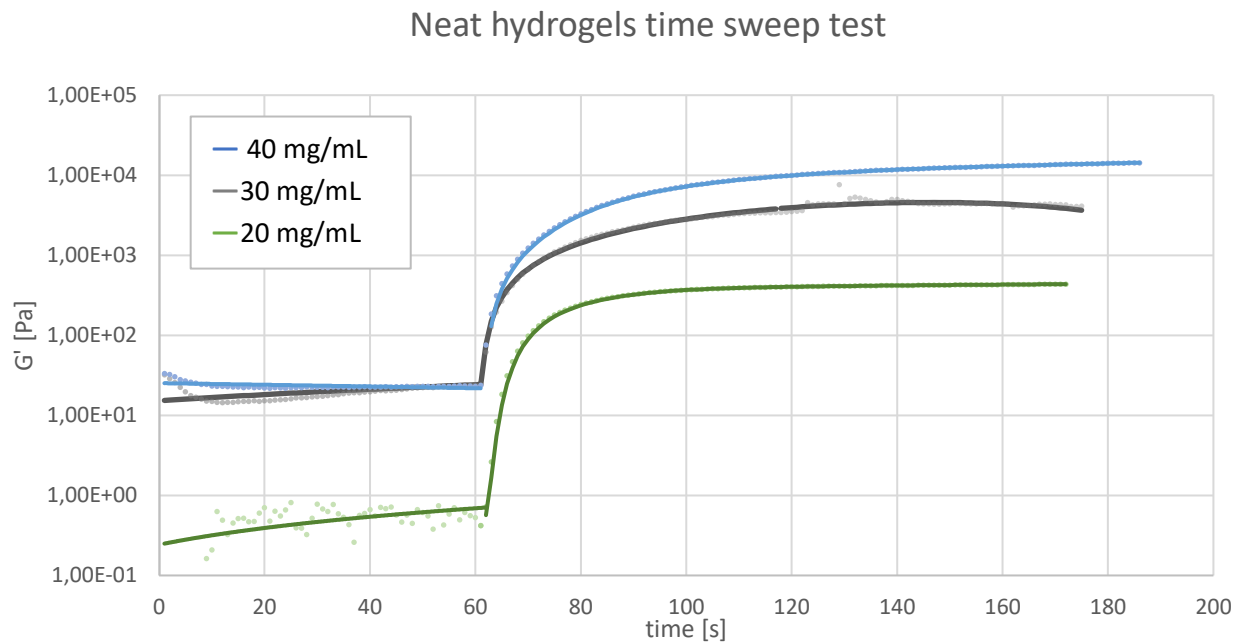


FIGURE 45. TIME SWEEP TEST ON NEAT SAMPLES WITH DIFFERENT CONCENTRATION OF M-CMC

The fast rise of G' after the lamp was turned on, demonstrated that all three formulations reacted to UV light, and that the curing times were rapid.

figure 46 shows an enlargement of the curve of 20 mg/mL formulation. For the 20 mg/mL formulation, t_{cr} and t_{gel} were more evident, due to the more liquid nature than that of 30 mg/mL and 40 mg/mL formulations. This aspect, that is caused by the lower concentration of M-CMC, meant that 20 mg/mL formulation was the one chosen for the 3D-printing.

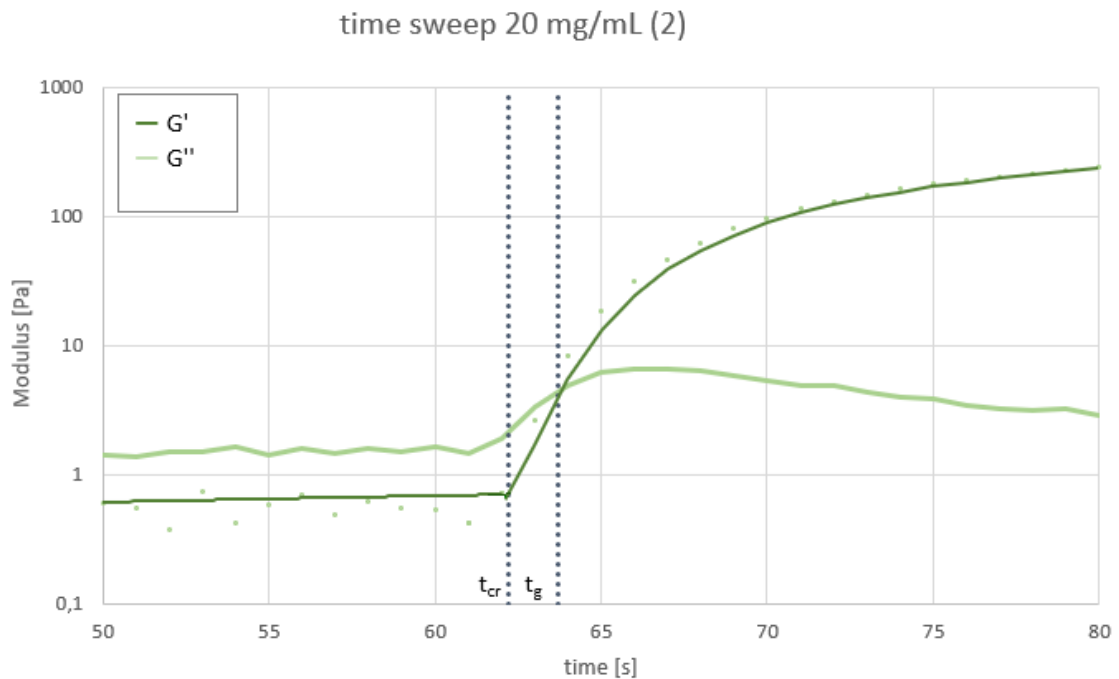


FIGURE 46. DETAIL OF THE TIME SWEEP CURVE OF 20 MG/ML SAMPLE OF NEAT M-CMC. THE VALUE OF G' AND G'' ARE REPORTED IN THE RANGE OF TIME BETWEEN 50 S AND 80 S.

Initially, $G'' > G'$, meaning that the material acts like a viscous liquid system. At the end of the test, $G' > G''$, due to the solid-nature of the cured hydrogel.

At $t=t_{cr}$, G' started growing faster, due to the crosslinking reactions. The hydrogel formed at $t=t_{gel}$, when $G'=G''$. Thereafter, G' became larger than G'' , indicating the prevalence of the elastic solid component. This attested that the formulations were photocurable and, then, potentially printable by DLP.

The influence of the M-CMC concentration is showed in figure 47. The final value of G' ($G_{plateau}$) increased with M-CMC concentration, according to a power-law correlation.

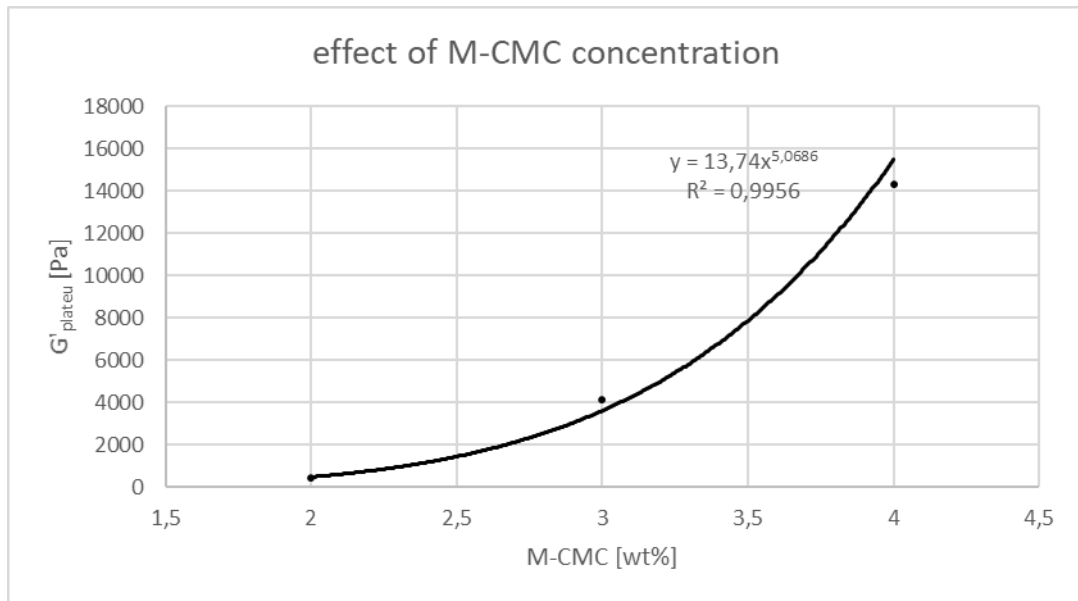


FIGURE 47. DEPENDANCE OF THE FINAL STORAGE MODULUS ON THE M-CMC CONCENTRATION IN NEAT HYDROGELS.

The result of the amplitude sweep tests (figure 48) attested that every formulation was cured ($G' > G''$) and that each hydrogel was stable in a large range of strain rate.

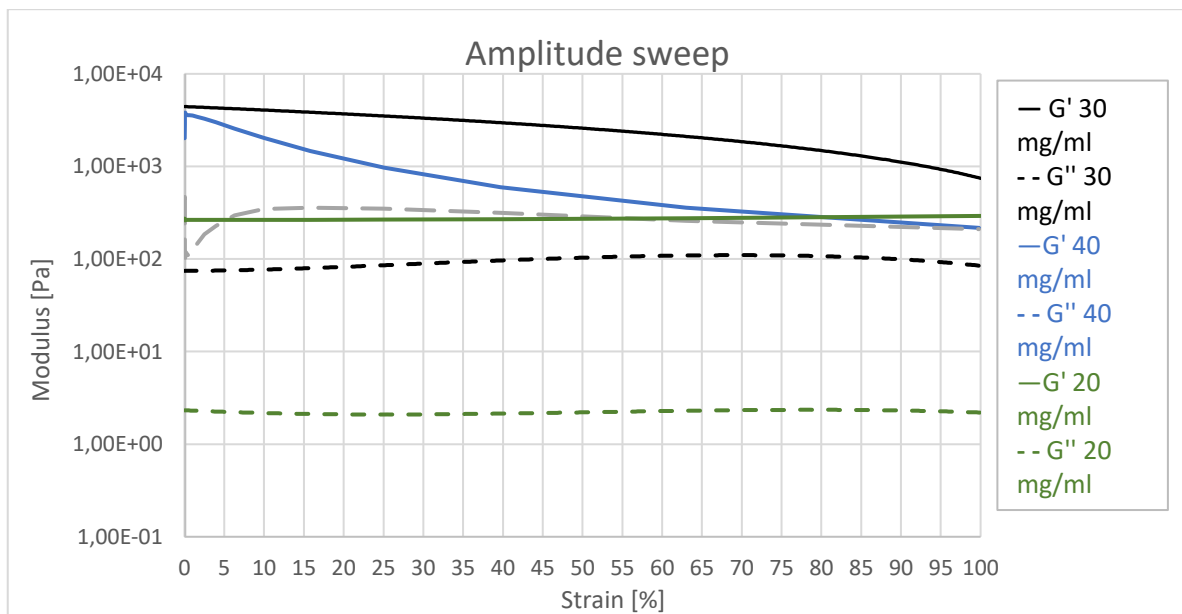


FIGURE 48. AMPLITUDE SWEEP TESTS OF NEAT SAMPLES

8.1.2 COMPOSITE SAMPLES

On the basis of the previous results, it was decided to continue the work with the 20 mg/mL formulations, as a compromise between initial viscosity and final G' value.

Several formulations were tried, in order to analyze the material's behavior at various concentrations of CNC.

The reinforced samples were compared to a neat formulation of 20 mg/mL of M-CMC.

Likely to the neat samples, the composite samples demonstrated to be pseudo-plastic materials, as shown in figure 49.

In addition, the increase of viscosity with concentration of CNCs was observed.

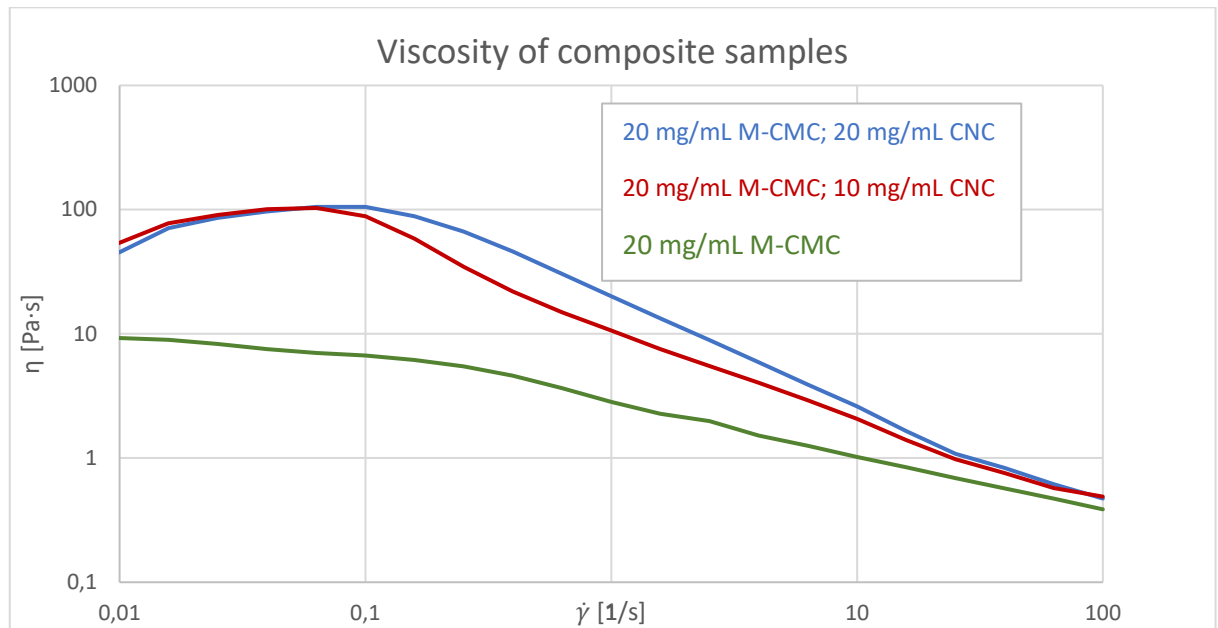


FIGURE 49. VISCOSITY VS SHEAR RATE CURVES OF COMPOSITE SAMPLES

The time sweep tests proved that the composite samples present a good reactivity.

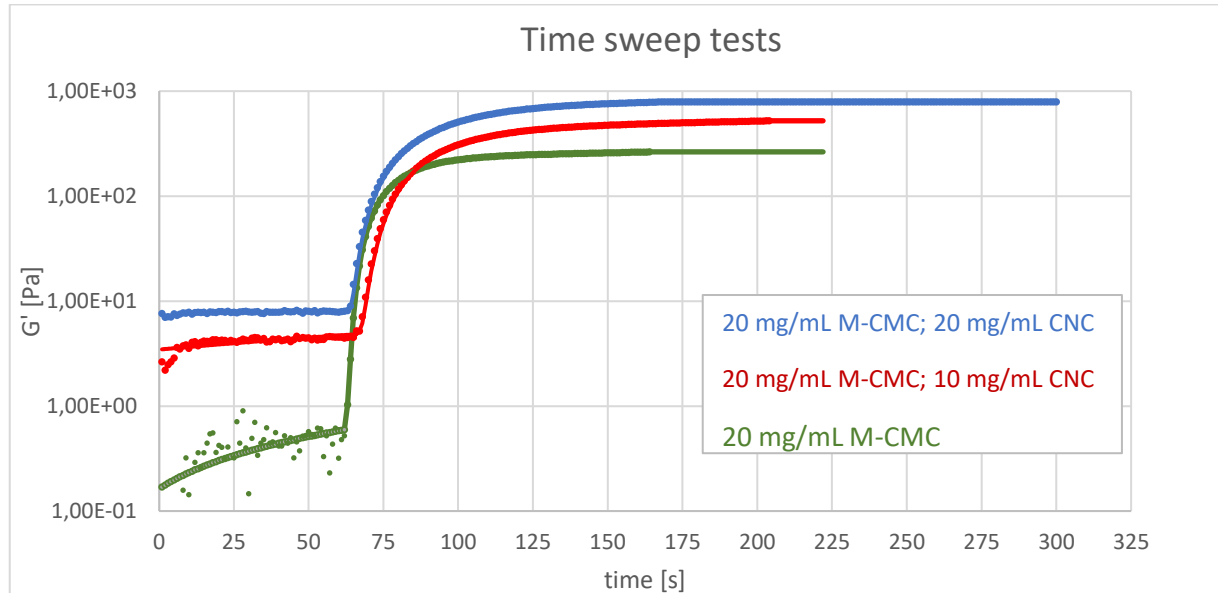


FIGURE 50. TIME SWEEPS TEST OF COMPOSITE SAMPLES

Nevertheless, the presence of CNCs led to a slight delay in the photopolymerization: t_{cr} was 3-seconds larger, and t_{gel} increased as a consequence (Table 5). Also the G' plateau is reached after longer exposure times for the composite samples.

CNC [mg/mL]	t_{cr} [s]	t_{gel} [s]
0	62	63
10	65	68
20	65	/

TABLE 5. KINETICS OF PHOTPOLYMERIZATION. THE AMOUNT OF M-CMC IS 20 MG/ML. t_{GEL} OF THE HYDROGEL WITH 20 MG/ML OF CNCs WAS NOT DETECTED BY THE SOFTWARE.

This effect can be ascribed either to the screening effect of the CNCs on the light or the increased viscosity, that limits the chain mobility (thus lowering the rate of reaction).

Nevertheless, the photocuring of composite samples was still rapid, and an increase of G' was recorded.

figure 51 shows the linear relationship between G' and the concentration of CNCs.

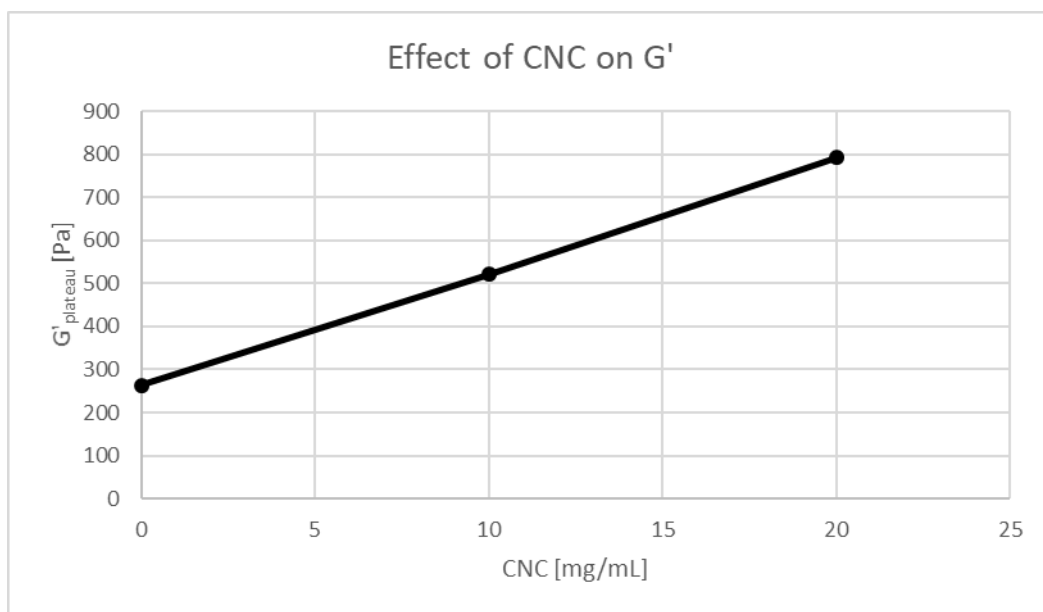


FIGURE 51. G' AS A FUNCTION OF CNCs CONTENT IN A FORMULATION OF 20 MG/ML OF M-CMC AND 2 PHR OF BAPO-OH (WITH RESPECT TO M-CMC).

The results of the amplitude sweeps tests on the cured samples are reported in figure 52. For every formulation, $G' > G''$, which is the evidence of the solid-like structure. All the hydrogels were stable in the range $\gamma = 0.01-100\%$.

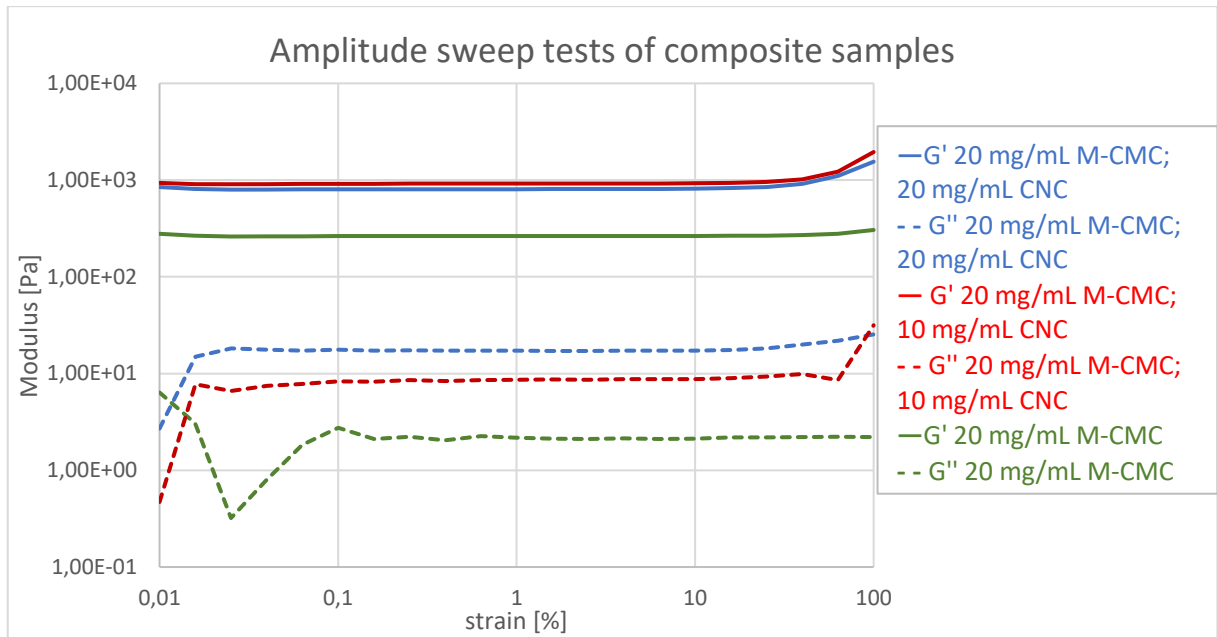


FIGURE 52. AMPLITUDE SWEEPS TESTS OF CNC/M-CMC SAMPLES, COMPARED TO 20 MG/ML NEAT SAMPLE.

8.2 3D PRINTING

After having evaluated the reactivity of the formulations through photorheology and confirmed their suitability for DLP printing, several printing tests were performed in order to optimize the printing parameters for the production of different samples. Firstly simple cylinders and parallelepiped were produced. The success or failure of printing (intended as resolution, fidelity and self-supporting of the part) depended on the setting of parameters and on the amount of formulation.

In figure 53, the same two objects (neat formulation, 20 mg/mL) were 3D-printed by varying the light intensity, burn-in exposure time and the exposure time. From left to right, these parameters were increased. Intermediate values yielded the most fulfilling result.



FIGURE 53. EFFECT OF PRINTING PARAMETERS IN DLP.

1 st printing	2 nd printing	3 rd printing
Light intensity 25 mW/cm ²	Light intensity 30 mW/cm ²	Light intensity 30 mW/cm ²
Exposure time 7 s	Exposure time 15 s	Exposure time 20 s
Burn-in exposure time 9 s	Burn-in exposure time 12 s	Burn-in exposure time 15 s

TABLE 6. SETTLING PARAMETERS FOR PARTS REPORTED IN FIGURE 53.

The parts appeared clear and transparent. The setting of the third printing (Table 6), that included longer exposure time, was used to print the same components with a formulation containing CNCs (20 mg/mL of M-CMC, 10 mg/mL of CNC), that was characterized by a slower reactivity, as attested through the photoreology. They were successfully printed; their appearance was whitish and more opaque, due to the presence of the CNCs (figure 54).

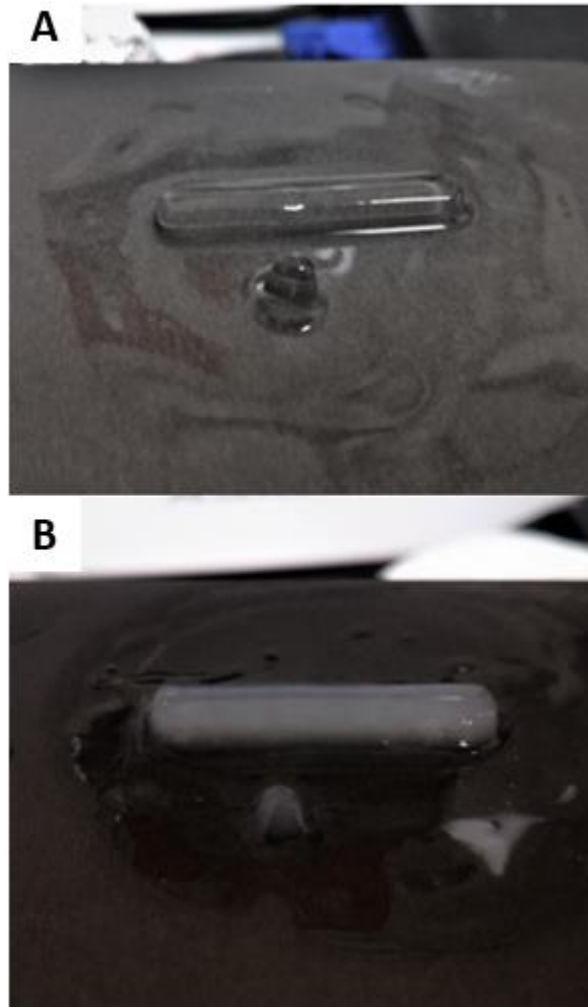


FIGURE 54. THE SAME STL FILE WAS 3D-PRINTED STARTING FROM NEAT FORMULATION (A) AND FROM THE FORMULATION CONTAINING CNCs (B).

Cylindrical samples were produced aiming to evaluate their mechanical properties under compression (figure 55).

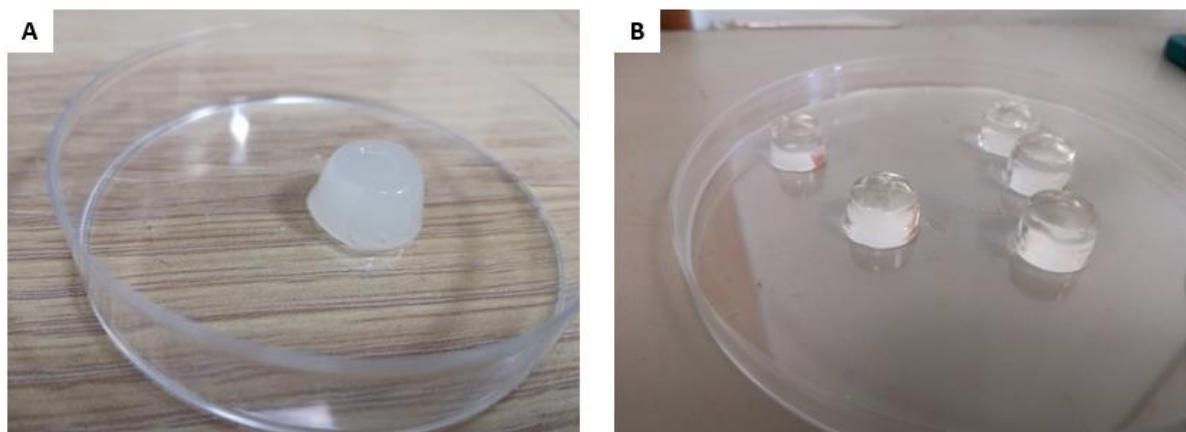


FIGURE 55. FILLED (A) AND NEAT (B) SAMPLES FOR COMPRESSION TESTS

Furthermore, printing test on the formulations containing higher amount of M-CMC were performed: figure 56 shows two attempts to print hydrogels with a concentration of 30

mg/mL of M-CMC. The adjustment of the parameters improved the final result, that was, however, not optimal, probably due to the high viscosity. For this reason only the sample based on the formulation containing 20 mg/ml were studied.



FIGURE 56. TWO ATTEMPTS TO PRINTING A 30 MG/ML FORMULATION. IN THE SECOND PICTURE, BURN-IN EXPOSURE TIME AND EXPOSURE TIME WERE INCREASED

Since one of the great advantages of 3D printing is the possibility to produce complex objects, different geometries were chosen in order to investigate the real printability of the studied formulations (figure 57 and figure 58).

In general, more complex structures can be 3D-printed thanks to the addition of a dye, that ensures finer resolution. Dulbecco's Modified Eagle Medium (DMEM) is a common medium for cell and tissue cultures. It contains phenol red molecules, used as pH indicator, that may act as dyes.-The presence of DMEM allowed the penetration of light and yielded to a higher resolution of the components. The phenol molecules of DMEM provided a reddish colour to the hydrogels.

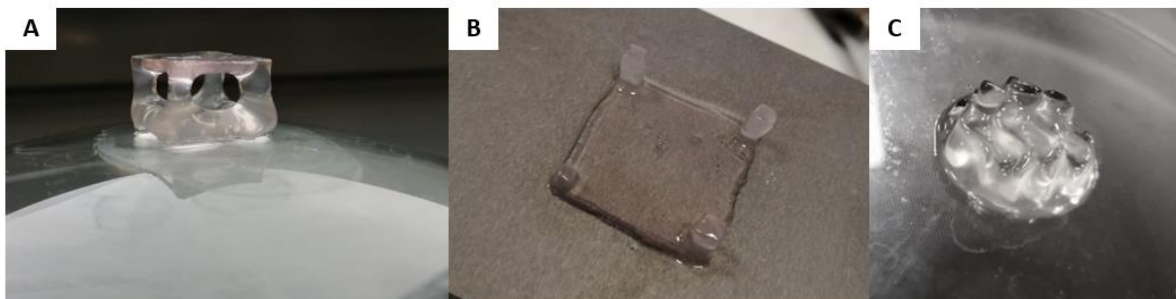


FIGURE 57. 3D-PRINTING OF M-CMC/DMEM (A AND B) AND NEAT M-CMC (C) FORMULATIONS.

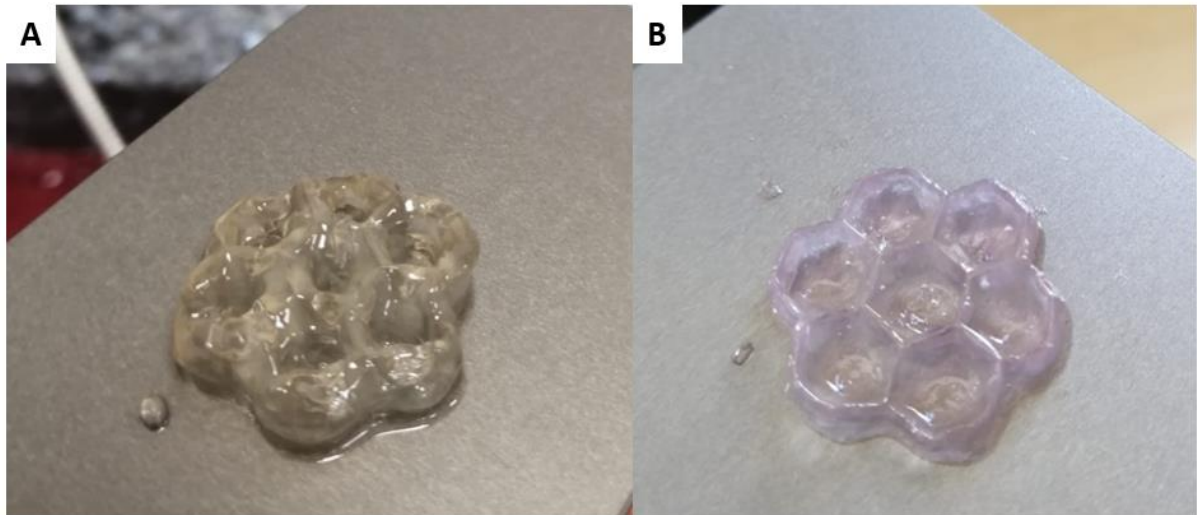


FIGURE 58. THE SAME COMPONENT PRINTED WITHOUT AND WITH DMEM (RESPECTIVELY FIGURE A AND B).

8.3 COMPRESSION TESTS

8.3.1 SINGLE COMPRESSION TESTS

A typical stress strain curve is reported in figure 59.

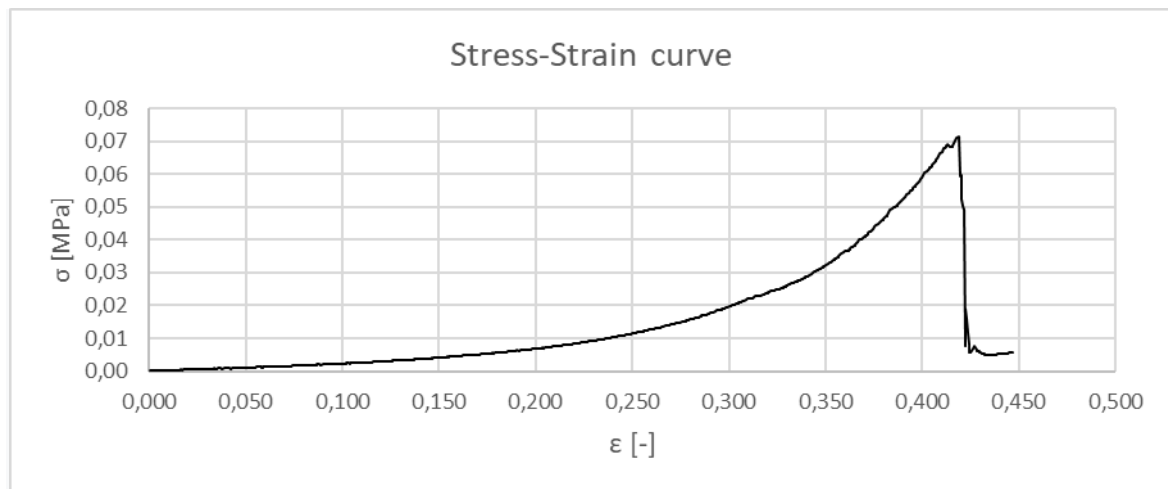


FIGURE 59. COMPRESSION CURVE.

Unfortunately, few samples could be tested. Consequently, the statistics should be verified by further tests.

Firstly, the mechanical performances of neat and composite hydrogel were characterized by:

- The compressive stress at maximal compression (σ_{\max});
- The deformation value recorded at σ_{\max} (ϵ_{\max}).

The calculation are reported in Table 7:

	σ_{\max} [kPa]	St. dev.	ϵ_{\max} [-]	St. dev.
MA-CMC	57.06	12.34	0.405	0.059
CNC/MA-CMC	68.76	10.6	0.483	0.125

TABLE 7. RESULTS OF SINGLE COMPRESSION TESTS

Reinforced samples resulted more resistant than neat ones, displaying a 20% rise in σ_{\max} . Even the elongation at break was slightly larger for reinforced hydrogels.

In addition, the different failure mode was interesting.

Neat samples appeared as completely smashed (figure 60), whereas reinforced hydrogels retained their shape, showing cracks that took place at the bottom border of the specimens (figure 60).



FIGURE 60. NEAT M-CMC HYDROGEL AT FAILURE

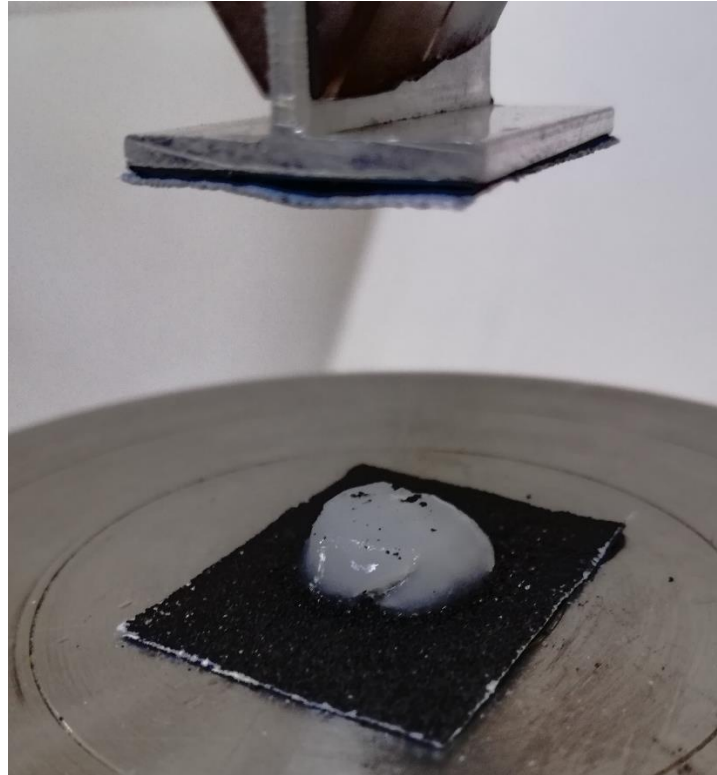


FIGURE 61. COMPOSITE CNC/M-CMC HYDROGEL AT FAILURE

As for the elasticity of the hydrogels, the ratio $d\sigma/d\varepsilon$ value rose in a broad range of deformation. So, the Young Modulus E was calculated in two range of deformation, according to the method reported by Buyanov et al. (46):

- $\varepsilon = 5\%-15\%$
- $\varepsilon = 15\%-25\%$

Results are summarized in table.

	$E_{5\%-15\%}$ [kPa]	St. dev.	$E_{15\%-25\%}$ [kPa]	St. dev.
MA-CMC	28.66	4.02	54.21	3.47
CNC/MA-CMC	29.32	6.82	62.95	19.24

TABLE 8. ELASTIC MODULUS OF NEAT AND COMPOSITE HYDROGELS

Composite hydrogels seemed stiffer; furthermore, it seemed clear that E increased with the increasing of strain, revealing a non-linear deformation-behaviour under compression stress.

8.3.2 CYCLIC COMPRESSION TESTS

The cyclic compression tests performed in this work must be regarded as preliminary.

Either neat or composite hydrogels, when subjected to cyclic loading, developed a hysteric loop, due to their viscoelastic nature.

figure 62 displays a typical test: the number of cycles increased until the sample's failure.

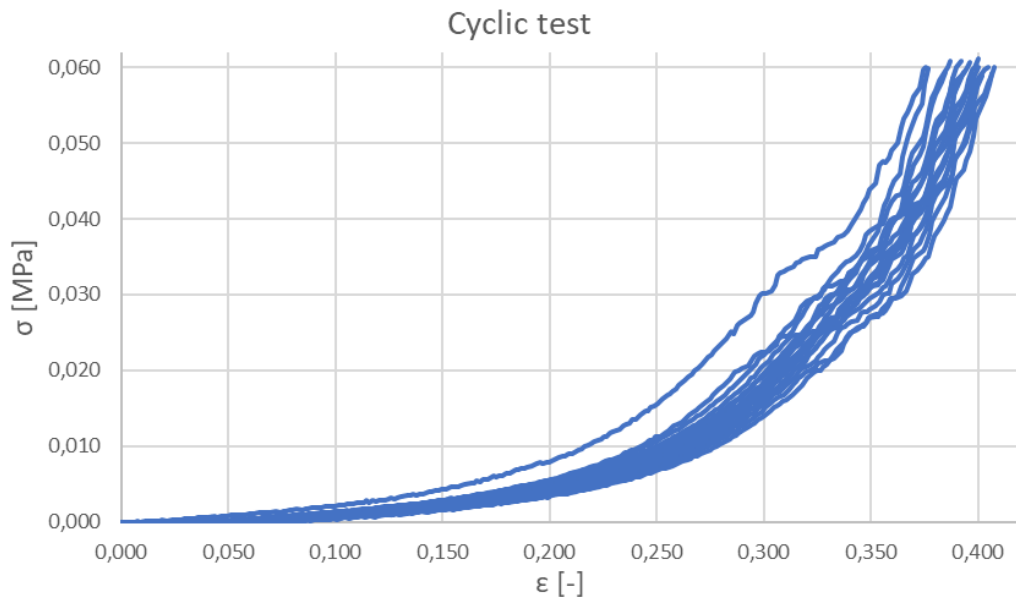


FIGURE 62. CYCLIC TEST

A typical cycle is showed in figure 63.

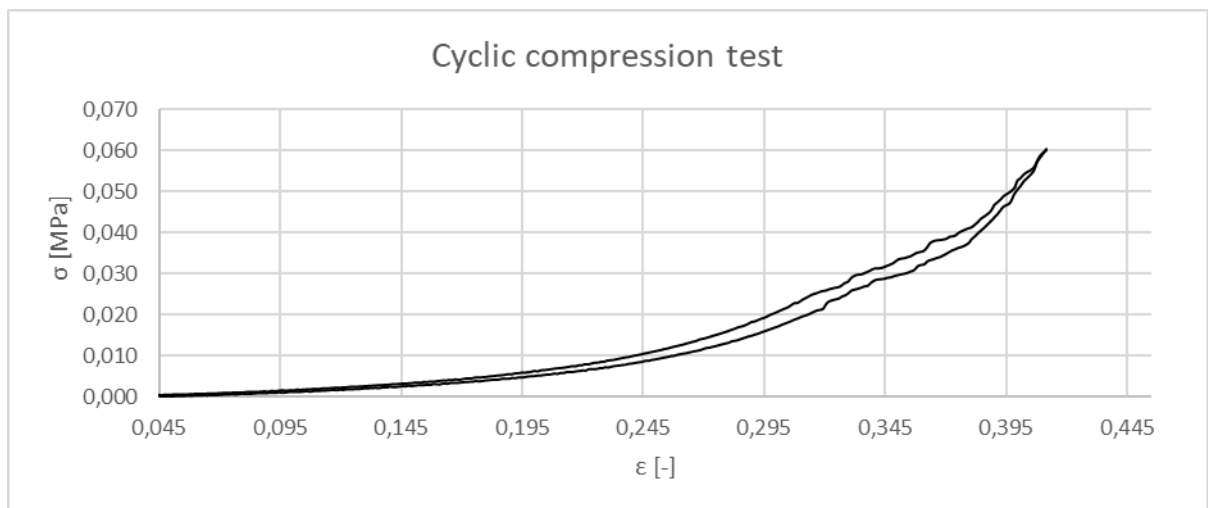


FIGURE 63. EXAMPLE OF A CYCLE OF CYCLIC COMPRESSION TESTS.

The stress at the loading part of the curve is larger than that at the unloading part, at the same deformation value. The phase displacement creates the loop, whose internal area quantifies the energy that is dissipated in a cycle. There are many contributions to the energy dissipation, such as the viscous flow and the friction between different components of the hydrogel. After the stress is released, the polymer chains, that had curled under the external load, return to their natural state and the deformation is restored (175). Nevertheless, the material undergoes to some modifications, that are reflected in the progressive decaying of the elastic modulus, until breaking.

This was particularly evident for neat M-CMC samples: excluding the first cycle (which can reasonably be considered as a settling cycle), the elastic modulus showed a decreasing trend, while the dissipated energy grew cycle by cycle.

On the contrary, in reinforced hydrogels a less pronounced reduction of E was detected, and each cycle was almost identical to other cycles, in terms of dissipative energy (only the first cycle showed a higher dissipative energy).

These results are summarized in figure 64.

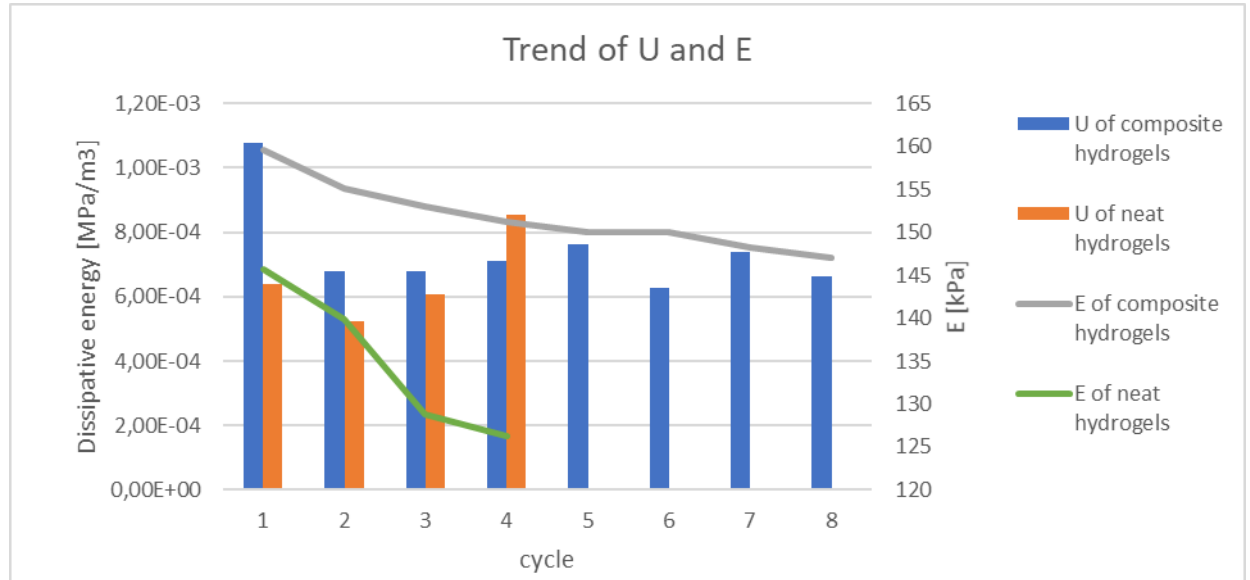


FIGURE 64. VALUE OF DISSIPATIVE ENERGY (U) AND YOUNG MODULUS (E) DURING THE CYCLIC TESTS.

In addition, relating to neat hydrogels, the strain recorded at the maximum stress (ϵ_{max}) was, for each cycle, higher than this of composite samples. Moreover, in M-CMC specimens, ϵ_{max} showed a more pronounced growth (figure 65).

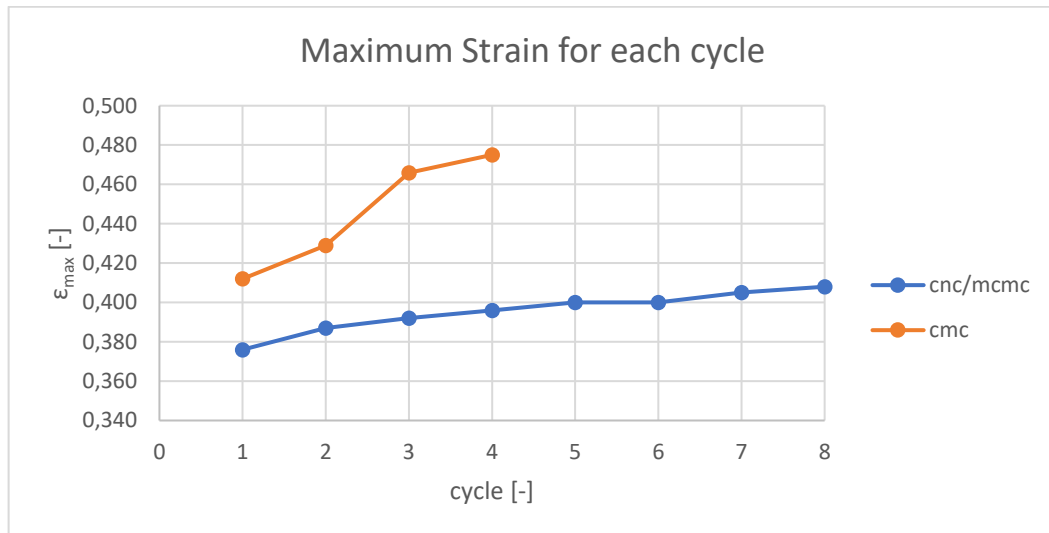


FIGURE 65. TREND OF THE STRAIN CORRESPONDING TO THE MAXIMUM STRESS AT EACH CYCLE

These results suggest that reinforced samples are more resistant to fatigue loading.

In neat hydrogels, the progressive damage of the network was primarily highlighted by the collapse of the Young Modulus and the clear rise of the dissipative energy. On the contrary, the CNCs were likely to keep the network more intact, preserving the elasticity and the stiffness of the material.

cycle	U [MPa/m ³]	E _{max} [kPa]	ε _{max} [-]
1	6,40E-04	145,63	0,412
2	5,24E-04	139,86	0,429
3	6,09E-04	128,76	0,466
4	8,54E-04	126,32	0,475

TABLE 9. VALUES OF DISSIPATIVE ENERGY U, YOUNG MODULUS E AND MAXIMUM STRAIN FOR NEAT HYDROGELS

cycle	U [MPa/m ³]	E _{max} [kPa]	ε _{max} [-]
1	1,08E-03	159,57	0,376
2	6,79E-04	155,04	0,387
3	6,79E-04	153,06	0,392
4	7,10E-04	151,16	0,396
5	7,63E-04	150	0,4
6	6,27E-04	150	0,4
7	7,39E-04	148,15	0,405
8	6,62E-04	147,06	0,408

TABLE 10. VALUES OF DISSIPATIVE ENERGY U, YOUNG MODULUS E AND MAXIMUM STRAIN FOR COMPOSITE HYDROGELS.

9. CONCLUSIONS

The work attested the 3D-DLP printability of cellulose-based hydrogels, which, according to the preliminary results achieved, possess promising properties.

Methacrylation endowed carboxymethylcellulose with photocurability, as attested through the photoreology tests. In fact, formulations with different concentrations of M-CMC proved to form a cured hydrogel after UV-light exposure. Viscosity and storage modulus G' , that is an index of the elastic, solid behaviour of the material, increased with the amount of M-CMC.

The addition of cellulose nanocrystals didn't affect drastically the kinetics of photopolymerization, that was completed within about one minute after the UV exposure. Nanocrystals enhanced the value of hydrogels' storage modulus, that grew linearly with the concentration of CNCs: the storage modulus is increased from 260 Pa (neat formulation, 20 mg/mL) to 522 Pa (20 mg/mL of M-CMC, 10 mg/mL of CNC) and to 800 Pa (20 mg/mL of M-CMC, 20 mg/mL of CNC).

M-CMC and CNC/M-CMC formulations were 3D-printed by DLP, using UV light and BAPO-OH photoinitiator, in order to build both simple and complex structures. The addition of DMEM, which acted as a dye, ensured better resolution.

Printed cylinders were utilized to determine the mechanical properties of neat and reinforced hydrogels.

Single compression tests established that CNC/M-CMC hydrogels are harder (E is up to 1.2-fold higher), more resistant (compressive strength grows from 57 kPa to 69 kPa) and slightly more deformable (maximum deformation of 48%).

Preliminary cyclic, compression tests seemed to suggest that nanocrystals improve fatigue behaviour, too, even though further analysis are required.

Enhanced mechanical properties can be related to an efficient load-transfer between fillers and matrix. Cellulose nanocrystals absorb the external stress due to their higher rigidity and dissipate it through filler-filler and filler-matrix friction.

Future work could include:

- Additional compression tests, to obtain more accurate results. Moreover, it would be interesting to analyse the trend of mechanical properties with varying concentrations of M-CMC and the ratio CNC/M-CMC.
- Cellular studies, aimed at verifying cells' survival and proliferation in the material, thus its suitability for biological and biomedical applications.
- Methacrylation of CNCs and its effect on the mechanical and photorheological properties of the composite hydrogels.

REFERENCES

1. *In situ-forming injectable hydrogels for regenerative medicine*. J.A. Yang, Jeong-A., et al. 2014, Progress in Polymer Science.
2. Bahram, Morteza, Mohseni, Naimeh and Moghtader, Mehdi. An Introduction to Hydrogels and Some Recent applications. *Intech open science*. 2016.
3. Mahinroosta, Author links open overlay panel Mostafa, et al. Hydrogels as intelligent materials: A brief review of synthesis, properties and applications. *Materials Today Chemistry*. 2018, Vol. 8.
4. Li, Ling and Lee, L. James. PHOTODSC ANALYSIS OF UV-CURABLE HYDROGELS. *Antec*. 2004.
5. Peppasa, N.A., et al. Hydrogels in pharmaceutical formulations. *European Journal of Pharmaceutics and Biopharmaceutics*. 2000.
6. Huaping, Tan and Marra, Kacey G. Injectable, Biodegradable Hydrogels for Tissue Engineering Applications. *Materials*. 2010.
7. *In situ hydrogelation of photocurable gelatin and drug release*. Okino, H., et al. Lausanne, Switzerland : s.n., 2000.
8. Hoffman, Allan S. Hydrogels for biomedical applications. *Advanced Drug Delivery Reviews*. 2012, 64.
9. Feng, Zhaoxuan, et al. Photocrosslinked Chitosan Hydrogels Reinforced with Chitosan-Derived Nano-Graphene Oxide. *Macromolecular Chemistry and Physics*. 2019.
10. Du, Wnbo, et al. An injectable self-healing hydrogel-cellulose nanocrystals conjugate with excellent mechanical strength and good biocompatibility. *Carbohydrate Polymers*. Carbohydrate Polymers, 223.
11. Z., Wei, et al. Self-healing gels based on constitutional dynamic chemistry and their potential applications. *Chemical Society Reviews*. 2014.
12. Boffito, Monica, et al. Thermosensitive Block Copolymer Hydrogels Based on Poly(ϵ -Caprolactone) and Polyethylene Glycol for Biomedical Applications: State of the Art and Future Perspectives. *J Biomed Mater Res A*. 2015.
13. Ali, A.El-Hag, et al. Synthesis and characterization of PVP/AAC copolymer hydrogel and its applications in the removal of heavy metals from aqueous solution. *European Polymer Journal*. 2003, Vol. 39.
14. Cui, Li, et al. Preparation and characterization of IPN hydrogels composed of chitosan and gelatin cross-linked by genipin. *Carbohydrate Polymers*. 2014, Vol. 99.
15. Nguyen, Kytai Truong and West, Jennifer L. Photopolymerizable hydrogels for tissue engineering applications. *Biomaterials*. 2002, 23.
16. Freytes, Donald O., et al. Preparation and rheological characterization of a gel form of the porcine urinary bladder matrix. *Biomaterials*. 2008, 29.
17. Jiang, Dan, et al. Characterization of bladder acellular matrix hydrogel with inherent bioactive factors. *Materials Science and Engineering: C*. 2017, 77.

18. Fan, Wenshuai, et al. Injectable double-crosslinked hydrogels with kartogenin-conjugated polyurethane nano-particles and transforming growth factor β 3 for in-situ cartilage regeneration. *Materials Science and Engineering: C*. 2020, 110.
19. Lau, Ting Ting, Ho, Li Wen and Wang, Dong-An. Hepatogenesis of murine induced pluripotent stem cells in 3D micro-cavitary hydrogel system for liver regeneration. *Biomaterials*. 2013, Vol. 34.
20. Hwang, Youngmin, et al. Injectable and detachable heparin-based hydrogel micropatches for hepatic differentiation of hADSCs and their liver targeted delivery. *Biomaterials*. 2018, Vol. 165.
21. Xu, Guohui, et al. Injectable biodegradable hybrid hydrogels based on thiolated collagen and oligo(acryloyl carbonate)–poly(ethylene glycol)–oligo(acryloyl carbonate) copolymer for functional cardiac regeneration. *Acta Biomaterialia*. 2015, Vol. 15.
22. Si, Rui, et al. Human mesenchymal stem cells encapsulated-coacervated photoluminescent nanodots layered bioactive chitosan/collagen hydrogel matrices to indorse cardiac healing after acute myocardial infarction. *Journal of Photochemistry and Photobiology B: Biology*. 2020.
23. Fujita, Masanori, et al. Antagomir-92a impregnated gelatin hydrogel microsphere sheet enhances cardiac regeneration after myocardial infarction in rats. *Regenerative Therapy*. 2016, Vol. 5.
24. Wu, Jiezhou, et al. Stem cell-laden injectable hydrogel microspheres for cancellous bone regeneration. *Chemical Engineering Journal*. 2020, Vol. 393.
25. Zuidema, Jonathan M., et al. Fabrication and characterization of tunable polysaccharide hydrogel blends for neural repair. *Acta Biomaterialia*. 2011, 7.
26. Li, Lan, et al. Biofabrication of a biomimetic supramolecular-polymer double network hydrogel for cartilage regeneration. *Materials & Design*. 2020, Vol. 189.
27. Xu, Jianbin, et al. Injectable stem cell-laden supramolecular hydrogels enhance in situ osteochondral regeneration via the sustained co-delivery of hydrophilic and hydrophobic chondrogenic molecules. *Biomaterials*. 2019, Vol. 210.
28. Matthias P. Lutolf, Penney M. Gilbert, Helen M. Blau. Designing materials to direct stem-cell fate. *Nature*. 2009, Vol. 462.
29. Chena, Nusheng, et al. Cellulose-based injectable hydrogel composite for pH-responsive and controllable drug delivery. *Carbohydrate Polymers*. 2019, 225.
30. Hu, Y., Hollinger, J.O. and Marra, K.G. Controlled release from coated polymer microparticles embedded in tissue-engineered scaffolds. *J. Drug Targeting*. 2001.
31. Chen, Xueyun, et al. Magnetic and self-healing chitosan-alginate hydrogel encapsulated gelatin microspheres via covalent cross-linking for drug delivery. *Materials Science and Engineering: C*. 2019, Vol. 101.
32. Duman, Osman, et al. Agar/ κ -carrageenan composite hydrogel adsorbent for the removal of Methylene Blue from water. *International Journal of Biological Macromolecules*. 2020.
33. Lv, Qingyun, et al. Highly efficient removal of trace metal ions by using poly(acrylic acid) hydrogel adsorbent. *Materials & Design*. 2019, Vol. 181.

34. Kamel, Samir, et al. Carboxymethyl cellulose-hydrogel embedded with modified magnetite nanoparticles and porous carbon: Effective environmental adsorbent. *Carbohydrate Polymers*. 2020, Vol. 242.
35. Tadeu, Paulino Alexandre, et al. Efficiency of hydrogels based on natural polysaccharides in the removal of Cd²⁺ ions from aqueous solutions. *Chemical Engineering Journal*. 2011, Vol. 168.
36. Khan, Suhail Ayoub, Siddiqui, Mohammad Fuzail and Khan, Tabrez Alam. Ultrasonic-assisted synthesis of polyacrylamide/bentonite hydrogel nanocomposite for the sequestration of lead and cadmium from aqueous phase: Equilibrium, kinetics and thermodynamic studies. *Ultrasonics - Sonochemistry*. 2019, Vol. 60.
37. Uddin, F. Clays, nanoclays, and montmorillonite minerals. *Metallic Materials Science*. 2008.
38. Pathak, Akhilesh Kumar and Singh, Vinod Kumar. A wide range and highly sensitive optical fiber pH sensor using polyacrylamide hydrogel. *Optical fiber technology*. 2017, Vol. 39.
39. An, Ran, et al. Healing, flexible, high thermal sensitive dual-network ionic conductive hydrogels for 3D linear temperature sensor. *Materials Science and Engineering*. 2019.
40. Elkhoury, Kamil, et al. Soft-Nanoparticle Functionalization of Natural Hydrogels for tissue engineering applications. *Advanced healthcare materials*. 2019.
41. Zhao, Wen, et al. Degradable natural polymer hydrogels for articular cartilage tissue engineering. *Wiley Online Library*. 2012.
42. Bao, Ziting, et al. Natural Polymer-Based Hydrogels with Enhanced Mechanical Performances: Preparation, Structure, and Property. *Advanced healthcare materials* . 2019.
43. Sannino, Alessandro, Demitri, Christian and Madaghiele, Marta. Biodegradable Cellulose-based Hydrogels: Design and Applications. *Materials*. 2009, Vol. 2.
44. Mariano, Marcos, Kissi, Nadia El and Dufresne, Alain. Cellulose Nanocrystals and Related Nanocomposites: Review of some Properties and Challenges. *Journal of polymer science*. 2014.
45. Ul-Islam, Mazhar, et al. Comparative study of plant and bacterial cellulose pellicles regenerated from dissolved states. *International Journal of Biological Macromolecules*. 2019, Vol. 137.
46. Buyanov, A.L., Gofman, I.V. and Saprykina, N.N. High-strength cellulose–polyacrylamide hydrogels: Mechanical behavior and structure depending on the type of cellulose. *Journal of the Mechanical Behavior of Biomedical Materials*. 2019, Vol. 100.
47. M., Gupta K. and J., Jiang. Cellulose dissolution and regeneration in ionic liquids: A computational perspective. *Chemical Engineering Science*. 2015, Vol. 121.
48. Markstedt, K., Sundberg, J. and Gatenholm, P. 3D bioprinting of cellulose structures from a ionic liquid. *3D Printing and Additive Manufacturing*. 2014, Vol. 1.
49. 8 - Cellulose and Cellulose-Based Hydrocolloids. [book auth.] Author links open overlay panel James N. BeMiller. *Carbohydrate Chemistry for Food Scientists (Third Edition)*. 2019.
50. Zhang, Qing, et al. Methods and applications of nanocellulose loaded with inorganic nanomaterials: A review. *Carbohydrate Polymers*. 2020, Vol. 229.
51. Kontturi, E., Laaksonen, P., Linder, M. B., Nonappa, Groschel, A. H., Rojas, O. J. Advanced materials through assembly of nanocelluloses. *Advanced Materials*. 2018, Vol. 39.

52. Moon, R. J., Martini, A., Nairn, J., Simonsen, J., & Youngblood, J. Cellulose nanomaterials review: Structure, properties and nanocomposites. *Chemical Society Reviews*. 2011, Vol. 40.
53. Jiang, Qiwen, et al. Preparation of cellulose nanocrystals based on waste paper via different systems. *International Journal of Biological Macromolecules*. 2020, Vol. 149.
54. Pourmoazzen, Zhaleh, et al. The morphology, self-assembly, and host-guest properties of cellulose nanocrystals surface grafted with cholesterol. *Carbohydrate Polymers*. 2020, Vol. 23.
55. Buffa, J. M., Casado, U., Mucci, V., Aranguren, M. I. Cellulose nanocrystals in aqueous suspensions: Rheology of lyotropic chiral liquid crystals. *Cellulose*. 2019, Vol. 26.
56. Jiménez Saelices, C., Save, M., & Capron, I. Synthesis of latex stabilized by unmodified cellulose nanocrystals: The effect of monomers on particle size. *Polymers chemistry*. 2019.
57. Zhang, H., et al. A facile and efficient strategy for the fabrication of porous linseed gum/cellulose superabsorbent hydrogels for water conservation. *Carbohydrate Polymers*. 2017, Vol. 157.
58. I.Raafat, Amany, Eid, Mona and B.El-Arnaouty, Magda. Radiation synthesis of superabsorbent CMC based hydrogels for agriculture applications. *Nuclear Instruments and Methods in Physics Research Section B: Beam Interactions with Materials and Atoms*. 2012, Vol. 283.
59. Sannino, A., et al. Cellulose-based hydrogels as body water retainers. *Journal of Materials Science: Materials in Medicine*. 2000, Vol. 11.
60. Liu, Xinwei, Luan, Sen and Li, Wei. Utilization of waste hemicelluloses lye for superabsorbent hydrogel synthesis. *Macromolecules*. 2019, Vol. 132.
61. Sannino, A., et al. Biomedical application of a superabsorbent hydrogel for body water elimination in the treatment of edemas. *Journal of Biomedical Materials Research A*. 2003, Vol. 63.
62. Lina, Huizi Anna, et al. Injectable cellulose-based hydrogels as nucleus pulposus replacements: Assessment of in vitro structural stability, ex vivo herniation risk, and in vivo biocompatibility. *Journal of the Mechanical Behavior of Biomedical Materials*. 2019, Vol. 96.
63. Thomas, D. J. and Claypole, T. C. Printing on Polymers. 2016.
64. Yu, Yin, et al. Three-dimensional bioprinting using self-assembling scalable scaffold-free “tissue strands” as a new bioink. *Scientific Reports*. 2016, Vol. 6.
65. Hammed Abiodun Balogun, Reyihangu Sulaiman, Sarah Sayed Marzouk, Adewale Giwa, Shadi Wajih Hasan. 3D printing and surface imprinting technologies for water treatment: A review. *Journal of Water Process Engineering*. 2019, Vol. 31.
66. Lee, Jian-Yuan, An, Jia and Chua, Chee Kai. Fundamentals and applications of 3D printing for novel materials. *Applied Materials Today*. 2017, 7.
67. L. Wang, M. Zhang, B. Bhandari, C. Yang. Investigation on fish surimi gel as promising food material for 3D printing. *Journal of Food Engineering*. 2018, Vol. 220.
68. F. Yang, M. Zhang, B. Bhandari, Y. Liu. Investigation on lemon juice gel as food material for 3D printing and optimization of printing parameters. *LWT - Food Science and Technology*,. 2018, Vol. 87.
69. E. Pei, J. Shen, J. Watling. Direct 3D printing of polymers onto textiles: experimental studies and applications. *Rapid Prototyping Journal*. 2015, Vol. 21.

70. L. Sabantina, F. Kinzel, A. Ehrmann, K. Finsterbusch. Combining 3D printed forms with textile structures – mechanical and geometrical properties of multi-material systems. *IOP conference series materials science and engineering*. 2015, Vol. 87.
71. Gaget, L. 3D printed clothes: Top 7 of the best projects. *Sculpteo*. 2018.
72. Wikipedia Photopolymer. *Wikipedia, the free encyclopedia*. [Online] <https://en.wikipedia.org/wiki/Photopolymer>.
73. Gibson, Ian, Rosen, David W. and Stucker, Brent. Chapter 4 Photopolymerization Processes. *Additive Manufacturing Technologies: Rapid Prototyping to Direct Digital Manufacturing*. Boston : Springer, 2010.
74. Junyi, Zhou, et al. Progress in the development of polymeric and multifunctional photoinitiators. *Progress in Polymer Science*. 2019, Vol. 99.
75. Fouassier, J.P. and Rabek, J.F. *Radiation curing in polymer science and technology*. London : Chapman and Hall, 1993.
76. Lalevée, Jacques and Fouassier, Jean-Pierre. *Photoinitiators for Polymer Synthesis : Scope, Reactivity, and Efficiency*. s.l. : John Wiley & Sons, Incorporated, 2012.
77. Ng, Wei Long, et al. Vat polymerization-based bioprinting—process, materials, applications and regulatory challenges. *Biofabrication*. 2020, Vol. 12.
78. Crivello, J.V. and Dietliker, K. *Photoinitiators for free radical, cationic & anionic*. s.l. : John Wiley & Sons, 1998.
79. Tumbleston, John R., et al. Continuous liquid interface production of 3D objects. *Science*. 2015.
80. [Online] [Cited: 23 3 2020.] <https://www.pcimag.com/articles/104755-use-of-amino-acrylates-to-reduce-photoinitiator-concentration-or-increase-cure-speed-in-uv-led-curable-opsv-and-flexo-inks>.
81. Hoyle, C. E., Keel, M. and Kim, K. Photopolymerization of 1,6-hexanediol diacrylate: The effect of functionalized amines. *Polymer*. 1988, 29.
82. KiKim, Soon and Guymon, C. Allan. Effects of polymerizable organoclays on oxygen inhibition of acrylate and thiol-acrylate photopolymerization. *Polymer*. 2012, Vol. 53.
83. *Validating continuous digital light processing (cDLP) additive manufacturing accuracy and tissue engineering utility of a dye-initiator package*. Wallace, Jonathan F. and Wang, Martha O. 2014, Materials Science, Medicine Biofabrication.
84. SLA vs. DLP: Compare Resin 3D Printing Technologies (2019 Guide). *formlabs*. [Online] <https://formlabs.com/blog/3d-printing-technology-comparison-sla-dlp/>.
85. You, Shangting, et al. High-fidelity 3D printing using flashing photopolymerization. *Additive Manufacturing*. 2019, 30.
86. Quan, Haoyuan, et al. Photo-curing 3D printing technique and its challenges. *Bioactive Materials*. 2020.
87. Lia, Jinhua, et al. 3D printing of hydrogels: Rational design strategies and emerging biomedical applications. *Materials Science & Engineering R*. 2020, Vol. 140.

88. Brigo, Laura, et al. 3D high-resolution two-photon crosslinked hydrogel structures for biological studies. *Acta Biomaterialia*. 2017, 55.
89. Giustina, Gioia Della, et al. Polysaccharide hydrogels for multiscale 3D printing of pullulan scaffolds. *Materials and Design*. 2019, 165.
90. Bracaglia, Laura G., et al. 3D printing for the design and fabrication of polymer-based gradient scaffolds. *Acta Biomaterialia*. 2017, 56.
91. Ergul, Necdet Mekki, et al. 3D printing of chitosan/ poly(vinyl alcohol) hydrogel containing synthesized hydroxyapatite scaffolds for hard-tissue engineering. *Polymer Testing*. 2019, 79.
92. Xue, Dai, et al. Digital Light Processing-Based 3D Printing of Cell-Seeding Hydrogel Scaffolds with Regionally Varied Stiffness. *Acta Biomaterials Science and Engineering*. 2019, 5.
93. Discher, D. E., Janmey, P. and Wang, Y. L. Tissue Cells Feel and Respond to the Stiffness of Their Substrate. *Science*. 2005, Vol. 310.
94. Kirkpatrick, C. J., Fuchs, S. and Unger, R. E. Co-culture systems for vascularization. 2011, Vol. 63.
95. Annabi, Nasim, et al. Controlling the Porosity and Microarchitecture of Hydrogels for Tissue Engineering. *Tissue Engineering Part B: Reviews*. 2010, Vol. 16.
96. Brigo, Laura, et al. 3D high-resolution two-photon crosslinked hydrogel structures for biological studies. *Acta Biomaterialia*. 2017, Vol. 55.
97. Kadry, Hossam, et al. Digital light processing (DLP) 3D-printing technology and photoreactive polymers in fabrication of modified-release tablets. *European Journal of Pharmaceutical Sciences*. 2019, Vol. 135.
98. Li, F., et al. Novel spacers for mass transfer enhancement in membrane separation. *J. Memb. Sci*. 2005.
99. Sreedhar, N., et al. 3D printed feed spacers based on triply periodic minimal surfaces for flux enhancement and biofouling mitigation in RO and UF. *Desalination*. 2018, 45.
100. Yanar, N., et al. Investigation of the performance behaviour of a forward osmosis membrane system using various feed spacer materials fabricated by 3D printing technique . *Chemosphere* . 2018, Vol. 202.
101. Kerdi, S., et al. Fouling resilient perforated speed spacers for membrane filtration. *Water Res*. 2019, 164.
102. Ali, S.M., et al. Energy efficient 3D printed column type feed spacer for membrane filtration. *Water Res*. 2019, 164.
103. Valentin, Thomas M., et al. Alginate-graphene oxide hydrogels with enhanced ionic tunability and chemomechanical stability for light-directed 3D printing. *Carbon*. 2019.
104. Shahbazi, Mahdiyar, et al. Electron beam crosslinking of alginate/nanoclay ink to improve functional properties of 3D printed hydrogel for removing heavy metal ions. *Carbohydrate Polymers*. 2020.
105. Appuhamillage, Gayan A, et al. A biopolymer-based 3D printable hydrogel for toxic metal adsorption from water. *Polym Int*. 2019.

106. Chan, V., et al. Three-dimensional photopatterning of hydrogels using stereolithography for long term cell encapsulation. *Lab. Chip.* . 2010, Vol. 10.
107. Vehse, M., et al. Drug delivery from poly(ethylene glycol) diacrylate scaffolds produced by DLC based micro-Stereolithography. *Macromol. Symp.* 2014, 346.
108. Shepherd, J.N. Hanson, et al. 3D microperiodic hydrogel scaffolds for robust neuronal cultures. *Advanced Functionalised Materials.* 2011, 21.
109. Arcaute, K., Mann, B.K. and Wicker, R.B. Stereolithography of three-dimensional bioactive poly(ethylene glycol) constructs with encapsulated cells. *Annual Biomedical Engineering.* 2006, 34.
110. Dhariwala, B., Hunt, E. and Boland, T. Rapid prototyping of tissue-engineering constructs, using photopolymerizable hydrogels and stereolithography. *Tissue Engineering.* 2004, 10.
111. Fisher, J.P., Dean, D. and Mikos, A.G. Photocrosslinking characteristics and mechanical properties of diethyl fumarate/poly(propylene fumarate) biomaterials. *Biomaterials.* 2002, 23.
112. Martinez, Pamela Robles, et al. Fabrication of drug-loaded hydrogels with stereolithographic 3D printing. *International Journal of Pharmaceutics.* 2017, Vol. 532.
113. Yin, Jun, et al. 3D Bioprinting of Low-Concentration Cell-Laden Gelatin Methacrylate (GelMA) Bioinks with a Two-Step Cross-linking Strategy. *Applied Materials & Interfaces.* 2018, Vol. 10.
114. Zhao, Xin, et al. Photocrosslinkable Gelatin Hydrogel for Epidermal Tissue Engineering. *Advanced Healthcare Materials.* 2016, Vol. 5.
115. Billiet, Thomas, et al. The 3D printing of gelatin methacrylamide cell-laden tissue-engineered constructs with high cell viability. *Biomaterials.* 2014, Vol. 35.
116. Shen, Yi, et al. DLP printing photocurable chitosan to build bio-constructs for tissue engineering. *Carbohydrate Polymers.* 2020.
117. Kolawole, Oluwadamilola M., Lau, Wing Man and Khutoryanskiy, Vitaliy V. Methacrylated chitosan as a polymer with enhanced mucoadhesive properties for transmucosal drug delivery. *International Journal of Pharmaceutics.* 2018, Vol. 550.
118. AD, Rouillard, et al. Methods for photocrosslinking alginate hydrogel scaffolds with high cell viability. *Tissue Engineering Part C.* 2011, Vol. 7.
119. Mu, Changjun, et al. Preparation of cell-enclosing microcapsules through photopolymerization of methacrylated alginate solution triggered by irradiation with visible light. *Journal of Bioscience and Bioengineering.* 2010, Vol. 109.
120. Xiao, Wenqian, et al. Synthesis and characterization of cell-laden double-network hydrogels based on silk fibroin and methacrylated hyaluronic acid. *European Polymer Journal.* 2019, Vol. 118.
121. Tavsanlı, Burak and Okay, Oğuz. Mechanically strong hyaluronic acid hydrogels with an interpenetrating network structure. *European Polymer Journal.* 2017, Vol. 94.
122. Na, Kyunga, et al. Effect of solution viscosity on retardation of cell sedimentation in DLP 3D printing of gelatin methacrylate/silk fibroin bioink. *Journal of Industrial and Engineering Chemistry.* 2018, Vol. 61.
123. Kim, S. H., et al. Digital light processing 3D printed silk fibroin hydrogel for cartilage tissue engineering. *Nature Communication.* 2019.

124. Ma, X., et al. Deterministically patterned biomimetic human iPSC-derived hepatic model via rapid 3D bioprinting. *Proceedings of the National Academy of Sciences*. 2016, Vol. 113.
125. Z., Wang, et al. A simple and high-resolution stereolithography-based 3D bioprinting system using visible light crosslinkable bioinks. *Biofabrication*. 7, 2015.
126. O., Håkansson K. M., et al. Solidification of 3D printed nanofibril hydrogels into functional 3D cellulose structures. *Advanced Materials & Technologies*. 2016.
127. Lille, Martina, et al. Applicability of protein and fiber-rich food materials in extrusion-based 3D printing. *Journal of Food Engineering*. 2018, Vol. 220.
128. Schütz, K., et al. Threedimensional plotting of a cell-laden alginate/methylcellulose blend: towards biofabrication of tissue engineering constructs with clinically relevant dimensions. *Tissue Engineering Regeneration Medicine*. 11.
129. Law, N., et al. Characterisation of hyaluronic acid methylcellulose hydrogels for 3D bioprinting. *Mechanical Behaviour Biomedical Materials*. 2018, 77.
130. Negrini, N.C., et al. 3D printing of methylcellulose-based hydrogels. *Bioprinting*. 2018, Vol. 10.
131. You, Shangting, et al. High-fidelity 3D printing using flashing photopolymerization. *Additive Manufacturing*. 2019, 30.
132. Mondschein, Ryan J., et al. Polymer structure-property requirements for stereolithographic 3D printing of soft tissue engineering scaffolds. *Biomaterials*. 2017, Vol. 140.
133. Ji, Shen, Almeida, Emily and Guvendiren, Murat. 3D bioprinting of complex channels within cell-laden hydrogels. *Acta Biomaterialia*. 2019, Vol. 95.
134. Wadnap, Soham, et al. Biofabrication of 3D cell-encapsulated tubular constructs using dynamic optical projection stereolithography. *Journal of Materials Science: Materials in Medicine*. 2019.
135. Kufelt, Olga, et al. Water-soluble photopolymerizable chitosan hydrogels for biofabrication via two-photon polymerization. *Acta Biomaterialia*. 2015, Vol. 18.
136. Bencherif, Sidi A., et al. Influence of the degree of methacrylation on hyaluronic acid hydrogels properties. *Biomaterials*. 2008.
137. Lee, Jae Yoon and Kim, Geun Hyung. A cryopreservable cell-laden GelMa-based scaffold fabricated using a 3D printing process supplemented with an in situ photo-crosslinking. *Journal of Industrial and Engineering Chemistry*. 2020.
138. Nichol, J.W., et al. Cell-laden microengineered gelatin methacrylate hydrogels,. *Biomaterials*. 2011.
139. Hong, Heesun, et al. Digital light processing 3D printed silk fibroin hydrogel for cartilage tissue engineering. *Biomaterials*. 2020, 232.
140. Fairbanks, B.D., et al. Photoinitiated polymerization of PEG-diacrylate with lithium phenyl-2,4,6-trimethylbenzoylphosphinate: polymerization rate and cytocompatibility. *Biomaterials*. 2009, 30.
141. [Online] <https://www.sigmaaldrich.com/catalog/product/aldrich/900889?lang=it®ion=IT>.
142. [Online] 05 2020. <http://www.xtgchem.cn/upload/20110629045632.PDF>.

143. Bagheri, Ali and Jin, Jianyong. Photopolymerization in 3D printing. *ACS Appl. Polym. Mater.* . 2019, Vol. 1.
144. Gerola, Adriana P., et al. The effect of methacrylation on the behavior of Gum Arabic as pH-responsive matrix for colon-specific drug delivery. *European Polymer Journal*. 2016, Vol. 78.
145. Sampath, U.G. Thennakoon Mudiyansele, et al. Preparation and characterization of nanocellulose reinforced semi-interpenetrating polymer network of chitosan hydrogel. *Cellulose*. 2017, Vol. 24.
146. Leipzig, N. D., & Shoichet, M. S. The effect of substrate stiffness on adult neural. *Biomaterials*. 2009, Vol. 30 , 36.
147. Li, B., Wang, L., Xu, F., Gang, X., Demirci, U., Wei, D., ... Zhou, Y. Hydrosoluble, UV-crosslinkable and injectable chitosan for patterned cell-laden microgel and rapid transdermal curing hydrogel in vivo. *Acta Biomaterialia*. 2015, Vol. 22.
148. Matsuda, T. and Magoshi, T. Preparation of vinylated polysaccharides and photofabrication of tubular scaffolds as potential use in tissue engineering. *Biomacromolecules*. 2002, Vol. 5.
149. A.X. Sun, H. Lin, A.M. Beck, E.J. Kilroy, R.S. Tuan,. Projection stereolithographic fabrication of human adipose stem cell-incorporated biodegradable scaffolds for cartilage tissue engineering. *Front. Bioeng. Biotechnol*. 2015, Vol. 3.
150. K.S. Masters, D.N. Shah, L.A. Leinwand, K.S. Anseth. Crosslinked hyaluronan scaffolds as a biologically active acarrier for valvular cells. *Biomaterials*. 2005.
151. P. Zorlutuna, J.H. Jeong, H. Kong, R. Bashir. Stereolithography-based hydrogel microenvironments to examine cellular interactions . *Advanced Functionalised Materials*. 2011, Vol. 21.
152. E.M. Chandler, C.M. Berglund, J.S. Lee, W.J. Polacheck, J.P. Gleghorn, B.J. Kirby,. Stiffness of photocrosslinked RGD-alginate gels regulates adipose progenitor cell behavior. *Biotechnol. Bioeng.* . 2011, Vol. 108.
153. AD, Rouillard, et al. Methods for photocrosslinking alginate hydrogel scaffolds with high cell viability. *Tissue Eng Part C Methods*. 2011, Vol. 17.
154. Billiet, Thomas, et al. The 3D printing of gelatin methacrylamide cell-laden tissue-engineered constructs with high cell viability. *Biomaterials*. 2014.
155. R. Gauvin, Y.-C. Chen, J.W. Lee, P. Soman, P. Zorlutuna, J.W. Nichol, H. Bae, S. Chen, A. Khademhosseini,. Microfabrication of complex porous tissue engineering scaffolds using 3D projection stereolithograph. *Biomaterials*. 2012.
156. X. Zhao, Q. Lang, L. Yildirimer, Z.Y. Lin, W. Cui, N. Annabi, K.W. Ng, M.R. Dokmeci, A.M. Ghaemmaghami, A. Khademhosseini. Photocrosslinkable gelatin hydrogel for epidermal tissue engineering. *Adv. Healthcare Mater.* . 2016.
157. Krishnamoorthy, Srikumar, et al. Investigation of gelatin methacrylate working curves in dynamic optical projection stereolithography of vascular-like constructs. *European Polymer Journal*. 2020, Vol. 124.
158. Ye, Wensong, et al. 3D printing of gelatin methacrylate-based nerve guidance conduits with multiple channels. *Materials & Design*. 2020, Vol. 192.

159. Skardal, A., et al. Photocrosslinkable Hyaluronan-Gelatin Hydrogels for Two-Step Bioprinting. . *Tissue Eng., Part A*. 16, 2010.
160. Chung, J. H. Y., et al. Bio-ink Properties and Printability for Extrusion Printing Living Cells. *Biomater. Sciences*. 2013.
161. S.H. Kim, Y.K. Yeon, J.M. Lee, J.R. Chao, Y.J. Lee. Precisely printable and biocompatible silk fibroin bioink for digital light processing 3D printing. *Nat. Commun.* 2018, Vol. 9.
162. H.H. Kim, J.W. Kim, J. Choi, Y.H. Park, C.S. Ki. Characterization of silk hydrogel formed with hydrolyzed silk fibroinmethacrylate via photopolymerization. *Polymer*. 2018.
163. Mata, Jitendra, et al. Interaction of cationic surfactants with carboxymethylcellulose in aqueous media. *Journal of Colloid and Interface Science*. 2006, Vol. 297.
164. [Online] <https://www.scbt.com/p/carboxymethylcellulose-sodium-salt-9004-32-4>.
165. Javanbakht, Siamak and Shaabani, Ahmad. Carboxymethyl cellulose-based oral delivery systems. *International Journal of Biological Macromolecules*. 2019, Vol. 133.
166. *sigmaaldrich*. [Online] [Cited: 12 05 2020.] <https://www.sigmaaldrich.com/catalog/substance/methacrylicanhydride1541676093011?lang=it®ion=IT>.
167. Sahin, Melahat, et al. Tailoring the interfaces in glass fiber-reinforced photopolymer composites. *Polymer*. 2018, Vol. 141.
168. [Online] 27 03 2020. <http://www.xtgchem.cn/upload/20110629045602.PDF>.
169. M., Hassan, et al. Enzyme-assisted isolation of microfibrillated cellulose from date palm fruit stalks. *Industrial Crops and Products*. 2014, Vol. 55.
170. W.D.Wanrosli, R.Rohaizu and A.Ghazali. Synthesis and characterization of cellulose phosphate from oil palm empty fruit bunches microcrystalline cellulose. *Carbohydrate Polymers*. 2011, Vol. 84.
171. Chang, S.H. An overview of empty fruit bunch from oil palm as feedstock for bio-oil production. *Biomass and Bioenergy*. 2014, Vol. 62.
172. *Optimization of process parameters for digital light processing (DLP) 3D printing*. Ibrahim, A., N., Sa'ude and Ibrahim, M. Seoul, South Korea : s.n., 2017.
173. Bhutani, Utkarsh, et al. Sodium alginate and gelatin hydrogels: Viscosity effect on hydrophobic drug release. *Materials Letters*. 2016.
174. Colosi, Cristina, et al. Microfluidic Bioprinting of Heterogeneous 3D Tissue Constructs Using Low-Viscosity Bioink. *Advanced Materials*. 2016.
175. Gao, Yuxue, et al. Preparation and properties of a highly elastic galactomannan-poly(acrylamide- N, N-bis (acryloyl) cysteamine) hydrogel with reductive stimuli-responsive degradable properties. *Carbohydrate Polymers*. 2020, Vol. 231.
176. Lingli Li, †,§ Conglie Lu, et al. Gelatin-Based Photocurable Hydrogels for Corneal Wound Repair. *Applied materials and interfaces*. 2018, 10.

177. XU, BIN, et al. Chitosan hydrogel improves mesenchymal stem cell transplant survival and cardiac function following myocardial infarction in rats. *EXPERIMENTAL AND THERAPEUTIC MEDICINE*. 2017, 13.
178. Masanori Fujita, M.D., et al. Inhibition of Vascular Prosthetic Graft Infection Using a Photocrosslinkable Chitosan Hydrogel. *Journal of Surgical Research*. 2004, 121.
179. Amsden, Brian G., et al. Methacrylated Glycol Chitosan as a Photopolymerizable Biomaterial. *Biomacromolecules*. 2007, 8.
180. Geever, Luke M., Lyons, John G. and Higginbotham, Clement L. Photopolymerisation and characterisation of negative temperature sensitive hydrogels based on N,N-diethylacrylamide. *J Mater Sci*. 2011, 46.
181. Crompton, K.E., et al. Polylysine-functionalised thermoresponsive chitosan hydrogel for neural tissue engineering. *Biomaterials*. 2007, Vol. 28.
182. Fukaya, Chie, et al. Development of a photocurable gelatin-based gelation material for application to periodontal regeneration. *Journal of Photochemistry and Photobiology A: Chemistry*. 2008, Vol. 199.
183. Zuidema, Jonathan M., et al. Fabrication and characterization of tunable polysaccharide hydrogel blends. *Acta Biomaterialia*. 2011, Vol. 7.
184. Chen, Shixuan, et al. A laminin mimetic peptide SIKVAV-conjugated chitosan hydrogel promoting wound healing by enhancing angiogenesis, re-epithelialization and collagen deposition. *Journal of Material Chemistry B*.
185. Rabbani, Shahram, Rabbani, Abbas and al, Mohammad Ali Mohagheghi et. A novel approach for repairing of intestinal fistula using chitosan hydrogel. 2009.
186. Ishihara, Masayuki, et al. Chitosan hydrogel as a drug delivery carrier to control angiogenesis. *The Japanese Society for Artificial Organs*. 2016, Vol. 9.
187. Hamed, Hamid, et al. Chitosan based hydrogels and their applications for drug delivery in wound dressings: a review. *Carbohydrate Polymers*. 2018, Vol. 199.
188. Xu, Bin, et al. Chitosan hydrogel improves mesenchymal stem cell transplant survival and cardiac function following myocardial infarction in rats. *Experimental and therapeutic medicine*. 2017, Vol. 13.
189. Rinaudo, Marguerite. Chitin and chitosan: Properties and applications. *Progress in polymer science*. 2006, Vol. 31.
190. Han, Hee Dong, et al. Preparation and Biodegradation of Thermosensitive Chitosan Hydrogel as a Function of pH and Temperature. *Macromolecular Research*. 2004, Vol. 12.
191. Khan, Suhail Ayoub, Siddiqui, Mohammad Fuzail and Khan, Tabrez Alam. Ultrasonic-assisted synthesis of polyacrylamide/bentonite hydrogel nanocomposite for the sequestration of lead and cadmium from aqueous phase: Equilibrium, kinetics and thermodynamic studies. *Ultrasonics-Sonochemistry*. 2020, Vol. 60.
192. Crompton, K.E., et al. Polylysine-functionalised thermoresponsive chitosan hydrogel for neural tissue engineering. *Biomaterials*. 2007, Vol. 28.

193. Huang, Biao, Liu, Mingxian and Zhou, Changren. Chitosan composite hydrogels reinforced with natural clay nanotubes. *Carbohydrate polymers*. 2017, Vol. 175.
194. Sreedhar, N., et al. 3D printed feed spacers based on triply periodic minimal surfaces for flux enhancement and biofouling mitigation in RO and UF. *Desalination*. 2018, 45.
195. . S. Kerdi, A. Qamar, J.S. Vrouwenvelder, N. Ghaffour.
196. Liu, Jun, et al. Current advances and future perspectives of 3D printing natural-derived biopolymers. *Carbohydrate Polymers*. 2019, 207.
197. Tijging, Leonard D., et al. 3D printing for membrane separation, desalination and water treatment. *Applied Materials Today*. 2019.
198. B., Vernon, S.W., Kim and Y.H., Bae. Insulin release from islets of Langerhans entrapped in a poly(N-isopropylacrylamide-co-acrylic acid)polymer gel. *Biomaterial Science Polymers*. 1999, 10.
199. DrorBen-David, et al. Cell-scaffold transplant of hydrogel seeded with rat bone marrow progenitors for bone regeneration. *Journal of Cranio-Maxillofacial Surgery*. 2011, Vol. 39.
200. Deng, Jiajia, et al. PDGFBB-modified stem cells from apical papilla and thermosensitive hydrogel scaffolds induced bone regeneration. *Chemico-Biological Interactions*. 2020, Vol. 316.
201. Jin R, Moreira Teixeira LS, Krouwels A, Dijkstra PJ, van Blitter-swijk CA, Karperien M, Feijen J. Synthesis and characterization of hyaluronic acid-poly(ethylene glycol) hydrogels via Michael addition: an injectable biomaterial for cartilage repair. *Acta Biomaterialia*. 2010, Vol. 6.
202. Tan, H., et al. Gelatin/chitosan/hyaluronan scaffold integrated with PLGA. *Acta Biomaterialia*. 2009, Vol. 5.
203. Leach, J.B., et al. Development of photocrosslinkable hyaluronic acid polyethylene glycol-peptide composite hydrogels for soft tissue engineering. *Journal of Biomedical Materials Research*. 2004, Vol. 70.
204. Tan, H., et al. Thermosensitive Injectable Hyaluronic Acid Hydrogel for Adipose Tissue Engineering. *Biomaterials* . 2009, Vol. 30.
205. Hemmrich, K., et al. Autologous in vivo adipose tissue engineering in hyaluronan-based gels a pilot study. *Journal of Surgical Research*. 2008, Vol. 144.
206. Kanitkar, Ryan J. Mondschein, Akanksha, et al. Polymer structure-property requirements for stereolithographic 3D printing of soft tissue engineering scaffolds. *Biomaterials*. 2017, Vol. 140.
207. Matinfar, M., Mesgar, A.S. and Mohammadi, Z. Evaluation of physicochemical, mechanical and biological properties of chitosan/carboxymethyl cellulose reinforced with multiphasic calcium phosphate whisker-like fibers for bone tissue engineering. *Materials Science and Engineering: C*. 2019, Vol. 100.
208. Chen, J., et al. Two types of core/shell fibers based on carboxymethyl chitosan and sodium carboxymethyl cellulose with self-assembled liposome for buccal delivery of carvedilol across TR146 cell culture and porcine buccal mucosa. *International Journal of Biological Macromolecules*. 2019, Vol. 128.
209. Youssef, A.M. and El-Sayed, S.M. Bionanocomposites materials for food packaging applications: concepts and future outlook. *Carbohydrate Polymers*. 2018, Vol. 193.

210. A.M. Youssef, S.M. El-Sayed, H.S. El-Sayed, H.H. Salama, A. Dufresne. Enhancement of Egyptian soft white cheese shelf life using a novel chitosan/carboxymethyl cellulose/zinc oxide bionanocomposite film. *Carbohydrate Polymers*. 2016, Vol. 151.
211. Chen, Y., et al. Synthesis of high-performance sodium carboxymethyl cellulose-based adsorbent for effective removal of methylene blue and Pb (II). *International Journal of Biological Macromolecules*. 2019, Vol. 126.
212. Ure, D., et al. Greenhouse tomato plant roots/carboxymethyl cellulose method for the efficient removal and recovery of inorganic phosphate from agricultural wastewater. *Journal of Environmental Management*. 2019, Vol. 233.
213. Wang, W., et al. Comparative study of water-based LA133 and CMC/SBR binders for sulfur cathode in advanced lithium–sulfur batteries. *Journal of the American Chemical Society*. 2018, Vol. 123.
214. Y.C. Chen, R.Z. Lin, H. Qi, Y. Yang, H. Bae, J.M. Melero-Martin, A. Khademhosseini,. Functional human vascular network generated in photocrosslinkable gelatin methacrylate hydrogels. *Adv. Funct. Mater*. 2012.
215. Ying-Chieh Chen, Ruei-Zeng Lin , Hao Qi , Yunzhi Yang , Hojae Bae , Juan M. Melero-Martin , Ali Khademhosseini. Functional Human Vascular Network Generated in Photocrosslinkable Gelatin Methacrylate Hydrogels. *Advanced Functional Materials*. 2012, Vol. 22.
216. Gauvin, Robert, et al. Microfabrication of complex porous tissue engineering scaffolds using 3D projection stereolithography. *Biomaterials*. 2012, Vol. 33.
217. Taormina, Gabriele, Sciancalepore, Corrado and Messori, Massimo. 3D printing processes for photocurable polymeric materials: technologies, materials, and future trends. *Journal of Applied Biomaterials & Functional Materials*. 2018, Vol. 16.

Figure 1: procedure to inject the cells-loaded hydrogel precursor. The hydrogel forms in-situ, thus the tissue regeneration occurs in a no-invasive manner (6) 7

figure 2. trend of drug's concentration. In conventional dosing the drug is given by doses; controlled release consists in a gradual release from carriers. 9

figure 3: (a) Repeating unit of cellulose, the 'cellubiose'. (b) repeating unit of cellulose derivatives. "R" represents the substituent groups for each derivative, such as methylcellulose (MC), hydroxypropyl methycellulose (HPMC), ethyl cellulose (EC), hydroxyethyl cellulose (HEC) and sodium carboxymethylcellulose (NaCMC). (43) 13

figure 4. Amorphous and crystalline regions in cellulose fibrils (44) 14

figure 5. classification of 3D printing technologies (64) (65) 19

Figure 6. scheme of photopolymerization (72) 21

figure 7. Molecular structure of photo-monomers (73) 22

figure 8. photoinitiators (type I and type II). (75)..... 23

figure 9. Radical photopolymerization reaction's steps. PI is the photoinitiator, that absorbs the radiation and create a radical specie. The reaction proceeds with the formation of a macroradical

(initiation) and its growth by the addition of other monomers (propagation). The reaction ends with the termination step. (76)	23
figure 10. Quenching and scavenging reactions (80)	25
figure 11. Stereolithography (SLA) (83)	26
figure 12. Digital Light Processing (DLP) (83)	26
figure 13. Comparison between SLA and DLP. (84).....	27
figure 14. A PEGDA hydrogel cell-scaffold produced by DLP. The modification of exposure time allowed the production of a structure with regionally varied stiffness. (92).....	29
figure 15. DLP PRINTER TO FABRICATE TABLETS FOR DRUG CONTENT, USING PEGDA AND PEGDMA AS PHOTOREACTIVE (97)	30
figure 16. membranes' spacers produced by DLP technologies. (101).....	31
figure 17. cDAP hydrogels with different concentration of chitosan and dyacrylated pluronic F-127 were printed into various shapes (105).	31
figure 18. Repeating units of common polysaccharides (132).....	33
figure 19. Chemical structure of lithium acylphosphinate salt (LAP) (141)	34
figure 20. Chemical structure of 1-[4-(2-Hydroxyethoxy)-phenyl]-2-hydroxy-2-methyl-1-propane-1-one (Irgacure 2959) (142).....	34
figure 21. Reaction scheme for the synthesis of methacrylated chitosan (MeChi). LMeCHI and HMeChi are chitosan with respectively low and high degree of modification. (117).....	35
figure 22. Modification and DLP-3D printing of chitosan (109)	35
figure 23. Magnification of a CHI-MA scaffold produced by 2PP (135)	36
figure 24. Constructs of various shapes (B) mimic perfectly the CAD models (A) in paper (149).....	36
figure 25. printing approach that uses a sacrificial ink (131)	37
figure 26 Synthesis of GelMA (154).....	38
figure 27. Fabricated 3D vascular-like construct and the cell viability test. The part possesses a hollow cross section (157).....	39
figure 28. Synthesis of Silk-GMA (137)	40
figure 29. cell-loaded artificial trachea fabricated by DLP printer (137).....	40
figure 30. Synthesis of SFMA (139) with IEM	41
figure 31. Carboxymethyl cellulose sodium salt chemical structure (164)	43
figure 32. Methacrylic anhydride (166).....	43
figure 33. BAPO chemical structure. (168)	44
figure 34. CMC and MA solution after washing with ethanol.....	44
figure 35. dialysis.....	45
figure 36. DLP printer	46
figure 37. STL files for the 3D printing of various parts.....	47
figure 38. Photo-rheometer equipment	48
figure 39. Hydrogel sample subjected to compression test.....	50
figure 40. Displacement-controlled test. The displacement increases regularly and the machine measures the instantaneous load sustained by the sample.....	51
figure 41. TREND OF LOAD AND DISPLACEMENT IN A CYCLE	52
figure 42. Possible scheme for methacrylation of CMC	54
figure 43. 1 H-NMR spectra for M-CMC (red) and neat CMC (Black).....	54
figure 44. Viscosity vs Shear rate curves of neat M-CMC samples	55
figure 45. TIME SWEEP TEST ON NEAT SAMPLES WITH DIFFERENT CONCENTRATION OF M-CMC	55
figure 46. Detail of the time sweep curve of 20 mg/mL sample of neat M-CMC. The value of G' and G'' are reported in the range of time between 50 s and 80 s.	56

figure 47. DEPENDANCE OF THE FINAL STORAGE MODULUS ON THE M-CMC CONCENTRATION IN NEAT HYDROGELS.....	57
figure 48. Amplitude sweep tests of neat samples	57
figure 49. viscosity vs shear rate curves of composite samples.....	58
figure 50. Time sweeps test of composite samples	58
figure 51. G' as a function of CNCs content in a formulation of 20 mg/mL of M-CMC and 2 phr of BAPO-OH (with respect to M-CMC).	59
figure 52. Amplitude sweeps tests of CNC/M-CMC samples, compared to 20 mg/mL neat sample. ..	60
figure 53. Effect of printing parameters in DLP.....	61
figure 54. The same STL file was 3D-printed starting from neat formulation (A) and from the formulation containing CNCs (B).....	62
figure 55. Filled (A) and neat (B) samples for compression tests.....	62
figure 56. Two attempts to printing a 30 mg/mL formulation. In the second picture, burn-in exposure time and exposure time were increased.....	63
figure 57. 3D-printing of M-CMC/DMEM (A and B) and neat M-CMC (C) formulations.....	63
figure 58. the same component printed without and with DMEM (respectively figure A and B).	64
figure 59. Compression curve.....	64
figure 60. Neat M-CMC hydrogel at failure.....	65
figure 61. Composite CNC/M-CMC hydrogel at failure.....	66
figure 62. Example of a cycle of cyclic compression tests.....	67
figure 63. VALUE OF DISSIPATIVE ENERGY (U) AND YOUNG MODULUS (E) DURING THE CYCLIC TESTS.	68
figure 64. Trend of the strain corresponding to the maximum stress at each cycle	68